Interaction of igneous sills and host rocks of the Curtis Formation, Eastern Utah

Master of Geoscience

Kristin Aven

Department of Earth Science

University of Bergen

August 2023

Abstract

Sills and igneous intrusions are crucial components in volcanic plumbing systems because they transport magma through the crust. Understanding the development of sills in sedimentary basins is useful for executing efficient extraction of hydrocarbons and mineral resources, as well as understanding active volcanism. However, previous studies on sill development and emplacement mechanisms have mainly focused on the emplacement of sills in mudstone. The emplacement of sill intrusions in cemented sandstone deposits, with sparse mudstone beds, has not been studied in detail before. This study aims to enhance the understanding of the interaction between the igneous intrusion and the sandstone-dominated host rock. In this thesis, I have investigated a shallow (c. < 1 km) emplaced alkaline trachybasalt sill with a thickness of c. 15 m in the Mussentuchit Wash, San Rafael Swell, Utah. The host rock of this intrusion is the Middle to Late Jurassic Curtis Formation, which is dominated by sandy and tidally influenced sedimentary rocks. The relationship between the sill and surrounding host rock has been examined using sedimentological logs of the Curtis Formation and 3D virtual representations of the outcrop of the Mussentuchit Wash Sill. Four different facies associations (FAs) were determined for the host rock. Results of this study show that host rock lithology strongly controls the emplacement of the intrusion. In this study it has been established that the Mussentuchit Wash Sill exploits weak mudstone layers such as mudstone-draped foresets, even though its preference is staying in the (dune-dominated) sandstone layer. This study also results in observations of a shallow emplaced sill displaying emplacement structures caused by brittle deformation, such as steps and broken bridges. The results demonstrate that cementation of the host rock might be more important than the emplacement depth, given that the Mussentuchit Wash Sill predominantly displays brittle emplacement structures. This is contrary to previous studies, where shallow emplaced sills primarily display non-brittle emplacement structures. Thus, the findings of this study suggest that local lithology appears to control the architecture and emplacement of sills to a great extent in sedimentary basins.

Acknowledgments

This thesis is a part of my master's degree in the Geodynamics and Basin Studies Research Group at the Department of Earth Science, University of Bergen. This section is to show my deepest gratitude to all those who have been associated with this project and helped me on the way.

First and foremost, I would like to express my greatest gratitude to my main supervisor, Professor Christian Haug Eide (University of Bergen) for giving me the opportunity to work on such an exciting project, and for the excellent guidance. Thank you for the support and encouragement I have received during these last two years. I would also like to express my gratitude to my co-supervisor, PhD Candidate Martin Kjenes (University of Bergen) for great feedback, encouragement and for helping me with the photogrammetry modeling.

Thanks to NORCE for the academic license to the software LIME where I could interpret the processed 3D models.

I would also like to thank my fellow students for the great work environment with room for both academic discussions and social events during the last five years. It has been so much fun. Special thanks to Seline Bruun Berg for being an excellent field assistant in Utah, May 2022. For those of you who proofread my chapters, thank you for great feedback.

Finally, thank you to my family and friends for the endless support during these exciting years and during the time of writing my thesis. Thank you for helping me relax and keep me grounded during these stressful last few months.

Kristin Aven

Bergen, August 2023

Table of Contents

1.0 Introduction

1.1 Motivation

Sills are common in sedimentary basins, and understanding how they develop is crucial. By gaining this understanding, it becomes feasible to plan and execute the extraction of oil, gas, and mineral resources more efficiently in volcanic basins worldwide. Additionally, analyzing earthquake data and ground deformation enables us to predict volcanic eruptions and comprehend magma movement and transport within the Earth (Tibaldi & Pasquarè, 2008). Recent studies have revealed that sills create magma-filled fissures ahead of them (Hutton, 2009; Schofield et al., 2012), which could be responsible for inducing earthquakes (Ágústsdóttir et al., 2016).

Volcanic and igneous plumbing systems display an abundance of various shapes such as dykes (near vertical), sills (near horizontal sheets or saucers), laccoliths and inclined sheets. Magma travels from the lower crust to the Earth's surface mainly through the pathways of dykes. Recent studies, however, have highlighted that igneous sills also represent a significant part of these volcanic plumbing systems. Furthermore, sills contribute to lateral magma transport and storage in the Earth's crust (Schofield et al., 2012; Tibaldi, 2015; Magee et al., 2016). Sills are intrusions that form in tabular sheets that are decided by the layering of the host rock. They are commonly found in sedimentary basins, and mafic intrusions are particularly common in rift basins and passive margins. Moreover, they are commonly linked to flood basalt emplacement and large igneous provinces (Hutton, 2009; Jerram & Bryan, 2015; Magee et al., 2016; Spacapan et al., 2017). Mafic sill intrusions develop frequently as layer-parallel conduits of magma within sedimentary basins. Recent work has shown that emplacement of such sills is strongly controlled by host rock lithology, particularly by weak mudstone layers (Eide et al., 2018; Mark et al., 2018). The emplacement of sill intrusions in cemented sandstone deposits, with sparse mudstone beds, has not yet been studied in detail. This is due to the physics of sill emplacement being studied mainly based on seismic interpretation (Eide, Schofield, et al., 2016). An understanding of such concept is important to plan resource extraction in volcanic basins and to interpret earthquake activity during volcanic rest. If sills are emplaced into sedimentary sequences, they can impact basin history, hydrocarbon migration pathways and reservoir properties, both at the time of the intrusion and long after (Gardiner et al., 2019).

1.2 Aims and objectives

The aim of this thesis is to describe and investigate the interaction between igneous sills and their host rocks of the Curtis Formation in SE Utah. How host rock heterogeneity has controlled emplacement features of the sill, such as steps, broken bridges, and the contact between the sill and the host rock will be investigated during this study. Additionally, enhancing the sedimentological comprehension of the Curtis Formation within the designated study area will be conducted. This will facilitate a better understanding of how the sill has exploited the distribution of heterogeneities. These primary aims were achieved through a case study of the Curtis Formation and the Mussentuchit Wash Sill in SE Utah, where there will be conducted detailed investigations of the outcrop in 3D virtual outcrop models and detailed sedimentological analysis of the study area.

1.3 Study area

This master thesis focuses on the well-exposed Mussentuchit Wash Sill in San Rafael Swell, Utah, and the host rock, the Curtis Formation. The sill is an alkaline trachybasalt sill emplaced into a sandstone-dominated package of Jurassic host rock (Germa et al., 2020). The contact between the sill and the host rock displays different geometries, such as planar to the bedding and crossbedding of the Curtis Formation, and irregular. The Mussentuchit Wash Sill seems to follow local sedimentary discontinuities, such as sedimentary structures (crossbedding, and bed boundaries). This thesis will go into depth on the sill-host rock contact. The emplacement of the sill occurred at an approximate depth of 0.8-1 km, related to volcanism along the transition zone of the Colorado Plateau and the Basin and Range Province (Delaney & Gartner, 1997; Kjenes et al., 2022).

The study area is located in the San Rafael Volcanic Field, in the San Rafael Swell, SE Utah, on the northwestern margin of the Colorado Plateau. More precisely, an ephemeral, meandering river channel referred to as the Mussentuchit Wash (Fig. 1.1). The sedimentary host rock that was intruded in the San Rafael Volcanic Field consists of the Middle to Late Jurassic strata of the San Rafael Group (Delaney & Gartner, 1997). In the Mussentuchit Wash, there is a c. 15 m thick sill that has been emplaced in the Curtis Formation. These rocks are mainly shallow-marine packages of tidally influenced heterolithic strata (Gilluly & Reeside, 1928; Delaney & Gartner, 1997). These deposits are primarily sandstone; however, thin mudstone, limestone,

and gypsum beds are present. This locality provides a world-class outcrop for investigating the relationship between host rock and mafic intrusions.

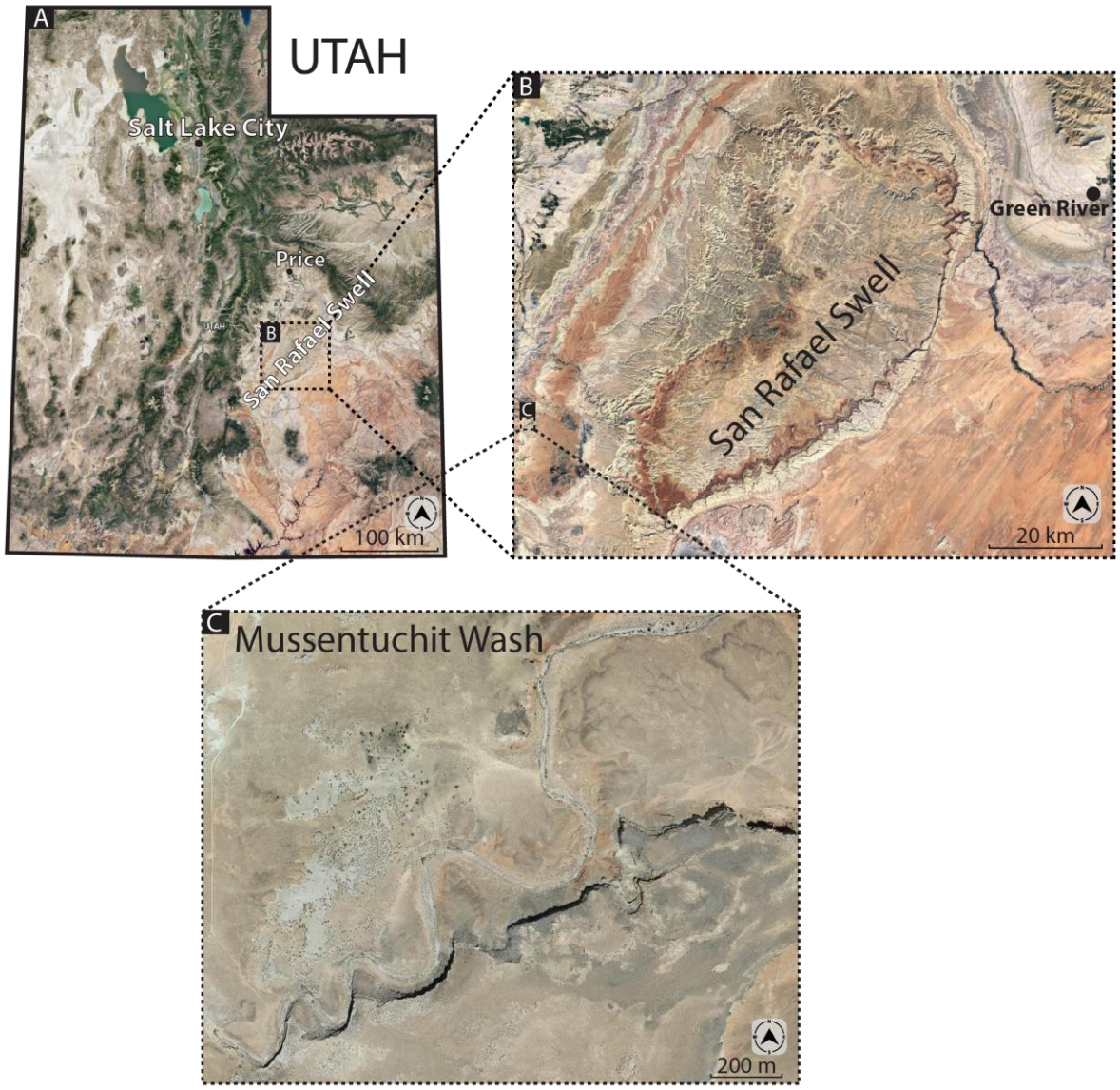

Fig. 1.1: Overview of the study area. (**A**) Map of the state of Utah with the San Rafael Swell and other key areas. (**B**) Close-up of the San Rafael Swell where the study area is located. (**C**) Close-up of the study area, the Mussentuchit Wash.

2.0 Geological framework

The purpose of this chapter is to provide the reader with an introduction to the tectonic and geological setting of the San Rafael Volcanic Field, located in Southeastern Utah, USA. The following chapter consists of three subchapters: 2.1. Tectonic setting, 2.2. Paleogeography and climate, and 2.3. Stratigraphic setting. Particularly, the depositional history of host rock, which is the Middle Jurassic Curtis Formation, and the emplacement of the studied Mussentuchit Wash Sill will be explained.

2.1 Tectonic setting

2.1.1 Overall setting

From late Precambrian through the Jurassic, the regions of the Southern Rocky Mountains as well as the Colorado Plateau was located on the southwest margin of cratonic North America (Blakey, 2019). Since the Mesozoic, Utah's geological history has been heavily influenced by tectonic events, especially by the evolution of the North American Cordillera (Zuchuat et al., 2018). There are several orogenies associated with the North American Cordillera: (1) the Middle Jurassic-Early Cretaceous Nevadan orogeny, where granitic intrusions occurred in Utah-Nevada, (2) the Middle Jurassic Elko orogeny, experiencing periods of both contraction and extension, and leading to the formation of a foreland basin, (3) the Early Cretaceous to Paleogene Sevier orogeny, characterized by fold-thrust belt structures oriented in an eastward direction across Idaho, Utah, and Wyoming, and (4) the Late Cretaceous to Paleogene Laramide orogeny, linked with the formation of monoclines such as the San Rafael Swell (Thompson & Zoback, 1979; Bump & Davis, 2003; Zuchuat et al., 2018). This series of orogenies is said to be initiated by the breakup of Pangaea in Late Triassic, around 200 Ma, and North America began to drift westward, continuing to this day, causing subduction along the western margin (Blakey & Ranney, 2018b).

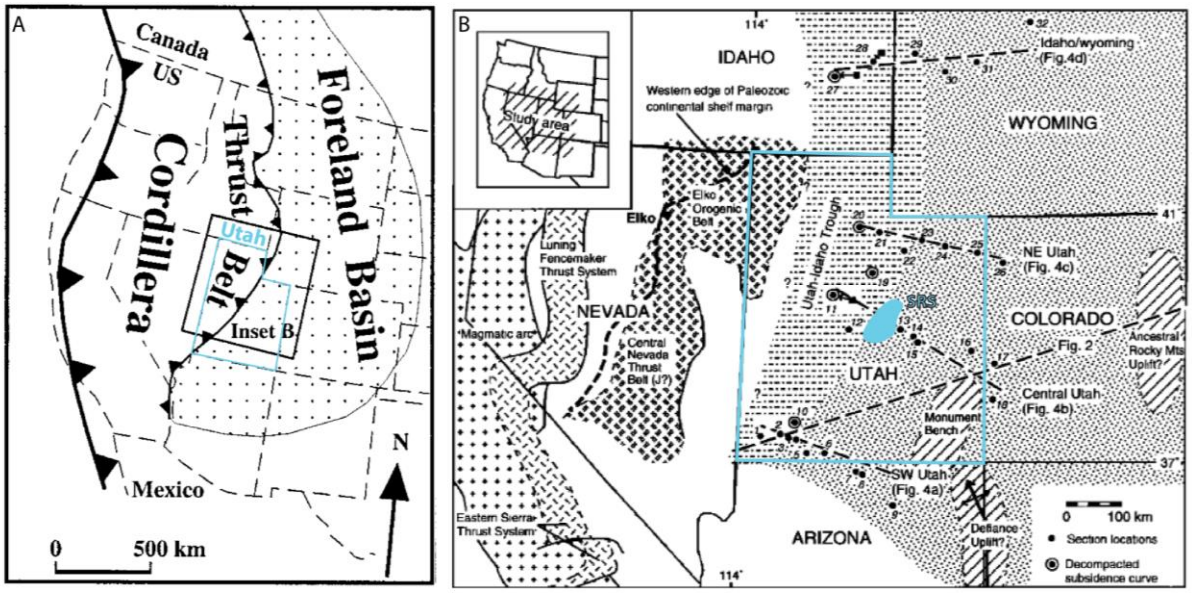

Fig. 2.1: Map of the western interior, United States. (**A**) Map showing the Cordilleran Arc and the Foreland Basin that developed. (**B**) Map showing the San Rafael Swell (light blue) and the Utah-Idaho Trough. Modified from Bjerrum & Dorsey (1995) and Currie (1998).

2.1.2 Setting during deposition of the Curtis Formation

As stated by Blakey and Ranney (2018), the entry of the Farallon plate during the Early Jurassic period played a crucial role in the evolution of modern-day North American Cordillera. The Farallon plate and the Cordillera both subducted, dipping eastward beneath the North American plate (Blakey & Ranney, 2018b). Heating and burial of the subducting slab through Late Triassic and Jurassic, caused partial melting and development of volcanic arcs on the surface (Blakey & Ranney, 2018b). The first orogeny in the North American Cordillera happened in Middle Jurassic and is called the Elko orogeny, where metamorphism and thrusting occurred. This orogeny was first proposed in 1990 by Thorman et al. (Thorman et al., 2020). A foreland basin advanced along the Wasatch Line, known as the Utah-Idaho Trough due to the subsiding basin during the Elko orogeny (Fig. 2.1) (Bjerrum & Dorsey, 1995). The subsidence phase ceased in the Late Jurassic (Bjerrum & Dorsey, 1995). Under deposition of the Curtis Formation during Late Jurassic, which is the host rock for the studied intrusion in this thesis, the Elko orogeny was still active. This basin initiated its subsidence in the Middle Jurassic due to the Elko orogeny and amassed over 2000 m of marine sediment during the Middle Jurassic. This process is illustrated in the burial curve from Nuccio and Condon (1996) (Fig. 2.2). The green curve represents Middle Jurassic sediments. It is indicated that the sediments experienced gradual burial to depths of approximately 600 m. Following a period of quiescence, the basin underwent further burial during the Upper Cretaceous due to the Sevier Orogeny. During this

phase, the burial rate was notably higher, leading to significant depths of sediment burial (Blakey, 2019). Nuccio and Condon (1996) propose that the Curtis Formation was buried to maximum depths of 2.45 km and 2.86 km near the San Rafael Swell during Upper Cretaceous and Early Paleogene (Fig. 2.2). The orogeny that has impacted the study area and the San Rafael Swell the most, is the Late Cretaceous to Paleogene Laramide orogeny (65 Ma to 50 Ma). This caused uplift of the Colorado Plateau as well as the Rocky Mountains and folded the sedimentary succession in Central Utah from the Mesozoic resulting in the San Rafael Swell (Blakey & Ranney, 2018a). The sediments of the San Rafael Group were later exposed to erosion and uplift during the uplift during the Laramide orogeny (Fig. 2.2).

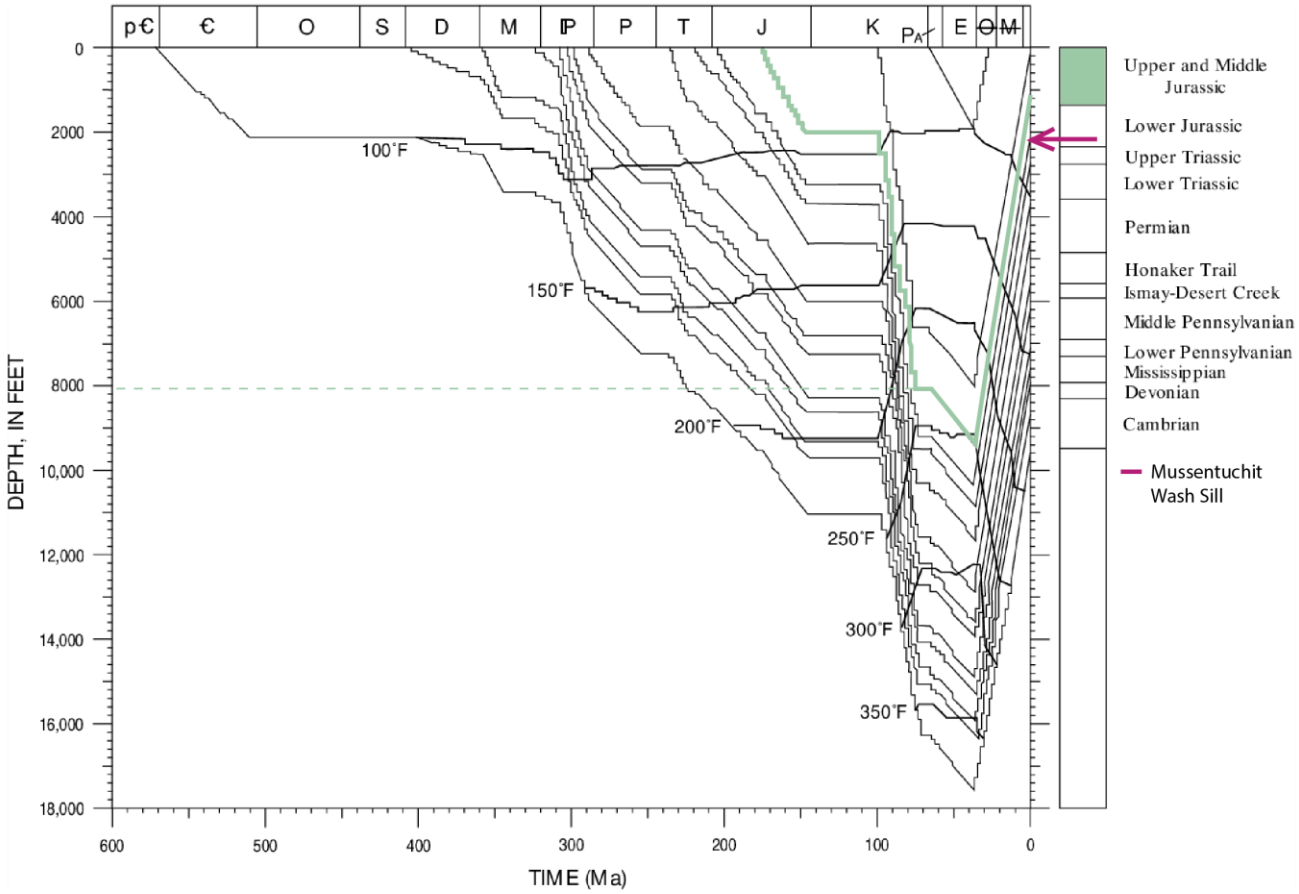

Fig. 2.2: Burial curve of the area near Green River, Utah. The burial depth is displayed on the y-axis in feet, and the time (and geological period/epoch) is displayed on the x-axis in Ma. Modified from Nuccio & Condon (1996).

2.1.3 Tectonic setting during emplacement of intrusions

The magmatism occurring in the San Rafael Volcanic Field is associated with the shallow subduction of oceanic lithosphere, the Farallon Slab, in Late Cretaceous to Early Cenozoic (Laramide orogeny). Nevertheless, the eruptions occurred much later, well after the subduction had ceased (Tingey et al., 1991; Humphreys, 1995). During the Neogene, there was a slab

rollback and lithospheric delamination causing crustal extension. Approximately 30 million years ago, asthenospheric melts might have underplated and heated the metasomatized lithosphere (Gonzales & Lake, 2017). The crustal extension along the margin, as well as intraplate volcanism occurring between the Colorado Plateau and the Basin and Range Province, lead to mantle magmatism that is assumed to be the source of magma for the intrusion studied in this thesis (Fig. 2.3) (Gonzales & Lake, 2017; Germa et al., 2020; Kjenes et al., 2022). The volcanic activity persisted from approximately 30 Ma to 800 years ago (Tingey et al., 1991; Gonzales & Lake, 2017; Germa et al., 2020).

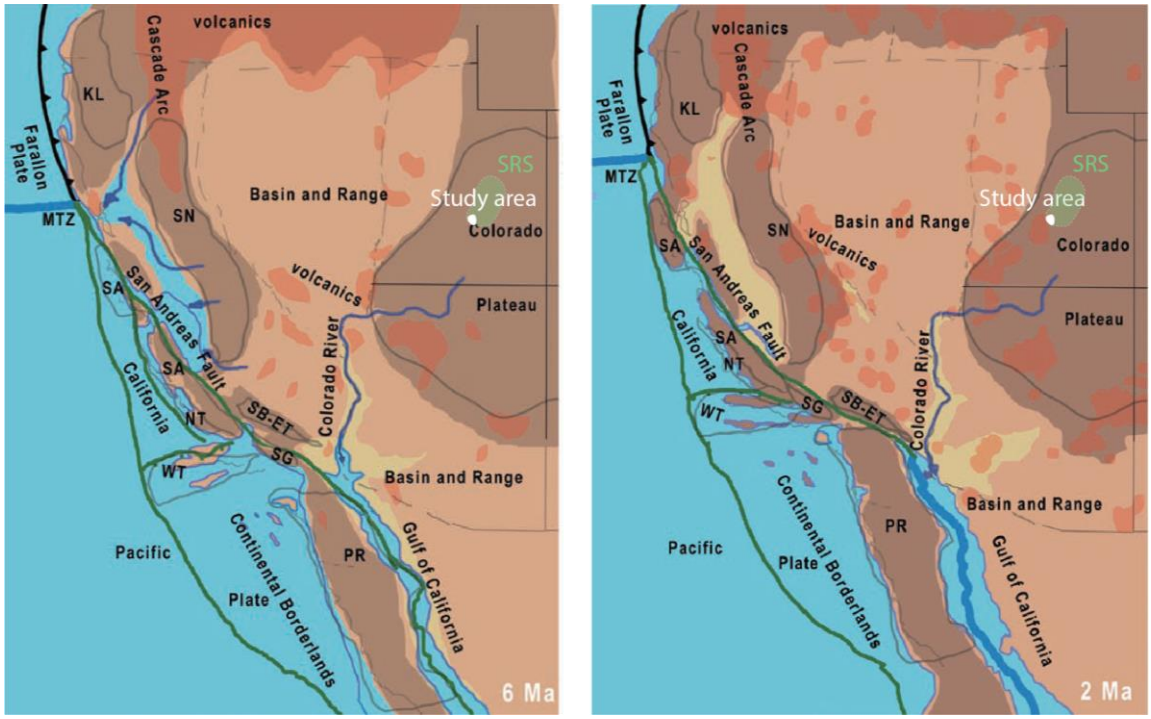

Fig. 2.3: Platotectonic maps from Miocene (6 Ma) and Pliocene (2 Ma) to display the evolution of the volcanism in the SW North America. The study area is marked in white, and the San Rafael Swell (SNS) is marked in green. Modified from Blakey & Ranney (2018a).

The San Rafael Volcanic Field comprises a crust that is approximately 40 kilometers thick, whereas 3 to 5 km of the crust is Phanerozoic sedimentary rocks. Underneath the crust, there is a basement made up of Precambrian igneous and metamorphic rocks (Thompson & Zoback, 1979). The San Rafael Volcanic Field is an example of an exposed shallow plumbing system comprising roughly 200 deeply eroded dykes and sills, with dykes predominately intersecting sills and exhibiting slightly chilled margins. These were first studied in detail by Delaney and Gartner (1997). According to K-Ar dating methods done by Delaney and Gartner (1997), the Mussentuchit Wash Sill and the rest of the sills and dykes in this swarm range between 3.4 to 4.7 Ma, which makes them of Pliocene age. The intrusions in the San Rafael are similar to

other types of alkaline mafic rocks found on the western margin of the North American Craton, and a great range of these are locally exposed along the transition zone between the Colorado Plateau and Basin and Range provinces (Fig.2.5) (Thompson & Zoback, 1979; Delaney & Gartner, 1997). Due to the stratigraphic position of the intrusions, as well as the evidence for vesicles in the igneous rocks, the depth of emplacement is suggested to be shallow (<1 km) (Williams, 1983; Díez et al., 2009; Richardson et al., 2015; Germa et al., 2020; Kjenes et al., 2022).

The intrusions in the San Rafael Volcanic Field comprises types of igneous rocks: 1) fine- to medium grained alkali trachybasalt comprising the bulk of the sills; 2) medium- to coarse-grained leucocratic syenite, which is found predominately within sills (Germa et al., 2020). The Mussentuchit Wash Sill belongs to the first type of igneous rock mentioned above, trachybasalt (Fig. 2.5). It is composed of 44-46 wt% SiO_2 with up to 60 vol. % crystals in an aphanitic to porphyritic groundmass (Williams, 1983; Delaney & Gartner, 1997; Germa et al., 2020). Aphanitic describes rocks that have a highly fine-grained texture (< 1 mm), where the individual crystals cannot be distinguished without using a microscope, whereas porphyritic texture describes groundmass with visible phenocrysts. The trachybasalt in the Mussentuchit Wash is melanocratic, meaning that it is composed of 50-60 % mafic minerals. According to Richardson et al. (2015), erosion has stripped away approximately 800 m to 1 km of overlying material since the volcanic activity came to a halt.

2.2 Paleogeography and climate during deposition of the Curtis Formation

The Mesozoic sedimentary sequences in Utah demonstrated alternating climatic conditions, which includes extensive eolian sequences deposited in Early and Middle Jurassic (Navajo Sandstone and Entrada Sandstone), as well as fluvial and marine conditions in the Late Jurassic to Early Cretaceous. Southwest North America is said to have been positioned around 15-20° north of the equator within an arid climate belt in the Jurassic (Blakey & Ranney, 2018b). The paleoclimate of the region changed from arid-hyperarid during the Middle Jurassic to semi-arid and more humid during the early Late Jurassic (Demko et al., 2004). The Morrison Formation marks the change in the climatic conditions from arid to fluvial and lacustrine (Blakey & Ranney, 2018b). The Curtis Formation is deposited earlier than the Morrison

Formation, which suggests that climatic conditions had begun to shift towards a more humid and less arid environment during its deposition.

The Utah-Idaho Trough was the dominant source of sediments during the Jurassic (Blakey, 2019). The Curtis Formation is widely exposed in the central and northern part of the Colorado Plateau, but its distribution is restricted by erosion linked to the overlying J-5 and sub-Cretaceous unconformities (Blakey, 2019). The deposition of the Curtis Formation occurred during the last Jurassic marine incursion into the Western Interior. Throughout the Early to Late Jurassic period, stream deposits reveal a shift in stream flow direction and changes in the sediment source. Initially, the sediments originated from Pangaean terranes and the North American craton at the beginning of the Jurassic, while towards the end of the period, they derived from Cordilleran terranes (Blakey, 2019). The sediments that make up the Curtis Formation came from the uplifted Paleozoic rocks of the Cordilleran region (Bjerrum & Dorsey, 1995; Blakey, 2019).

2.3 Stratigraphic setting of the Curtis Formation

2.3.1 San Rafael Group

The Mussentuchit Wash Sill is exposed in the Curtis Formation of Late Callovian-Early Oxfordian (about 161-159 Ma), Middle Jurassic strata of the San Rafael Group. This group consists of the Carmel Formation, Entrada Sandstone, and Curtis and Summerville Formations, ascending from oldest to youngest (Fig. 2.4) (Gilluly & Reeside, 1928). The Carmel Formation comprises marine- and sabkha-deposits and is overlain by the eolian erg and wet coastal deposits of the Entrada Sandstone. The fine-grained marine and tidal deposits of the Curtis Formation overlie an unconformity called the J-3 unconformity after Pipiringos and O'Sullivan (1978). This unconformity marks the separation of the Curtis Formation and the Entrada Sandstone. The Summerville Formation overlies the Curtis Formation, and it consists of sabkha-deposits. In the San Rafael Group, there is a change in deposits, from eolian deposits in the east to dominantly sabkha-marine deposition in the west (Blakey, 2019).

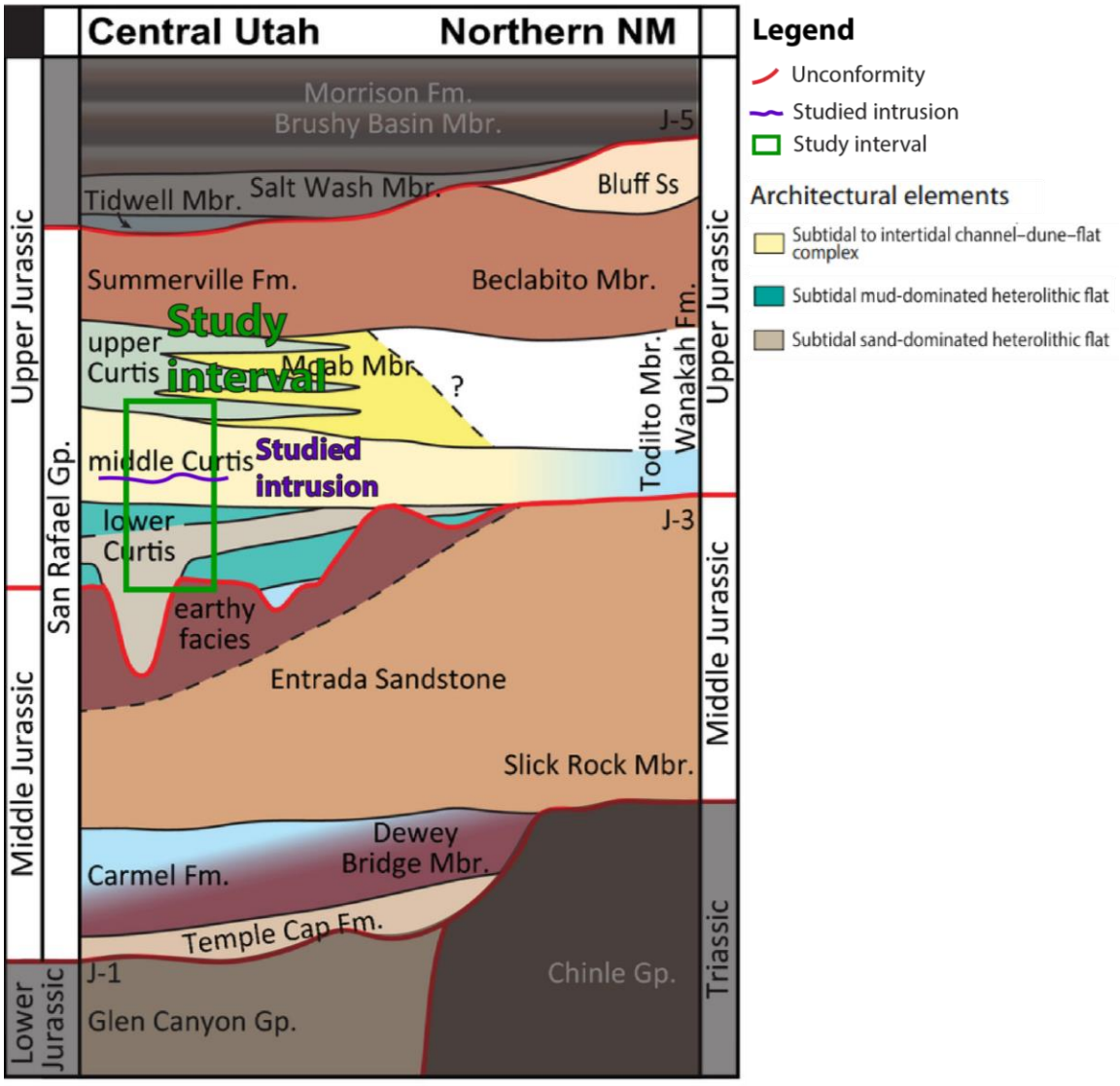

Fig. 2.4: Schematic lithostratigraphic column of Middle- and Upper Jurassic strata of the San Rafael Group in Central Utah (grey areas are not relevant for this study). The Curtis Formation is divided into lower, middle, and upper Curtis, and both study interval (green) and intrusion (purple) is visible. Modified from Zuchuat et al. (2019).

2.3.2 Curtis Formation

There have been several detailed studies investigating the development of the Curtis Formation (Gilluly & Reeside, 1928; Zuchuat et al., 2018), which is named after its exquisite exposure at Curtis Point, Utah. Gilluly and Reeside (1928) were the first to describe the formation, where the occurrence of greenish-gray glauconitic conglomerates, sandstones, and shales were used to identify it. The thickness varies from 30 to 80 meters throughout the formation in the study area in the San Rafael Swell (Gilluly & Reeside, 1928). Gilluly and Reeside (1928) collected fossils from the Northern part of the San Rafael Swell which confirmed that the Curtis

Formation has marine influence. Several different fossils were collected, i.e. Cidaris sp. and Pentacrinus asteriscus Meek and Hayden (Gilluly & Reeside, 1928).

As mentioned, the Curtis Formation is dominated by fine-grained sandstone and siltstone. The strata often display a greenish-gray color on fresh fracture, due to the glauconite contained (Gilluly & Reeside, 1928). However, weathering makes the rocks appear brownish in color. Gilluly and Reeside (1928) identified the lowermost part of the Curtis Formation as conglomerate composed of well-rounded pebbles, determined to be chert and flint. The rest of the Curtis Formation is fine-grained sandstone and siltstone, displaying sedimentary features such as cross-stratification (unidirectional and bidirectional current ripples) and oscillatory ripples. Shale and limestone are also commonly found in the Curtis Formation (Gilluly & Reeside, 1928).

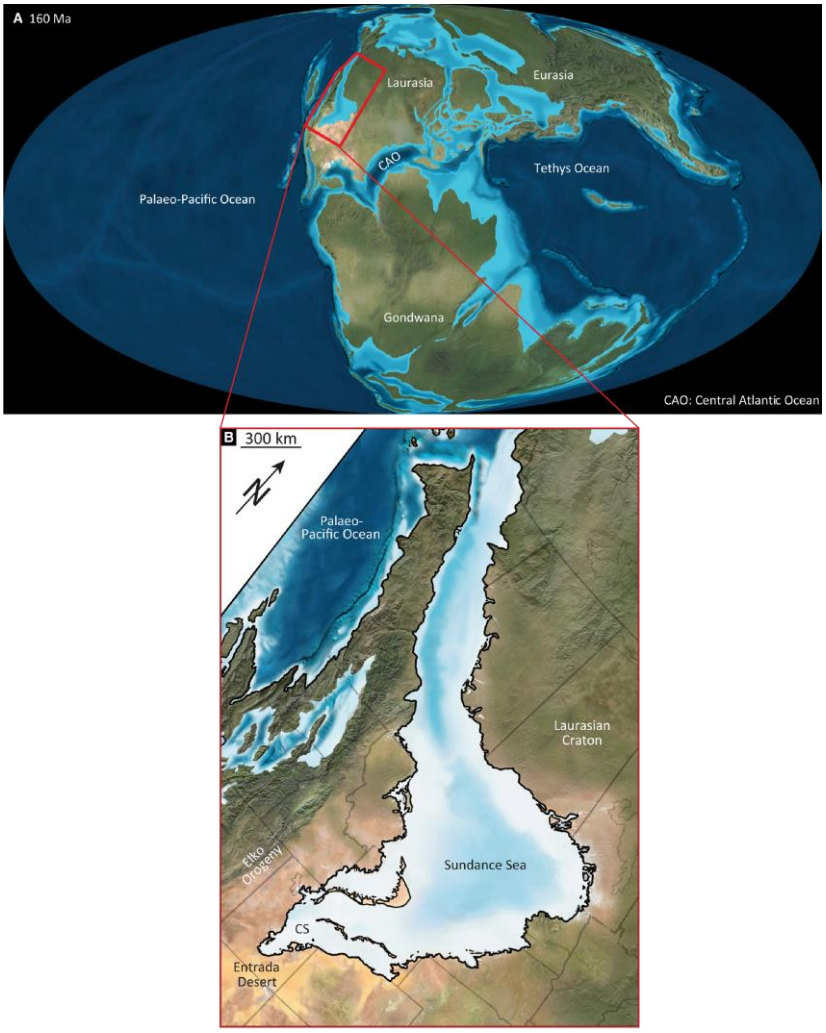

Fig. 2.5: (**A**) Palaeogeographical map depicting the world during the Oxfordian period of the Lower Jurassic, approximately 160 Ma. The red box displays the focused area. (**B**) Close-up palaeogeographical map of the Sundance and Curtis seas and the time when the lower Curtis was deposited (Zuchuat et al., 2018). Modified by Zuchuat et al (2022).

The Curtis Formation is believed to have been deposited during a transgression that inundated the Entrada Sandstone and subsequently altered its sediments. This rework of sediments might be the source of the J-3 unconformity (Pipiringos & O'Sullivan, 1978). Previous studies propose that the Curtis Formation was deposited in near-shore conditions, as well as coastal onlap and shelf sedimentation (Kreisa & Moiola, 1986; Caputo & Pryor, 1991; Zuchuat et al., 2018). A sandy subtidal to intertidal platform developed along the SE margin of an epicontinental sea in east-central Utah (Caputo & Pryor, 1991). During the Middle Callovian (c. 165 Ma), there was a marine transgression that initiated sedimentation in shelf and marginal marine environments of the Curtis-Summerville sea (Fig. 2.5) (Caputo & Pryor, 1991; Zuchuat et al., 2022). During Late Callovian (c. 163 Ma), the interior sea became narrower and more restricted, as opposed to the high-energy, tide-dominated sandflats during the deposition of the Curtis Formation (Caputo & Pryor, 1991). Sediments deposited during this period were muddy, silty, and sandy coastal plain deposits of the sabkha-environment of the Summerville Formation. The Curtis Formation, consisting of shallow marine sediments, has in recent decades been widely acknowledged to have been influenced by tidal forces, resulting in the formation of heterolithic strata (Kreisa & Moiola, 1986; Caputo & Pryor, 1991; Zuchuat et al., 2018). The limited presence of wave-related structures in the Curtis Formation might be attributed to the protective nature of the Curtis Sea, which was sheltered by its elongated basin configuration (Yoshida et al., 2007). Findings from Zuchuat et al. (2018) concluded that the oldest sediments of the Curtis Formation date back to the earliest flooding of the Entrada Sandstone. As the transgression went on, the heterolithic facies were deposited in a quieter environment. This area signifies a distal region of the Curtis Sea, influenced by tidal processes. Thereafter, there was a regression, as the Curtis Sea retreated rapidly. This lead to the deposits of dry eolian dunes, as well as a supratidal flat (Zuchuat et al., 2019).

Zuchuat et al (2018) divided the Curtis formation into three sub-units: lower Curtis, middle Curtis, and upper Curtis. Lower Curtis, at the base of the J-3 unconformity, consist of upper shoreface to beach deposits, mud-dominated and sand-dominated heterolithic subtidal flat, sand-rich sub- to supratidal flat and tidal channel infill (Zuchuat et al., 2018). Middle Curtis contains deposits from sub- to intertidal channel-dune-flat complex. Upper Curtis consists of heterolithic deposits from sub- to intertidal flat, as well as coastal dry eolian dunes that belong to the Moab Member of the Curtis Formation. The Moab Member is only recorded towards the border of Utah and Colorado (Zuchuat et al., 2018) and is therefore not relevant for this thesis.

Based on Zuchuat et al. (2019), the Jurassic Curtis Sea in the Utah-Idaho Trough foreland basin does not coincide with the typical modern tide-dominated and tide-influenced basins. In the case of the Curtis Sea, there have occurred several continuous aridity episodes. This has led to the starvation of the perennial fluvial input in the basin where the Curtis Formation was deposited (Zuchuat et al., 2019). Because of the elongated morphology of the shallow Curtis Sea and the semi-enclosed nature of the basin, wave energy has not been a significant contributor to the sediments deposited (Zuchuat et al., 2019). The biggest impacts has been tidal forces, resulting in intricate distribution of heterolithic deposits (Zuchuat et al., 2019).

3.0 Theoretical background

In the following subchapters, volcanic and sedimentological terms and concepts that will be used during this thesis will be explained. Firstly, Subchapter 3.1 will explain volcanic plumbing systems. Secondly, Subchapter 3.2 will go into detail on sill emplacement mechanisms. Lastly, Subchapter 3.3 will explain concepts and typical sediments deposited in tidal depositional systems.

3.1 Volcanic plumbing systems

Sills have been a hot topic for many decades (Galland et al., 2018; Jerram & Bryan, 2015; Magee et al., 2016; Schofield et al., 2012). In the last two decades, however, research regarding the existence of sills worldwide and their significance has increased.

To understand how igneous intrusions and volcanic processes work, one must first understand volcanic plumbing systems. Volcanoes are underlain by such volcanic plumbing systems, and they are the mechanism by which magma is transported from the Earth's mantle and crust towards the surface (Tibaldi, 2015). A large portion of the magma never reaches the surface and later becomes solidified in the Earth as magmatic intrusions (Tibaldi, 2015). What used to be understood as a simple balloon and stick-type model of magma chambers, is now widely accepted as a much more complex system (Jerram & Bryan, 2015). Volcanic plumbing systems are common in an abundance of sedimentary basins worldwide, where sills, dykes and laccoliths are crucial components. It is widely accepted that such systems are common in rifted basins and at passive margins, and associated with flood basalt emplacement and large igneous provinces (Hutton, 2009; Jerram & Bryan, 2015; Magee et al., 2016, 2019; Spacapan et al., 2017; Kjenes et al., 2022). However, the Mussentuchit

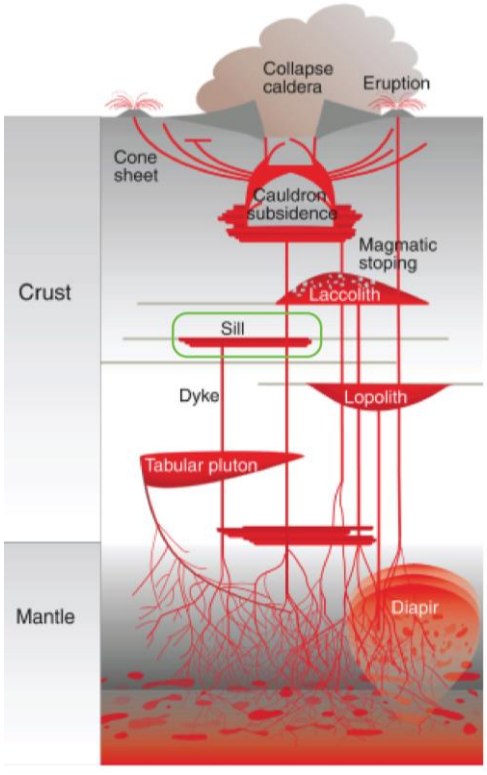

Fig. 3.1: Schematic sketch of volcanic plumbing systems. The figure depicts the network of magma transportation and storage chambers. The green box displays a sill. Modified from Burchardt (2018).

Wash Sill is not related to either category, but rather with intraplate volcanism along the transition zone of the Basin and Range Province and the Colorado Plateau (Delaney & Gartner, 1997), as described in Subchapter 2.1.4. Intraplate volcanism is volcanism unrelated to plate margins, e.g., the Hawaiian Islands. It is assumed that intraplate volcanism is associated with mantle convection underneath the lithospheric plates, where the pressure leads to melting and volcanism, however, intraplate volcanism is not very well understood (Turcotte & Oxburgh, 1978).

Magma moves through the crust through dykes, sills, and other magma chambers (Fig. 3.1). These can be heavily inclined or lateral, and Jerram and Bryan (2015) propose that intrusive sheets can be sorted into three categories based on the relationship between the host rocks and the intrusions: vertical to steep-dipping dykes, inclined sheets, and sills. Dykes are vertical pathways for magma transport that typically range in widths of meters to a few tens of meters. Sills, which are horizontal pathways for magma transport can extend over tens of kilometers (Jerram & Bryan, 2015). A classic text-book example of sills is near tabular sheet intrusions that follow the sedimentary strata that the sills are emplaced within. However, sills are not as planar as the classic text-book example. They can exhibit several different sill emplacement structures such as steps, bridges, and transgressive segments that will be discussed in the subchapters below. Sills are commonly found in sedimentary strata where they mostly correspond to with the layering of the host rock (Galland et al., 2018), and if the strata that the sill propagate into gets deformed, sills can appear inclined or even vertical.

3.2 Sill emplacement mechanisms

Emplacement structures of igneous intrusions such as sills and dykes have been studied in detail in several studies (Pollard, 1973; Pollard et al., 1975; Nicholson & Pollard, 1985; Hutton, 2009; Schofield et al., 2012). Nevertheless, much of the published studies on brittle structures have been centered around dykes (Rickwood, 1990). Sills can be classified in different categories based on the degree of concordance to the layering of the host rock. The classification is predominantly based on seismic data of sill complexes (Planke et al., 2005; Jackson et al., 2013): (A) Strata-concordant sills correspond to continuous sheets that are following the layers of the host rock (Fig. 3.2A), (B) Transgressive sills are sheets that move onto higher stratigraphical levels with an oblique angle to the layers of the host rock (transgressive sills can also be stepwise transgressive, meaning that they move in a manner that

is similar to a stairway (Fig. 3.2B-C)), (D) Saucer-shaped sills are approximately symmetric to strata-concordant sills in the middle, and similar to transgressive sills on the sides (Fig. 3.2D), and (E) V-shaped intrusions resemble saucer-shaped sills, however, the inner part of the sill is substantially smaller. They tend to occur in the shallow crust (Fig. 3.2E) (e.g. (Schofield et al., 2010). Hybrid sills also exist, and display a mix of the characteristics of transgressive, saucer-shaped, and V-shaped intrusions.

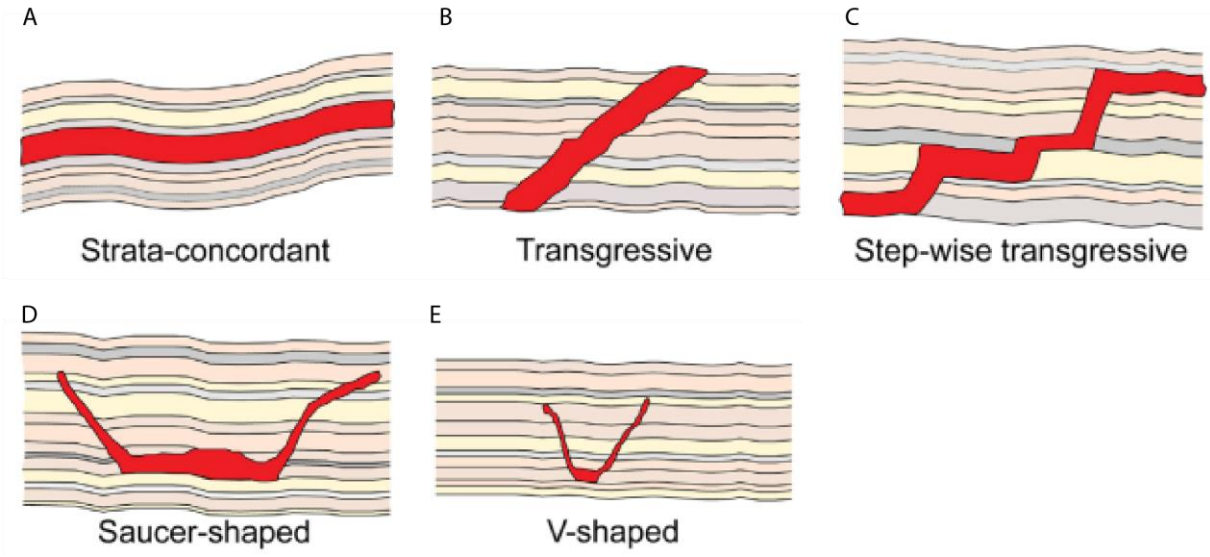

Fig. 3.2: Schematic illustrations depicting different shapes and the morphologies of sill intrusions. (**A**) strata concordant. (**B**) transgressive. (**C**) stepwise transgressive. (**D**) saucer shaped. (**E**) V-shaped. Modified from Galland et al. (2018).

It is crucial to understand the feeder-to-sill relationship so that one may make sense of how sills are formed and emplaced. Unfortunately, there are few outcrops large enough to understand linkage between different igneous elements (sill-sill, dyke-sill, sill-dyke) that can be studied in the field (Galland et al., 2018). This is why seismic imaging has been the primary source of the study of sill complexes. However, seismic imaging is not suitable for studying dyke-to-sill relationship, because seismic imaging is designed for displaying sub-horizontal structures (Galland et al., 2018). However, a few studies, such as the one by Eide, Schofield, et al. (2016) in Jameson Land, East Greenland has shown an example of a field observation of dykes feeding sills. Sills can also feed sills, and there are several examples in Greenland, where sills are connected in a network through inclined sheets (Fig. 3.3).

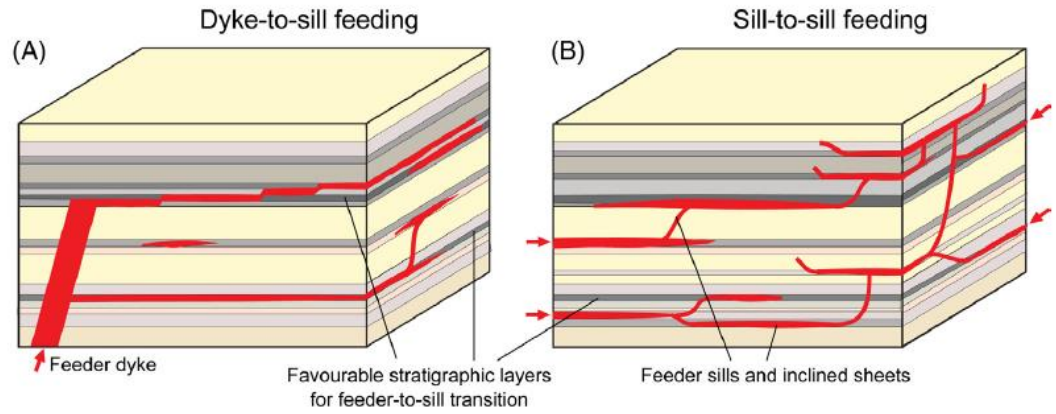

Fig. 3.3: (**A**) Illustrative drawings of a dyke feeding sills. (**B**) Illustrative drawing depicting sills feeding sills through inclined sheets. Modified from Galland et al. (2018).

Host rock cohesion strongly controls architecture of sills, evidenced by the fact that thick sills commonly occur in weakly cohesive materials *and vice versa* (Schmiedel et al., 2017). Brittle Coulomb properties of the Earth, which refer to the shear strength of rocks under varying stresses, might play a significant role in magma emplacement and propagation. This is evidenced by inelastic deformation of the layers above saucer-shaped, planar and cone-shaped sills (Haug et al., 2018). Rigidity in layers above sills also affect the magma emplacement, evidenced by sills being more likely to develop when the upper layer is more rigid than the lower layer (Kavanagh et al., 2006). Gill and Walker (2020) propose that the depth of emplacement, as well as magnitude of tectonic stress, can significantly influence the development of sills. In previous decades, there has been a classic model for sill emplacement arguing that magma spreads out horizontally along its level of neutral buoyancy (Francis, 1982). This model has been widely accepted for decades, however, several arguments in recent years have challenged this statement (Vigneresse & Clemens, 2000; Thomson & Schofield, 2008).

In recent decades, there have been many studies which have been focusing on the lithology of the host rock when discussing the emplacement of sills, however, the majority is focused on emplacement in mudstone (Eide, Schofield, et al., 2016; Mark et al., 2018; Eide et al., 2021). This stems from the fact that shales tend to undergo ductile deformation more easily than other lithologies, and that mudstones commonly have a prominent lamination (and how tensile strength normal to this lamination (Q. Gao et al., 2015) that makes it much easier for sill-related fractures to develop between bedding planes of these mudstones (Eide et al., 2021). The most common host rock for sill emplacement in the Faroe-Shetland Basin is claystone and shale,

evidenced by 245 of 251 total intrusions that were emplaced into claystone and shale (Mark et al., 2018). Furthermore, in deeply emplaced sill complexes in Jameson Land, East Greenland, sills favored mudstones. They were also taking advantage of discontinuities between strong and weak layers. The sill seemed to avoid homogenous, well cemented sandstone units (Eide, Schofield, et al., 2016).

3.2.1 Sill emplacement structures formed by brittle fracturing

What seems to be the most important factor for the architecture of sills is the mechanical strength of the host rock at the time of intrusion, and whether it reacts in a brittle or non-brittle manner (Schofield et al., 2012). In clastic rocks, the most important factor determining this is the degree of consolidation and cementation (Duffield et al., 1986). The emplacement mechanisms of sills have long been regarded as a result of brittle fracturing (Pollard, 1973), however, studies from Schofield et al. (2012) investigated the emplacement mechanisms in non-brittle processes. Findings of this study demonstrate that brittle and non-brittle sill emplacement exhibit different geometries, and therefore also propagation history. The propagation history during brittle emplacement involves initial fractures that occur due to the intrusion, as well as reactivation of pre-existing fractures. However, during non-brittle emplacement, ductile flow of the host rock might preserve some of the ductile interaction (Schofield et al., 2012).

The development of steps is common during emplacements of sills, first named by Rickwood (1990). Steps occur when the intruding sill changes the level between two sedimentary layers by either bending or stepping up or down. The result might resemble a step-stair morphology in a cross-section (Fig. 3.4A). Schofield et al. (2012) suggests that the morphology of the steps depends on the exploitation of preferential horizons. It can either have an en echelon step-stair morphology or an inconsistent up and down step morphology. Steps can form in two ways: 1) by utilizing horizons with slight offset and no overlap, or 2) by the creation of stepped fractures (en echelon fractures), which eventually will become one sheet, often due to magma inflation (Pollard, 1973; Schofield et al., 2012; Kjenes et al., 2022).

Bridging in sill emplacement structures happens when the sills are occupying different levels of the sedimentary strata they are intruding in (Fig. 3.4B) (Hutton, 2009), and was first described by Farmin (1941). The term “bridge” in igneous context, however, was first adopted by Delaney and Pollard (1981). These levels will overlap, and because of this, strata between

them will bend due to inflation. This bending causes longitudinal extension along the curved surfaces and contraction along the concave surface of the bridge (Fig. 3.4B) (Schofield et al., 2012). This continued inflation of the intrusive segments will increase the tensile stress within the bridge, and eventually, it becomes too much for the surrounding rock to bear. As a result, the bridge undergoes brittle failure, forming a broken bridge (Hutton, 2009).

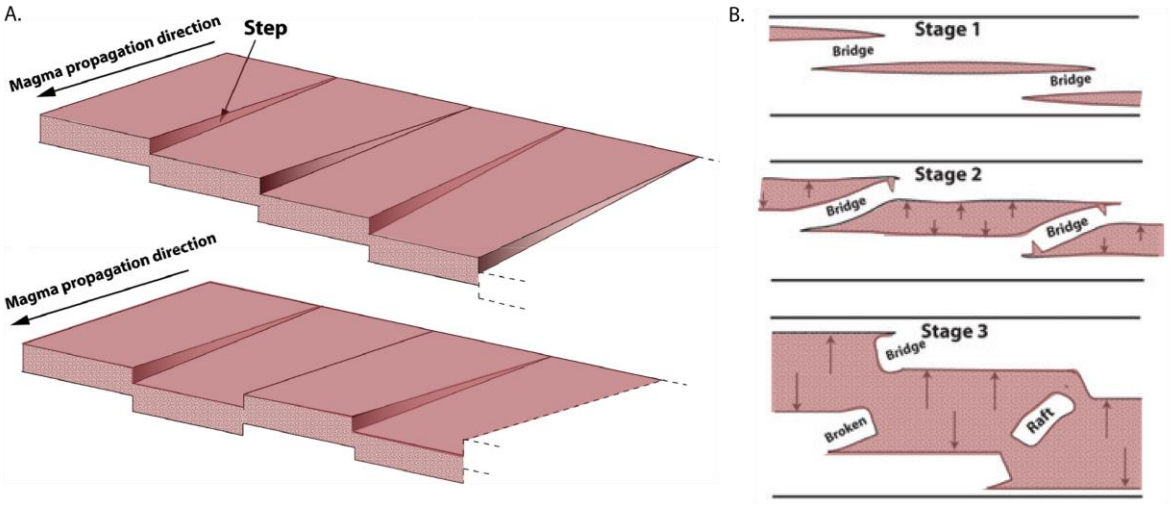

Fig. 3.4: (**A**) Schematic drawing depicting the development of en echelon steps within a sill. Depicting two step-developments: one where all trend in one direction, and another where stepping is in different directions. (**B**) Schematic drawing illustrating the development of broken bridges in different steps. Modified from Schofield et al (2012).

3.2.2 Magma finger emplacement in non-brittle processes

There are also emplacement structures in non-brittle processes, such as development of magma fingers. These tend to occur in host rocks with low rate of cohesion and mechanical strength, such as uncemented sediments (Pollard et al., 1975; Schofield et al., 2012). Important aspects of magma finger development are the viscosity of both the host rock and the magma, as well as how ductile deformation can promote magma finger formation. This type of emplacement in non-brittle processes is not relevant for this study and will therefore not be focused on later in the thesis.

3.3 Tidal depositional systems

As the host rock consists of the tidal deposits of the Curtis Formation, and tidal depositional features create important heterogeneities in the host rocks that may affect sill propagation and emplacement, an introduction to tidal depositional systems and tidal deposits is presented here.

Tides are regular variations in water level cause by the gravitational interaction between the moon and the sun (Dalrymple, 1992). Tides normally have a diurnal cycle (daily cycle) due to the Earth's rotation that gives high tides and low tides two times a day (Fig. 3.3a). As a consequence, this leads to the flow of water in and out during the day as the tides shift, as well as periods of slackwater and stillness between high tide and low tide. This is evident from the sediments, where bidirectional sedimentary structures are deposited by flowing water during low tide, and mud drapes when there is slackwater (van Straaten, 1954; Reineck & Wunderlich, 1968; Dalrymple, 1992). Tides also have neap-spring-cycles that are predominately due to the moon's rotation around the Earth. This results in stronger high tides called spring tides, and weaker low tides called neap tides every two weeks (Fig. 3.3a) (Dalrymple, 1992). This is often visible in deposits such as cross-stratification with mudstone drapes foresets (Fig. 3.3b). Weather and variation in water flow in rivers can also affect water levels and streams, which means that the sedimentary successions will not display a record of a perfect tidal cycle.

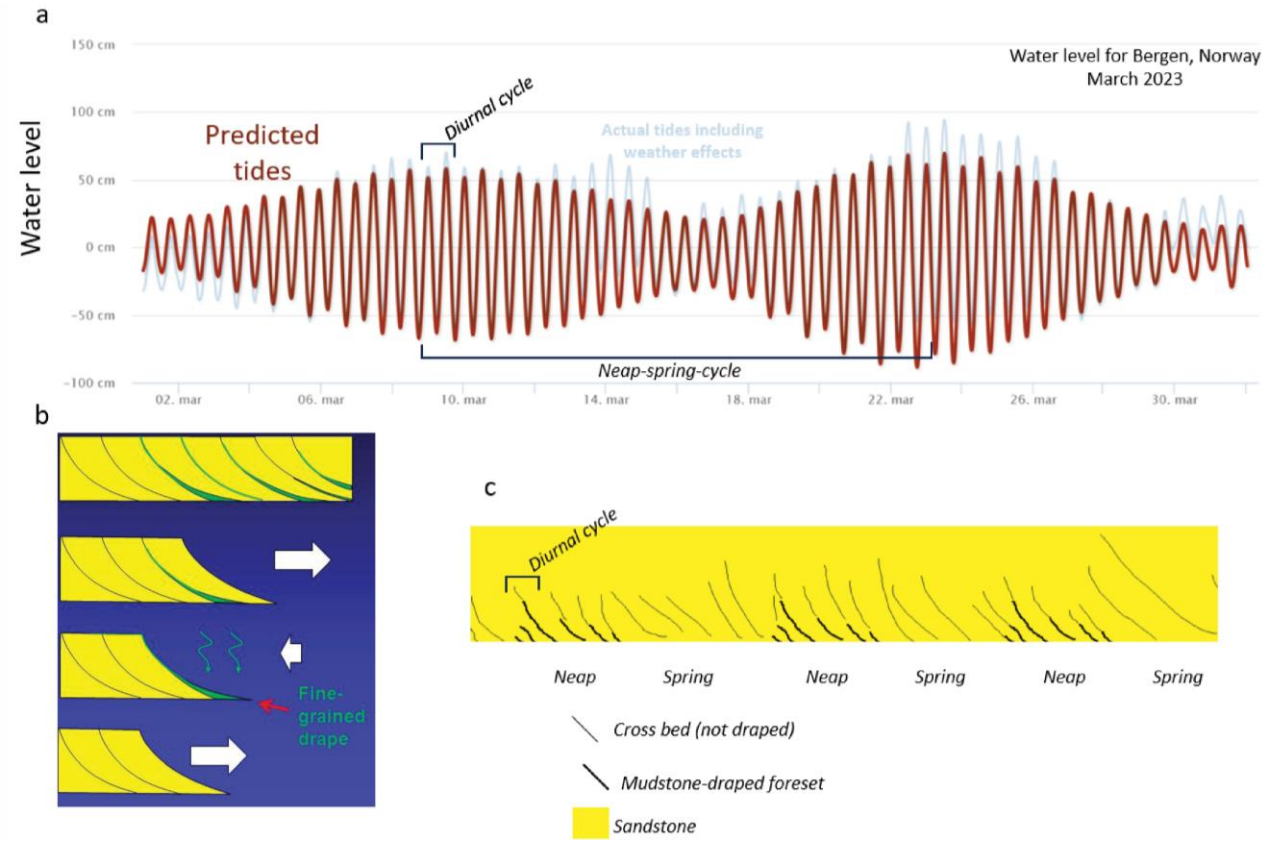

Fig. 3.5: (**a**) Water levels for Bergen, Norway, March 2023 displaying neap-spring cycles. (**b**) Formation of mudstone-draped foresets during slackwater, and crossbedding during low tides. (**c**) Schematic drawing of spring and neap cycles with and without mudstone-draped foresets. Water levels and predicted tides are from Kartverket's ocean levels data (2023).

Tidal flats are important depositional environments that are found on coasts worldwide, where they represent a crucial part of coastal wetlands (S. Gao, 2019). Tidal flats consist of three different zones based on the tidal water levels: subtidal zone, intertidal zone, and supratidal zone (Amos, 1995). The subtidal zone is located below the low water and is almost constantly covered with water. The intertidal zone is located between high and low water and is flooded regularly during the diurnal tidal cycles. The supratidal zone is for the most part not covered with water and is located over the high water and only under extreme circumstances will it be covered with water (Amos, 1995). The formation of tidal flats depends on the supply of fine-grained sediments, such as clay, silt, and very fine-grained sand, in addition to tides and tidal forces being the dominant depositional process (tides, waves, rivers) acting on the shoreline (Galloway, 1975). It is common to differentiate coasts based on tidal range, as this has key controls on the architecture of depositional systems (Dalrymple, 1992; Nyberg & Howell, 2016): microtidal, 2 m; mesotidal, 2-4 m; macrotidal, >4 m. Tidal currents are strongest under mesotidal and macrotidal conditions, compared to under microtidal conditions (S. Gao, 2019). In addition to the tidal range, the tidal cycle also plays a big part in the strength of the tidal currents, where tidal currents are stronger in semidiurnal areas than diurnal (once a day) areas (Dalrymple, 1992).

A typical facies model for an intertidal flat is displaying a “fining-upward sequence” (Fig. 3.6) (Klein, 1985). The sediments range from clays and silts deposited in the upper part of the flat, and sands, deposited in the lower and middle part of the flat. This leads to the vertical distribution in tidal flats (Fig. 3.6) (S. Gao, 2019). The general order from the supratidal zone to the subtidal zone, one can find salt marshes, mudflats, mixed sand-mud flats, and sand flats (Reineck & Singh, 1980). On salt marshes, the sediments are at their finest, and it is common to find organic matter from plants for example. The mudflats usually consist of clay and silt, which is plausible because the mudflat is located between high water levels on springs and neaps (S. Gao, 2019). The deposition of mud and clay occurs because of settling of fine-grained sediments from the water column. On the mixed sand-mud flats, sand is deposited during spring tides, and mud is deposited during neaps (S. Gao, 2019). This section of the tidal flats is associated with alternating deposition of mud in neaps and sand on springs. On the sand flats, well-sorted sands are deposited with different bedforms, such as dunes and ripples. Typical for tidal flat deposits are bidirectional cross-stratification, such as ‘herringbone cross-stratification’. ‘Herringbone cross-stratification’ is successive beds that show opposite paleocurrent directions and are generated by reversing tides, where crossbedding deposited

during flood dip in the opposite direction to those formed almost directly after during ebb tide (van Straaten, 1954).

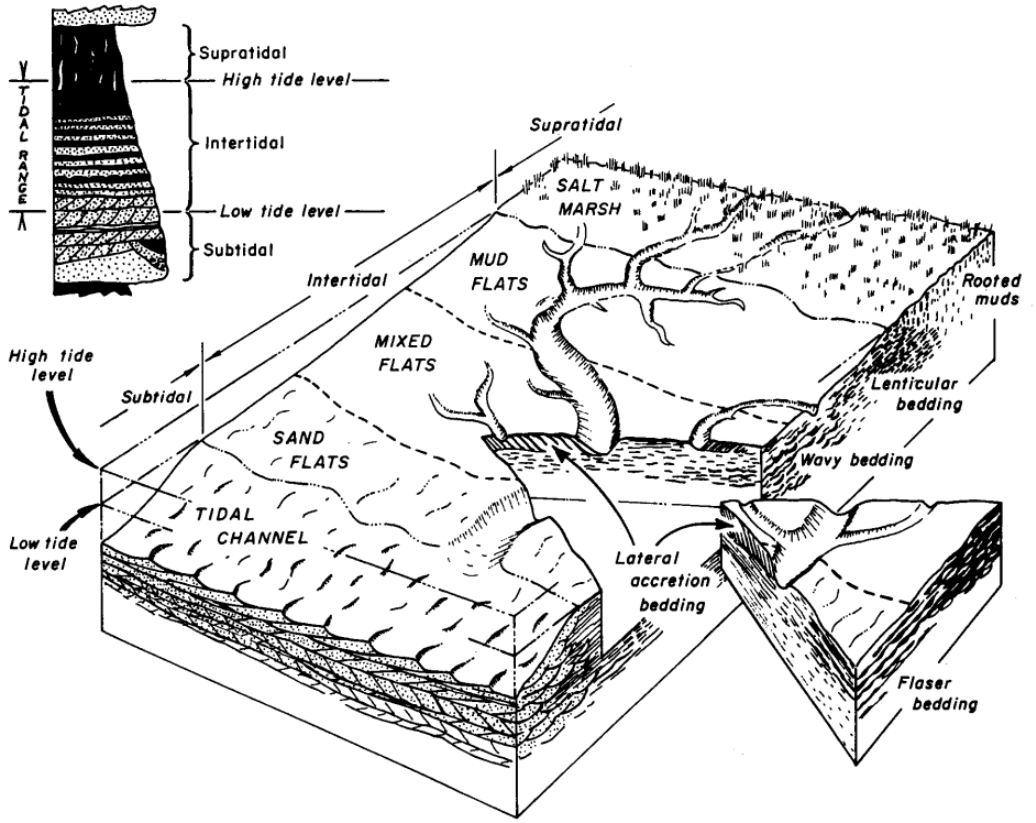

Fig. 3.6: Block diagram of a siliciclastic flat, consisting of a subtidal-, intertidal- and supratidal zone. Tidal channels closest to the sea, then sand flats, mixed flats, mud flats and then a salt marsh closest to land. A typical log for a tidal flat is displayed in the top left corner. Both the log and the diagram display a 'fining upwards sequence'. From Dalrymple 1992.

Tidal channels are also important components of a tidal depositional system as they are the main contributor to moving sediments between the inner and outer regions of the tidal system (Hughes, 2012). They serve as clear pathways for the offshore dispersal of sediments during the ebbing tide. Typical for tidal channels are the bidirectional flow of water, and they are defined by the alternating flow of ebb and flood currents. Tidal channels can either be intertidal, which means that they dry out or have standing water in the deepest parts during low tide), or they can be peri-subtidal, (Hughes, 2012). Tidal channels tend to be widest near the ocean, and narrower closer to land (Fig. 3.6). This is the opposite of fluvial systems. However, like fluvial channels, tidal channels have a diverse morphology. The channels can be straight, meandering, or dendritic for example. The most common type of channel on tidal flats are dendritic channel networks (Hughes, 2012).

Typical deposits in tidal flats are flaser bedding, wavy bedding and lenticular bedding, first classified by Reineck and Wunderlich (1968). The bedding consists of ripples interbedded with mud. Flaser bedding is characterized by layers of sand and discontinuous mud deposited on preexisting sand ripples (Fig. 3.7) Flaser bedding can be subdivided into simple flaser bedding and wavy flaser bedding, where mud is draping the troughs of the ripples (Reineck & Wunderlich, 1968). Wavy bedding is when the layers of mud has overlain both the ripple crests and in the ripple troughs displaying a wavy morphology (Reineck & Wunderlich, 1968). In lenticular bedding, mud dominates, and sand lenses are discontinuous. Lenticular bedding can be subdivided into lenticular bedding with connected lenses (<75% discontinuous lenses), and lenticular bedding with single lenses (>75% discontinuous lenses) (Reineck & Wunderlich, 1968). The origin of flaser, wavy and lenticular bedding is associated with alternating currents or wave action (Reineck, 1967). Under fast-moving water during rapid flow, the sand deposition generates ripples, whereas mud is deposited on top of the ripples in quieter times when there is slack water (Reineck & Wunderlich, 1968). Environments with such alternating currents have long been associated with tidal depositional systems. Although these conditions are not exclusive to tidal systems, fundamental studies from the last 70 years support this claim (Reineck, 1967; Reineck & Wunderlich, 1968; Terwindt & Breusers, 1972; van Straaten, 1954).

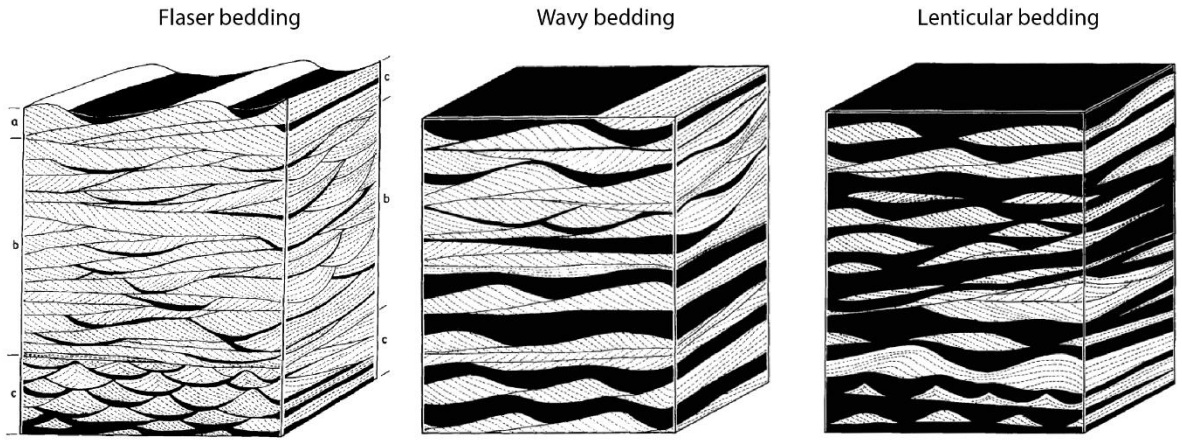

Fig. 3.7: Schematic representation of flaser-, wavy-, and lenticular bedding deposits. Modified from Reineck & Wunderlich (1968).

4.0 Data and methodology

The purpose of this chapter is to give the reader an understanding of the data acquired, and the methods utilized both in the field and in the computer lab, together with understanding the process of proceeding from outcrop to a 3D-model. This subchapter provides an overview of where the sedimentological logs were obtained from (Fig. 4.1) as well as an overview of the generated virtual outcrop models in the Mussentuchit Wash (Fig. 4.2).

4.1 Field work and data acquisition

4.1.1 Sedimentological field work

The data collected for this thesis are based on outcrop data acquisition from two different field seasons in Utah, USA. I was personally a part of one of the field seasons, during a 1-week-period in May 2022, where data types such as sedimentological logs and photos of the contact between the sill and the Curtis Formation were obtained. The other field season was conducted by Martin Kjenes and Nick Schofield in 2019, and this part led to the acquisition of photos for the 3D-models. The data were obtained through sedimentological field work and by an Unmanned Aerial Vehicle (UAV) or more informally, a *drone*. The drone photos were collected with the aim of building several 3D virtual outcrop models (VOMs) from photogrammetry of six accessible bends in the meandering canyon system Mussentuchit Wash. Two outcrops were studied to make two detailed sedimentological logs, which are visible in two of the virtual outcrop models created (Fig. 4.1).

The sedimentological fieldwork conducted included logging and photographing of the sill/host rock-boundary along with sedimentary structures. One log is from 3 South Swing and the other from 4 North Swing (Fig. 4.1). In total, 22.2 meters were logged, 8 m in 3 South Swing and 14.2 m in 4 North Swing. The data collected includes bed thickness, grain size, color, and sedimentary structures. Most of the outcrops were easily accessed by some hiking and walking, but a few of the bends were not possible to reach on foot. The focus was to map the boundary between the Mussentuchit Wash Sill and the Curtis Formation, examining if the intrusion followed any specific sedimentary layers or boundaries. The logging was carried out to provide an understanding of the sedimentology of the host rock where the magmatic intrusion occurred. The field equipment utilized for logging was measuring tape, compass, geological hammer,

mobile camera, and grain size chart. The logs were made on millimeter paper, with a scale of 1:25. They were later digitized and made into two continuous logs in Adobe Illustrator. The outcrops were easily accessed within 2 km from a location accessible by car (Fig. 1.1). From the twelve facies descriptions, four facies associations were determined for the study area. Facies and facies associations are presented in Chapter 5 (Results).

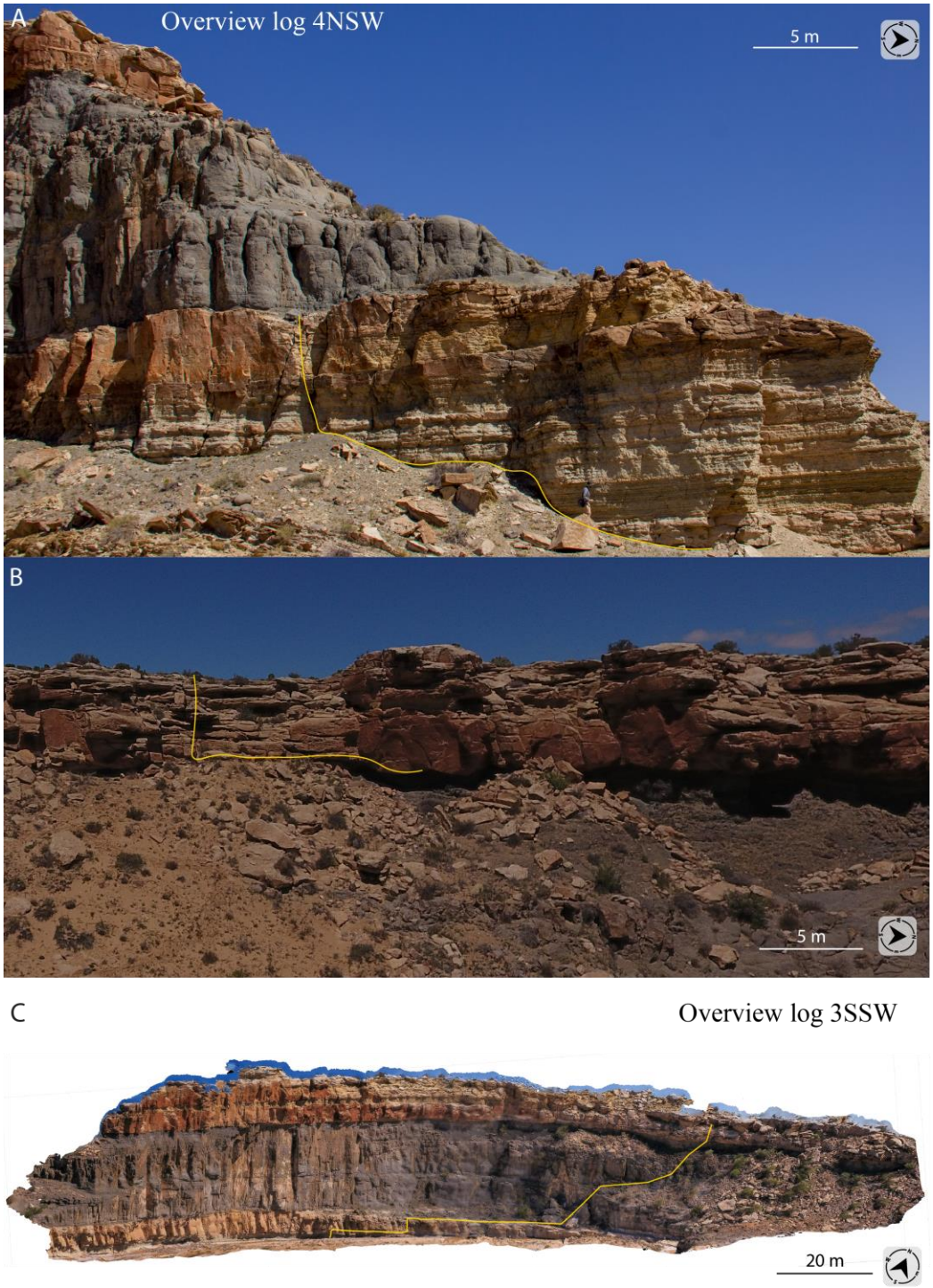

Fig. 4.1: Overview of the sedimentological logging. (**A**) Bottom log of 4 North Swing (4NSW) up to the sill. (**B**) Top log of 4 North Swing above the sill. (**C**) Sedimentological log of 3 South Swing (3SSW).

4.1.2 Drone/UAV/Outcrop mapping

Utah presents an exceptional opportunity for sedimentological research due to its favorable conditions. The region offers extensive exposure of geological formations, minimal vegetation cover, and consequently, convenient accessibility. However, many outcrops are of substantial size and may ultimately prove to be less accessible. For instance, the Mussentuchit Wash Sill has an average thickness of c. 15 meters across the entire study area, with a maximum thickness of 17 m. This makes it impractical to access the upper contact boundary between the sill and the Curtis Formation by foot. In addition, there are an abundance of scree slopes and areas that are difficult to reach by foot due to safety concerns. In such cases, photogrammetric techniques prove to be advantageous, offering both cost and time-efficiency for inaccessible outcrops. The only criteria for acquisition of 3D-data through these techniques, apart from a digital camera (such as a drone), is access to convenient software that can use the photos and make them into a virtual outcrop model (Bemis et al., 2014). Photogrammetry also presents the advantage of enabling researchers to revisit the outcrops and conduct more detailed studies, particularly when field time is limited, or the study area is too substantial to cover in one field season.

The aerial photographing by the UAV in this study was performed by Martin Kjenes and Nick Schofield in 2019 using a 'DJI Phantom 4' drone with a 35 mm lens that resulted in 362 photos. The photos were taken by manually flying the drone at c. 15 m from the outcrop, angling the camera perpendicular to the cliffs of Mussentuchit Wash, and taking photos with an overlap of ca. 60-70% (Kjenes et al., 2022). The images collected were processed by Kjenes to make a large-scale model with a resolution of 1.06-1.67 cm/pixel. For this thesis, I reprocessed these data into six new high-resolution 3D-models that will be used to assess propagation mechanisms for the sill. The workflow for these processing steps is presented in Fig. 4.3. The resulting models (Wavefront OBJ-files) were analyzed and interpreted in a software called LIME (Buckley et al., 2019). The interpretation made in LIME was made by outlining the sill/Curtis Formation-boundary, as well as other important lithological and stratigraphic boundaries (such as Entrada Sandstone/Curtis Formation-boundary).

4.2 3D Outcrop Modeling

Agisoft Metashape is a software product that performs photogrammetric processing of digital images and generates 3D spatial data (Agisoft Metashape, 2023). The photos from the drone were imported to Metashape, and several steps are needed to make a virtual outcrop model.

Processing steps include aligning of photos, editing and decimation of the point-cloud, triangulation of the points in order to build a topographic model (triangle mesh), and texturing of the model with the preferred images (Agisoft, 2023) (Fig. 4.3). This resulted in six 3D-models with ground pixel resolution ranging from 0.74 to 1.97 cm per pixel. The version used in the making of this thesis is Agisoft Metashape Professional version 1.7.3 build 12426 (64 bit) from 2021. A workflow of generating the 3D models is attached below (Fig. 4.3).

4.2.1 Aligning images

After selecting photos from the UAV, the photos need to be aligned, in order to get a defined amount of tie points between overlapping the photos. This was done with high accuracy, a key point limit of 20,000 and tie point limit to ”zero”. The camera position and orientation were found for each photo.

4.2.2 Build dense cloud

The next step is to build a dense cloud. This is done by using the aligned photos from the previous step. The quality was set to “high”, and the depth filtering to “mild”. When the depth filtering is set to mild, it makes small details visible in the model. This step calculates depth information for each camera to make a single dense point cloud. After the dense cloud is built, it resembles the actual outcrop.

4.2.3 Build mesh

By using the dense cloud as source data, a 3D polygonal mesh model was built. The mesh models were created with enabled interpolation, which automatically fills possible holes in the model, arbitrary surface type and a high face count. The polygonal mesh generates the shape of a polyhedral object, such as a virtual outcrop model.

4.2.4 Build texture

The final step in the making of the 3D-models is to build textures of the mesh models. Texture was added from diffuse maps, using images as source data, a generic mapping mode, mosaic blending and texture size 4096 px. After the 3D-models were created, the final step was to export the Wavefront OBJ-files to LIME.

4.2.5 Sources of error

Errors are highly important to be aware of when using software like these. By using Agisoft's gradual selection tool for reprojection error, reconstruction uncertainty and projection accuracy, they have been accounted for. The gradual selection tool filters out and removes points representing high amount of noise, which can be useful to eliminate. The reprojection error of the models ranged between 0.454-0.735 pixel. The technical details of all the processed virtual outcrop models are attached in Appendix I.

4.3 Interpretation in Lime and Adobe Illustrator

LIME (Lidar Interpretation and Manipulation Environment) is a software that is used for 3D viewing of models acquired using lidar, photogrammetry and other spatial measurements techniques, such as drone photos. It is developed by the Virtual Outcrop Geology Group (VOG) (Buckley et al., 2019). This software is used to interpret the 3D-models and measure geological features using line interpretation. LIME provides therefore a great way of mapping and representing outcrop 3D-models, which makes it possible to trace facies association across the outcrop. It also allows for display of level-of-detail photo-textured models, allowing scalable level-of-detail rendering of large-area terrain data (Buckley et al., 2019). The version used in this thesis is the LIME version 2.3.2 built January 28th, 2022.

Adobe Illustrator is a vector graphics editor and design software made by Adobe Inc., used to create drawings, illustrations, and figures. The use of Illustrator in this thesis has been to compose figures and show more detailed facies and sedimentary structures, because Illustrator is more suitable for drawing detailed sedimentological features on the outcrops. Screenshots were then taken in LIME in an orthographic projection and exported as a png-file, which was finally pasted onto an artboard in Adobe Illustrator. The geological units were filled with color, and the boundaries were marked. The version used in this thesis is the Adobe Illustrator version 26.5.1 (64-bit) from 2022.

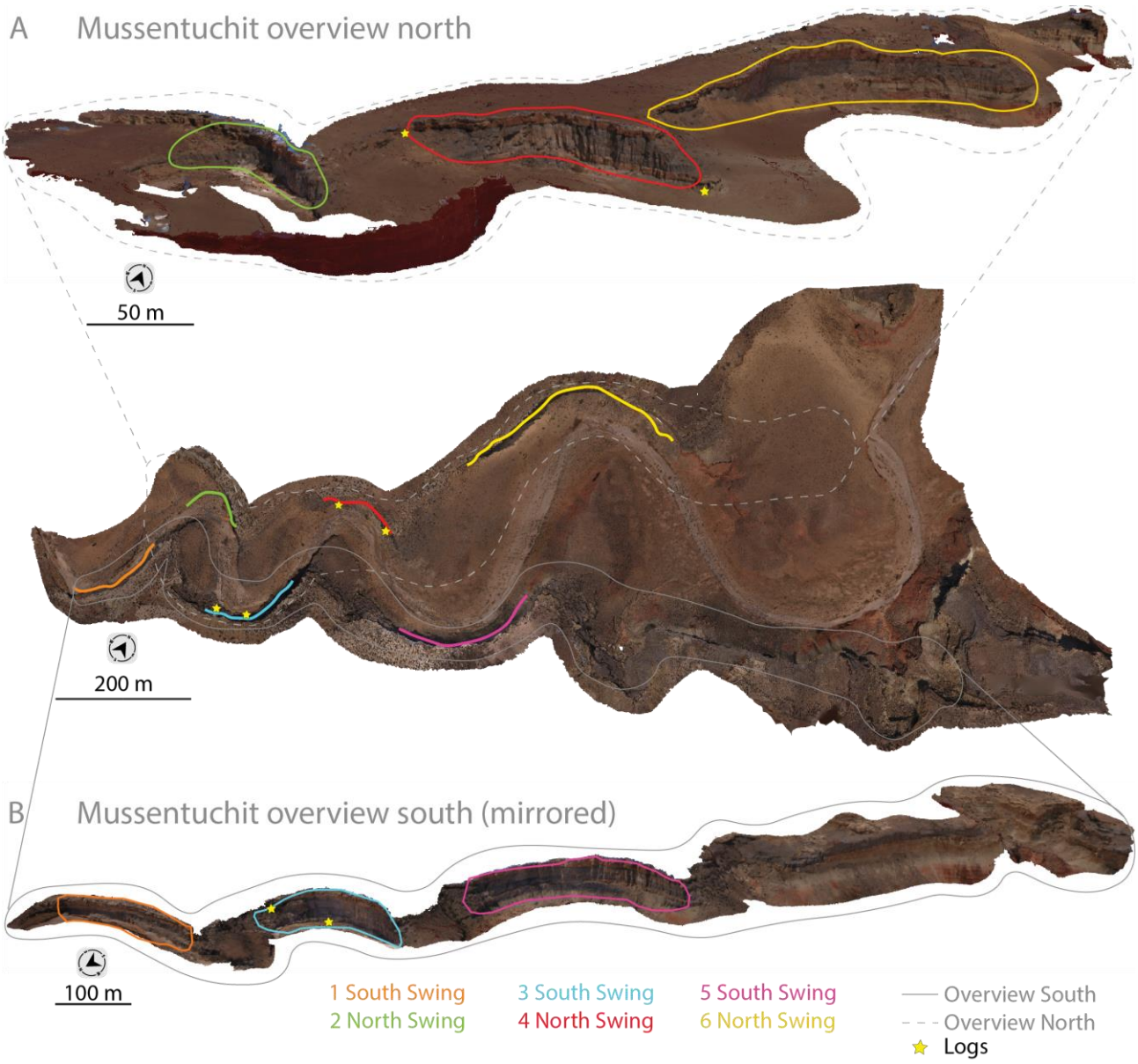

Fig. 4.2: Overview of the processed 3D models from Agisoft Metashape. (**A**) Overview of the models in the north side of the Mussentuchit Wash. (**B**) Overview of the models in the south side of the Mussentuchit Wash.

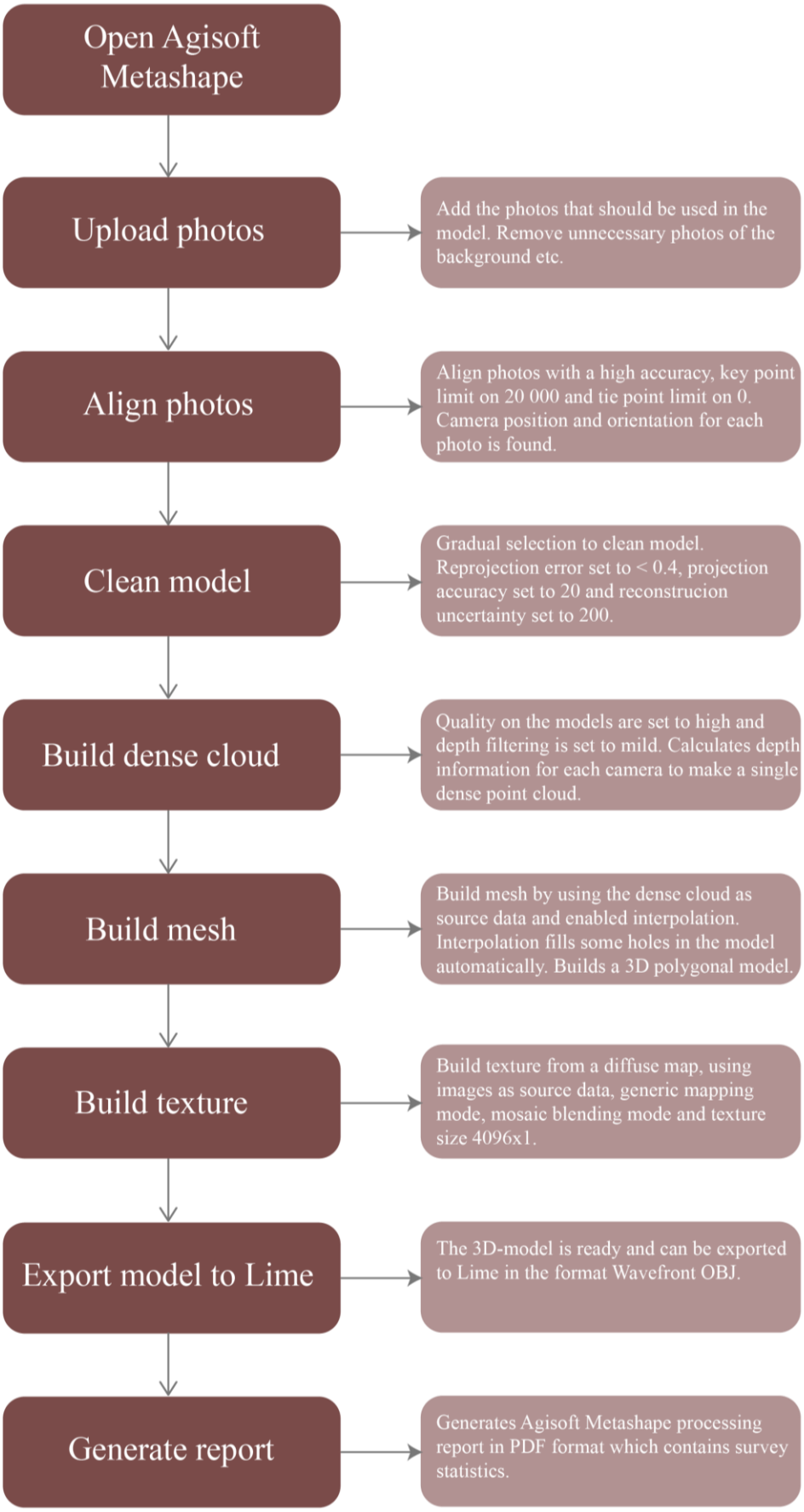

Fig. 4.3: Workflow of developing the virtual outcrop models (VOMs) using Agisoft Metashape.

5.0 Results

The purpose of this chapter is to present the new observations from the tidal depositional system of the outcrop in the Mussentuchit Wash, in both small scale and large scale, as well as observations from the Mussentuchit Wash Sill. Subchapters 5.1 and 5.2 present observations and models for the facies and the facies associations in the study area based on sedimentological logs. Subchapter 5.3 presents results from analysis of the facies associations on a larger scale in the virtual outcrop models, as well as the sedimentary architecture in the entire study area and a coherent model for the sedimentary environment here. Finally, sill geometry on a larger scale as well as the margins will also be presented.

5.1 Facies description

In the study area, twelve sedimentary facies have been identified based on their sedimentary structures, texture, and other distinguishable features. They are present in the sedimentary logs recorded during fieldwork (Fig. 5.10). As the study area is predominately affected by tidal influences, most of the facies consist of heterolithic sandstone and mudstone, as well as various types of sandstone. Table 5.1 lists the different facies as well as giving a brief description of the individual facies. Grain sizes on the sedimentary logs are classified in accordance with Wentworth (Wentworth, 1922).

These facies are determined only based on lithologies and sedimentary structures. This is because there have been no biogenic structures or fossils identified in the deposits that could supplement the facies analysis.

Table 5.1: List of facies in the study area with a brief description of each facies. The facies have been assigned to different facies associations that are described in a subchapter below.

Facies nr.	Lithofacies	Description	Thickness	Process interpretation
F1	Structureless silt with sparse sand laminae	Structureless siltstone with no structures and thin laminae of very fine-grained sand.	0.25 m	Settling of silt and very fine-grained sandstone from suspension
F2	Organic-rich siltstone	Siltstone with very fine-grained sandstone with current ripples and sparse wave ripples. Occasional organic fragments draping the layers.	0.47 m	Low-velocity, reversing currents. Suspension settling of mud and organic fragments during slackwater periods. Occasional wave-agitation in a standing body of water.
F3	Lenticular bedding	Heterolithic silt- and sandstone with lenticular bedding. Common, bidirectional current-ripples, sparse wave-ripples, very fine to fine-grained sandstone lenses within a matrix of laminated gray mudstones.	0.05 - 0.6 m	Reversing currents, with suspension settling of silt in low-velocity currents and rippled sand in higher-velocity currents. Dominance of low-velocity currents.
F4	Wavy bedding	Heterolithic silt- and sandstone with **wavy** bedding. Ripple cross-stratified very fine to fine-grained sand layers, with bidirectional current indicators and interbedded with laminated gray siltstone.	0.03 – 0.5 m	Reversing currents, with suspension settling of silt in low-velocity currents and rippled sand in higher-velocity currents. Equal amounts of deposits from low- and high-velocity currents.
F5	Flaser bedding	Heterolithic silt to very fine-grained sandstone with abundant sets of current ripples and sparse wave ripples and flaser bedding. Little mud content.	0.07 m	Reversing currents, with suspension settling of silt in low-velocity currents and rippled sand in higher-velocity currents. Dominance of high-water velocity.
F6	Silt- and sandstone with current ripples	Heterolithic silt to fine-grained sandstone with scattered bidirectional current ripples.	0.25 - 0.7 m	Reversing currents, with suspension settling of silt in low-velocity currents and rippled sand in higher-velocity currents.

F7	Combined flow rippled sandstone	Fine sand with combined flow ripples	0.25 m	Energy is too high to get preservation of mud. Reversing currents that have later been altered by weak waves.
F8	Wavy sandstone	Medium sandstone with wavy bedding where mud is draped over the layer.	0.1 - 0.25 m	Energy is high enough for transporting sand. Layers of flooding events where mud is deposited.
F9	Rippled sandstone	Sandstone with current ripples dipping E/SE and W/NW and scattered with wave ripples. FU-sequence from very fine sand to silt.	1.05 m	Environment with equal reversing currents. Energy is too high for deposition of mud.
F10	Cross-bedded sandstone	Medium-grained, sandstone beds with cross-bedding and occasional mudstone draped foresets and mud clasts. Sometimes stacked so that successive beds show opposite paleocurrent directions (“herringbone cross stratification”). Occasionally current ripples on basal part of some crossbed foresets/along the entire surface of some crossbeds.	0.25 – 1.25 m	Systematic alternation between flowing and standing water. Turbulent flow depositing cross-bedded sand and mudstone draped foresets deposited during slackwater.
F11	Conglomeratic sandstone	Tangential cross-stratified conglomeratic sandstone with a sub-horizontal erosive base, sub- to rounded clasts, maximum clast diameter 2 cm, unidirectional current trough cross-stratification. No preferred clast-orientation. From coarse- to medium-grained sandstone.	1.25 m	High energy flow in channel base
F12	Plane parallel-stratified sandstone	Plane parallel-stratified sandstone. Mm-scale organic fragments occur on some laminae in this facies.	0.25 m	High-velocity unidirectional current, deposited during rapid flow

5.2 Facies observations

A total of four facies associations (FA) have been identified in the study area, and their properties are presented below. Each facies association (FA) represents a specific depositional environment, which is based on facies with similar and closely linked sedimentary architecture and lithology. The facies associations include:

- FA 1 – Tidal flat facies association
- FA 2 – Prodelta-delta front facies association
- FA 3 – Tidal channel facies association
- FA 4 – Tide influenced fluvial channel facies association

A brief description of each facies association and their sedimentary architecture is given below (Table 5.2). The following subchapters will give the reader a detailed description and interpretation of each individual facies' association. The legend for the sedimentological logs is also attached (Fig. 5.1).

Table 5.2: List of facies associations (FAs) and a brief description of them.

Facies association (FA)	Depositional environment	Facies
FA 1 – Tidal flat facies association	Intertidal heterolithic mud-, silt- vf-grained sandstone, generally upward coarsening from laminated mudstone to wavy bedded sandstone	F1, F2, F3, F4, F5, F6, F7, F8
FA 2 – Prodelta- delta front facies association	Intertidal heterolithic mud-, silt- vf-grained sandstone, generally upward coarsening from laminated mudstone to wavy bedded sandstone	F1, F2, F3, F4, F5, F6, F7, F8
FA 3 – Tidal channel facies association	Tidal channel	F9, F10, F12
FA 4 – Tide influenced fluvial channel	Pebbly, conglomeratic sandstone	F11

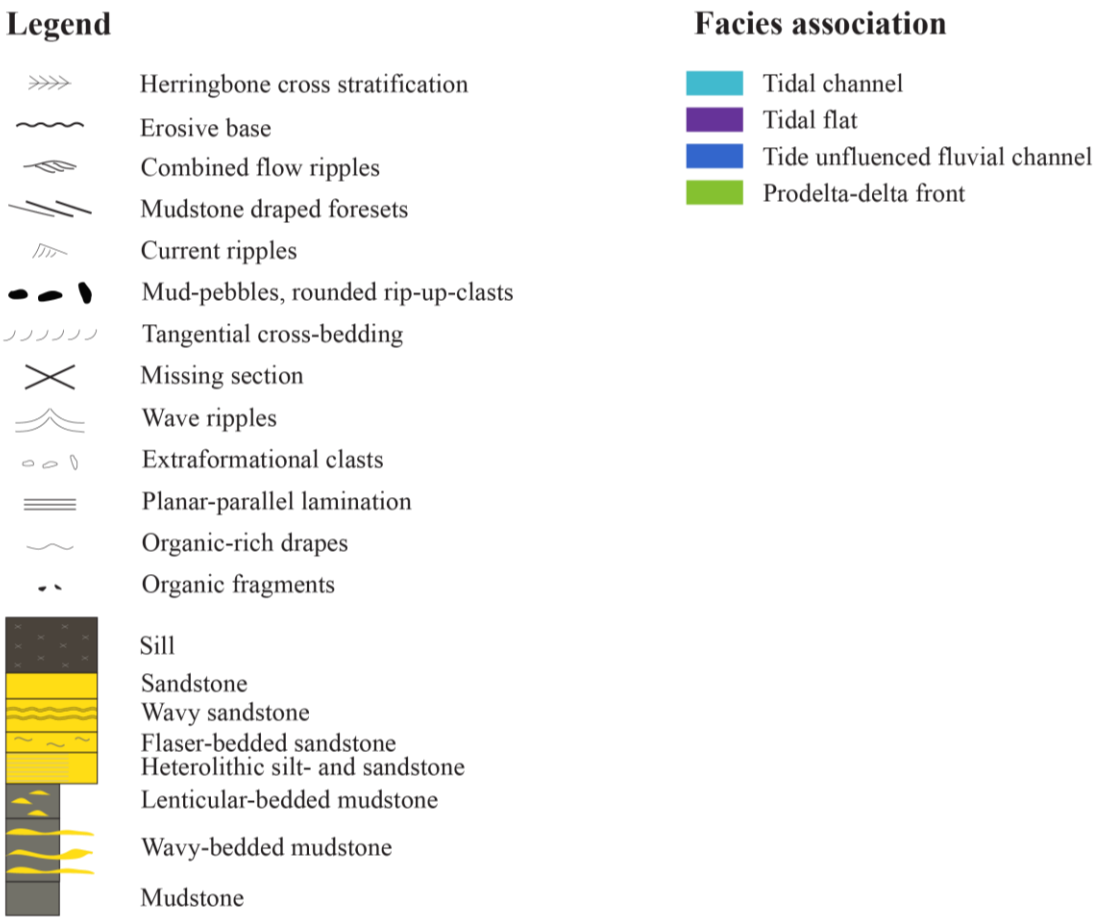

Fig. 5.1: The legend used for all the sedimentary logs and facies associations which are attached in the following subchapters.

5.2.1 FA1: Tidal flat facies association

5.2.1.1 Observations

The facies association FA1 is the most abundant in the study area, and it is found in both sedimentological logs (Fig. 5.10). It consists of heterolithic facies, with approximately 70 % heterolithic facies and 30 % sandy facies. It is well exposed, and the beds have crumbly characteristics and are commonly weathered. Hence, the detailed bed architecture requires some cleaning with a hammer to be investigated. They are covered by little to no vegetation, and the sedimentary structures are visible. FA1 consists of muddy/silty sediments without sedimentary structures, and sandy sediments with sedimentary structures (Fig.5.8). The facies included in this facies association is F1 (structureless silt with sparse sand laminae) (Fig. 5.2A), F2 (organic-rich siltstone) (Fig. 5.2B), F3 (lenticular bedding) (Fig. 5.2C), F4 (wavy bedding) (Fig. 5.2C), F5 (flaser bedding) (Fig. 5.2D), F6 (silt- and sandstone with current ripples) (Fig. 5.2E), F7 (rippled sandstone) and F8 (wavy sandstone) (Fig. 5.2F) (Table 5.2). The thickness

of the deposits is around 10 to 50 cm, with a maximum thickness of 70 cm. One of the facies contains organic fragments, and this facies is confined to a small area that has not been observed in many places (Fig. 5.2B). Bioturbation is 0, as there have been no burrows or fossils observed.

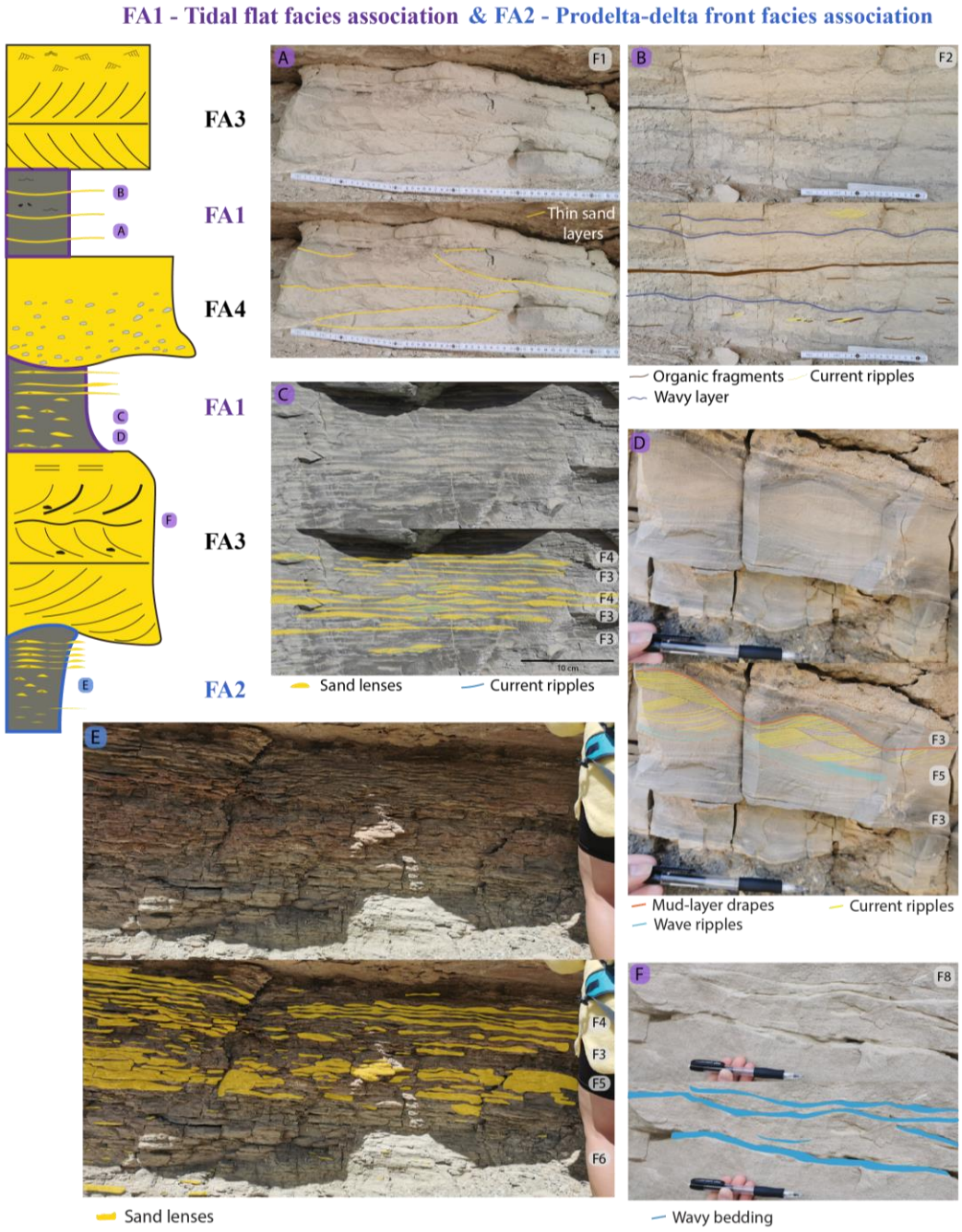

Fig. 5.2: FA1 (tidal flat association) & FA2 (prodelta-delta front facies association) visible. The log on the left side is a schematic log used to display the sedimentary environment. **A**: Facies 1 (structureless silt with sparse sand laminae). **B**: Facies 2 (organic-rich siltstone. **C**: Facies 3 (lenticular bedding) and facies 4 (wavy bedding) displayed. **D:** Facies 3 (lenticular bedding) and facies 5 (flaser bedding) displayed. **E**: Facies 3 (lenticular bedding), facies 4 (wavy bedding) and facies 6 (silt- and sandstone with current ripples) visible. **F**: Facies 8 (wavy sandstone).

Fig. 5.3 depicts the facies associations FA1 (tidal flat facies association) and FA3 (tidal channel facies association) in the virtual outcrop model 3SSW. The lowermost FA1 sequence seems to be thinning out towards the east, whereas above the sill, the sequence is planar and of the same thickness.

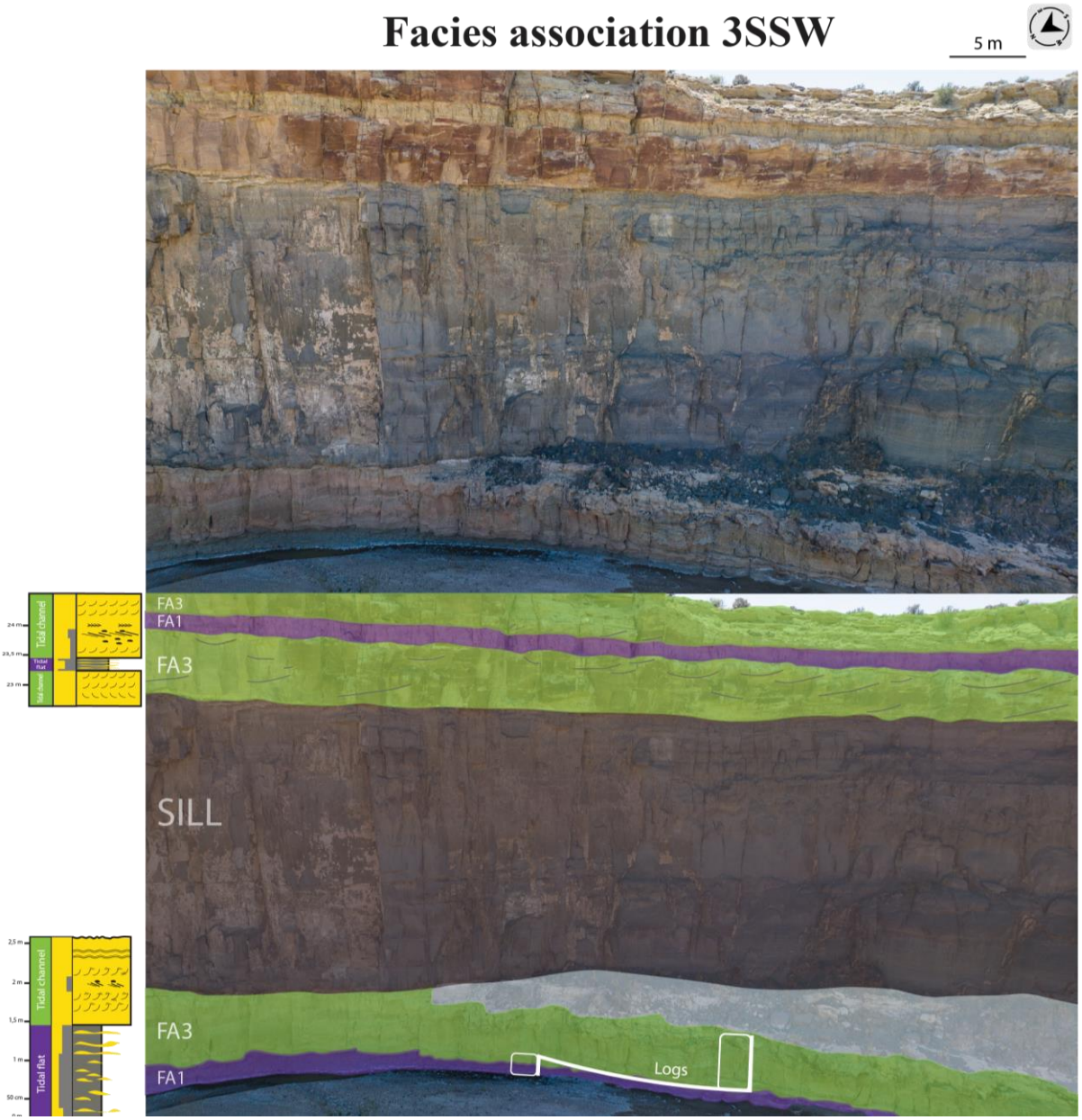

Fig. 5.3: Facies association found in log swing 3. Blue areas are FA1 (tidal flat facies association), yellow is FA3 (tidal channel facies association), and brown is the Mussentuchit Wash Sill. Black curved lines represent crossbedding. The white line and squares depict where one of the sedimentological logs was taken (3 South Swing).

In a different place in the study area, in 4NSW, FA1 occurs several times, where all instances are tabular (Fig. 5.4). FA1 displays a layered characteristic, what seems like several sequences of deposits in one sediment package. The sediment packages range from 0.5 m to 4 m.

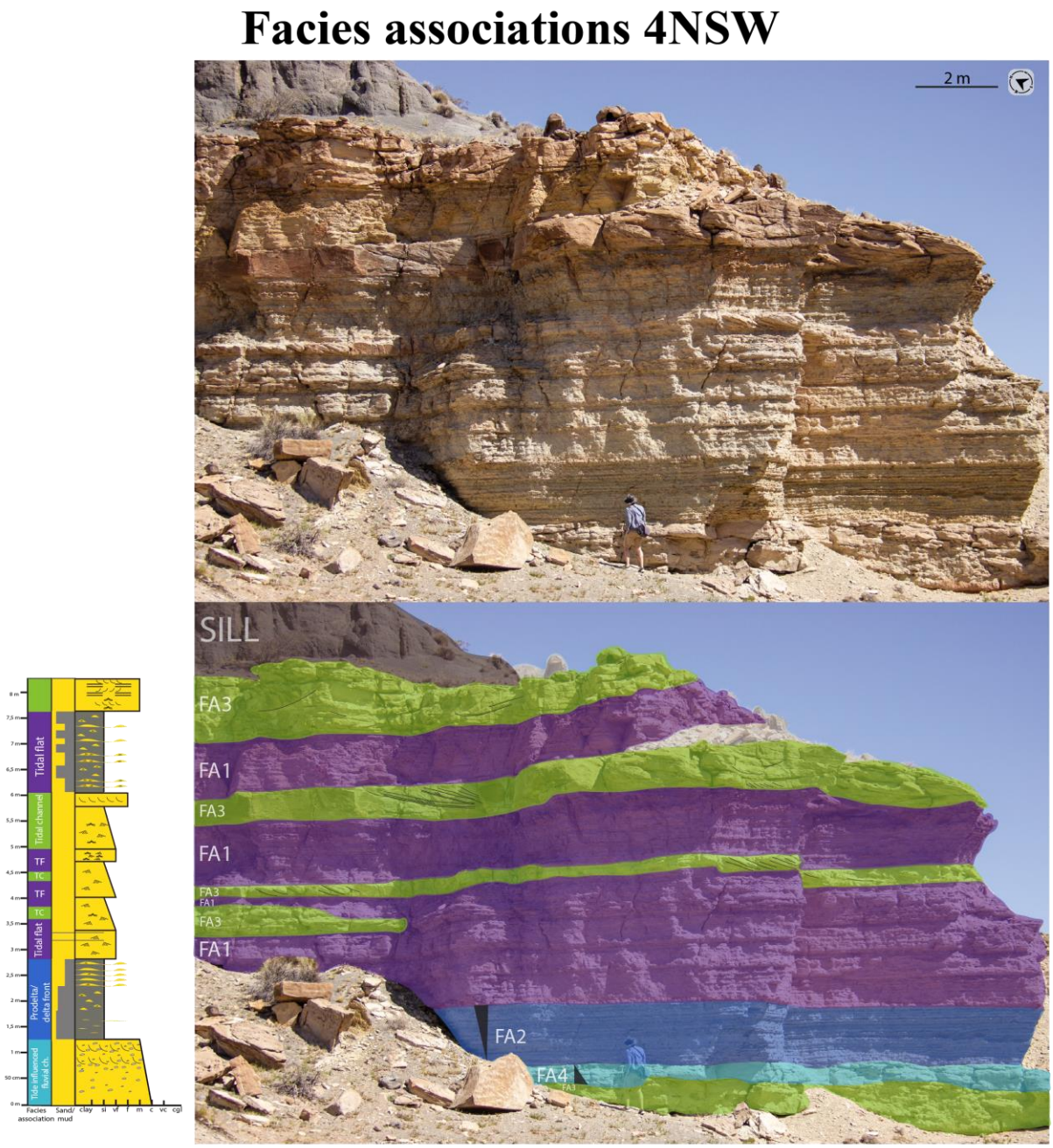

Fig. 5.4: Facies association found in log swing 4. Blue areas are FA1 (tidal flat facies association), grey represents FA2 (prodelta/delta front facies association), yellow is FA3 (tidal channel facies association), green is FA4 (tide-influenced fluvial channel), and brown is the Mussentuchit Wash Sill. Black curved lines represent crossbedding.

5.2.1.2 Interpretation

The dominance of mudstone and very fine-grained sandstone indicates relatively low energy levels. Deposition of mud, silt and very fine-grained sandstone is likely to have been from settling from suspension during slackwater. The heterolithic bedding indicates an environment with alternating episodes of higher energy currents, depositing sand, and slackwater, depositing mud. Bedding displaying bidirectional current ripples as well as sparse wave ripples, indicate

reversing currents. Reversing currents is widely accepted as being associated with tidal flats (van Straaten, 1954; Reineck, 1967; Dalrymple, 1992). Sandstone with wavy bedding is also an indicator for alternating high energy waters and slackwater (Fig. 5.2F). Following a period of high energy, flooding may occur, allowing suspended mud to settle and subsequently draping the sand (Fig. 3.5). Typical for any shallow marine depositional system, surfaces displaying no erosion and tabular successions are common in FA1 (Fig. 5.4). 'Fining upwards-sequences' are also very common for tidal flats (Dalrymple, 1992). The sediments in FA1 are generally fine-grained and show small tendencies of such sequences. The individual sediment packages are very thick, which makes it difficult to distinguish a complete 'fining- upwards' sequence. FA1 shows numerous indicators of tidal influence, such as lenticular, wavy and flaser bedding, mud drapes, sandstone with 'herringbone cross-stratification'. The sparse wave ripples observed, and the lack of hummocky cross-stratification suggest a limited reworking of the sediments after deposition, as well as indication for deposition below the storm wave base (Smyrak-Sikora et al., 2019). Absence of subaerial exposure, including rootlets, coal beds, or desiccation cracks, indicates deposition in the subtidal to lower intertidal zone (Dalrymple, 1992; Eide, Howell, et al., 2016). The low degree of bioturbation indicates environmental stress in a confined, tidal-influenced marginal-marine tidal flat area. This may suggest the presence of hypoxic conditions (low oxygen) and higher salinity levels compared to typical marine standards (Fan et al., 2013; Zuchuat et al., 2018).

5.2.2 FA2: Prodelta-delta front facies association

5.2.2.1 Observations

The facies association FA2 is not as laterally extensive as FA1 (Fig. 5.10). This facies association is similar to FA1, because it can have a lot of almost identical facies. The same facies as FA1 are displayed in FA2 (Table 5.2). Deposits in this facies association are well exposed with little to no vegetation. The facies included are F1 (structureless silt with sparse sand laminae), F2 (organic-rich siltstone), (F3 (lenticular bedding), F4 (wavy bedding), F5 (flaser bedding), F6 (silt- and sandstone with current ripples), F7 (rippled sandstone) and F8 (wavy sandstone) (Table 5.2). An example of the facies is displayed in Fig. 5.2E. Fig. A-F (excluding Fig. 2C) can also be interpreted as prodelta/delta front facies association, although it is marked as tidal flat facies association in this thesis. Bioturbation is 0, as there have been no burrows or fossils observed. The geometry of the deposits is planar and displays a 'coarsening-upwards' sequence (Fig. 5.4).

5.2.2.2 Interpretation

It can be difficult to distinguish between prodelta-delta front facies association and tidal flat facies association. A prodelta tends to have a gentle slope seaward, and according to Dalrymple et al. (2003), the deposits are predominantly mud and silt. This is because only a limited amount of sand can reach these areas in the suspension. According to the study from Eide, Howell, et al. (2016), typical for delta fronts are upward-coarsening heterolithic beds, including fine-grained sandstone with wavy bedding, current ripples, and wave ripples. Cross-stratified sandstone with mudstone drapes on the foresets can also occur (Eide, Howell, et al., 2016). One way to distinguish between prodelta/delta front facies deposits and tidal flat deposits, is on unidirectional currents vs. bidirectional currents. Tidal flats tend to have deposits like the former, whereas prodelta and delta front deposits display the latter deposits. Another way to distinguish deposits are based on 'fining-upwards' sequences or 'coarsening-upwards sequences (Eide, Howell, et al., 2016). In this study, it is difficult to determine in the field if it is a 'fining-upwards' sequence or a 'coarsening-upwards' sequence. It appears to only be distinguishable on the virtual outcrop models (Fig. 5.4). There have been several studies observing prodelta deposits similar as to this thesis (Ichaso & Dalrymple, 2014; Eide, Howell, et al., 2016). The studies described the facies as predominantly composed of mudstone heteroliths, with lenticular to wavy bedding and the presence of current-rippled and wave-rippled sandstone. As in FA1, the absence of hummocky cross-stratification and scarce wave ripples can indicate limited reworking of sediments as well as deposition below the storm wave base. Lack of bioturbation can indicate environmental stress or brackish conditions (Smyrak-Sikora et al., 2019).

5.2.3 FA3: Tidal channel facies association

5.2.3.1 Observations

FA3 is also present in the entire study area and found in both sedimentological logs (Fig. 5.10). Bedding appears exposed and covered with little to no vegetation. The facies included are F9 (rippled sandstone), F10 (cross-bedded sandstone) and F12 (plane parallel-stratified sandstone) (Table 5.2). The thickness of the layers range from 0.25 m to 1.25 m. F9 consists of 'fining-upwards' sequences of silt to fine sandstone with bidirectional current ripples, as well as packs of fine sandstone with bidirectional current ripples and sparse wave ripples (Fig. 5.5A). F10 displays a variety of sedimentary structures, such as bidirectional current ripples (Fig. 5.5A), crossbedding with and without single mudstone draped foresets (Figs. B-E) and 'herringbone

cross-stratification' (Fig. 5.5C). The grain size is confined to medium sandstone. There are visible mud clasts, both along the crossbed foresets and more randomly in the sandstone (Fig. 5.5D). There are also visible hollow crossbeds with some mudstone debris (Fig. 5.5E). The cross-stratification is tangential, which means that the cross-stratification tends to bend at the toesets. Successions of FA3 above the sill are planar with plenty visible cross-beddings (Fig. 5.3). These cross-beddings are oriented in opposite directions; however, the dominant direction is towards the west. Under the sill, FA3 seems to have eroded more into FA1, due to the irregular contact. In Fig. 5.4, black curved lines in FA3 display crossbedding with opposite dipping directions. The dominant direction of the cross-beddings is towards the south. The cross-beddings are of both small-scale and large-scale, and in some of the cross-beddings there are visible smaller cross-beddings on the foresets (Fig. 5.6). F12 displays plane parallel-stratification (Fig. 5.5F), and some of the plane parallel-stratification have mm-scale organic fragments on the laminae. Bioturbation is 0, as there have been no burrows or fossils observed.

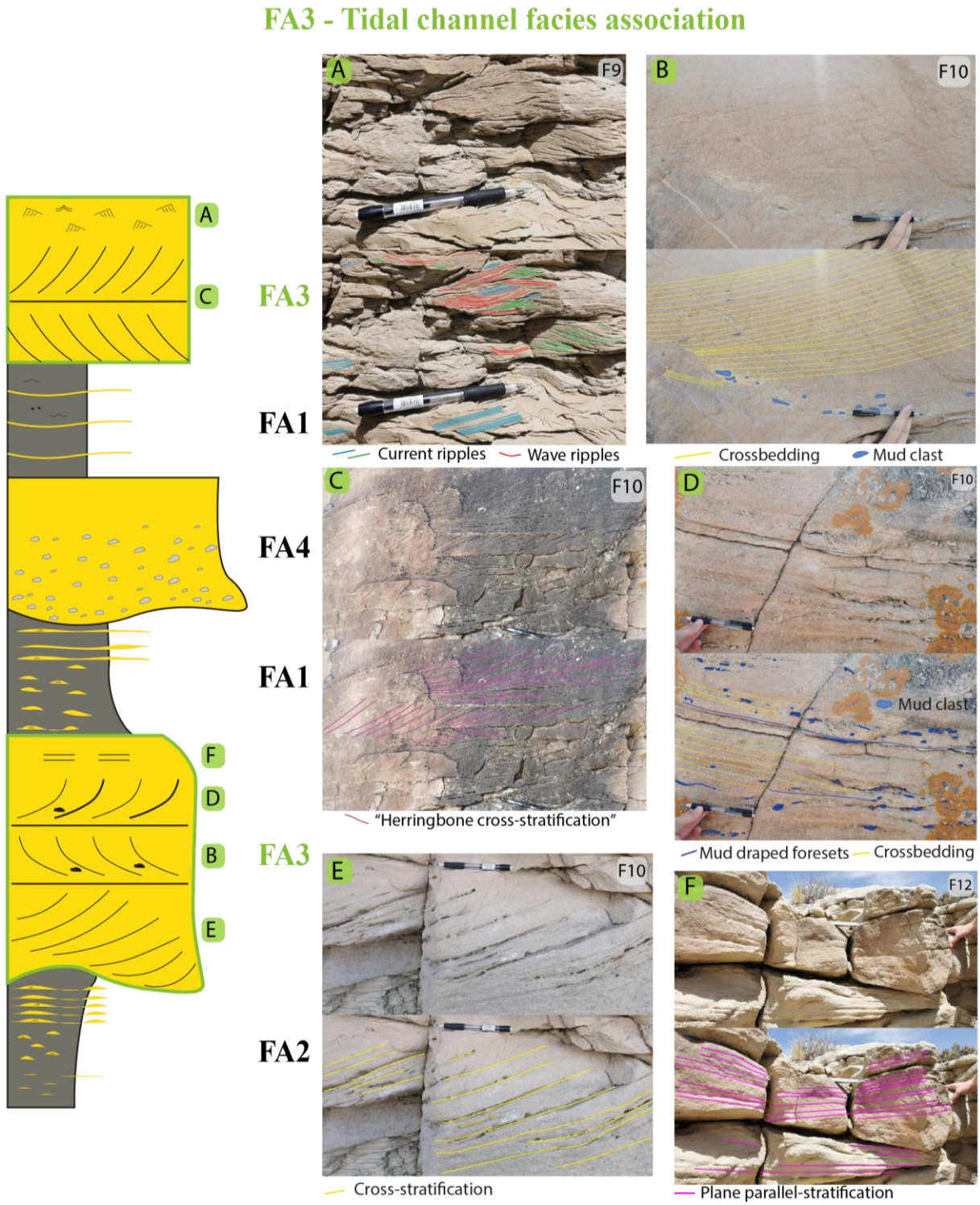

Fig. 5.5: Facies and a schematic log to display FA3 – Tidal channel facies association. **A:** Facies 9 (rippled sandstone). **B:** Facies 10 (cross-bedded sandstone with mud clasts). **C:** Facies 10 (cross-bedded sandstone with 'herringbone cross-stratification'). **D**: Facies 10 (cross-bedded sandstone with mudstone-draped foresets). **E:** Facies 10 (cross-bedded sandstone with hollow foresets). **F:** Facies 12 (plane parallel-stratified sandstone). The green letters on the schematic log to the left correspond to the facies and their letters to the right.

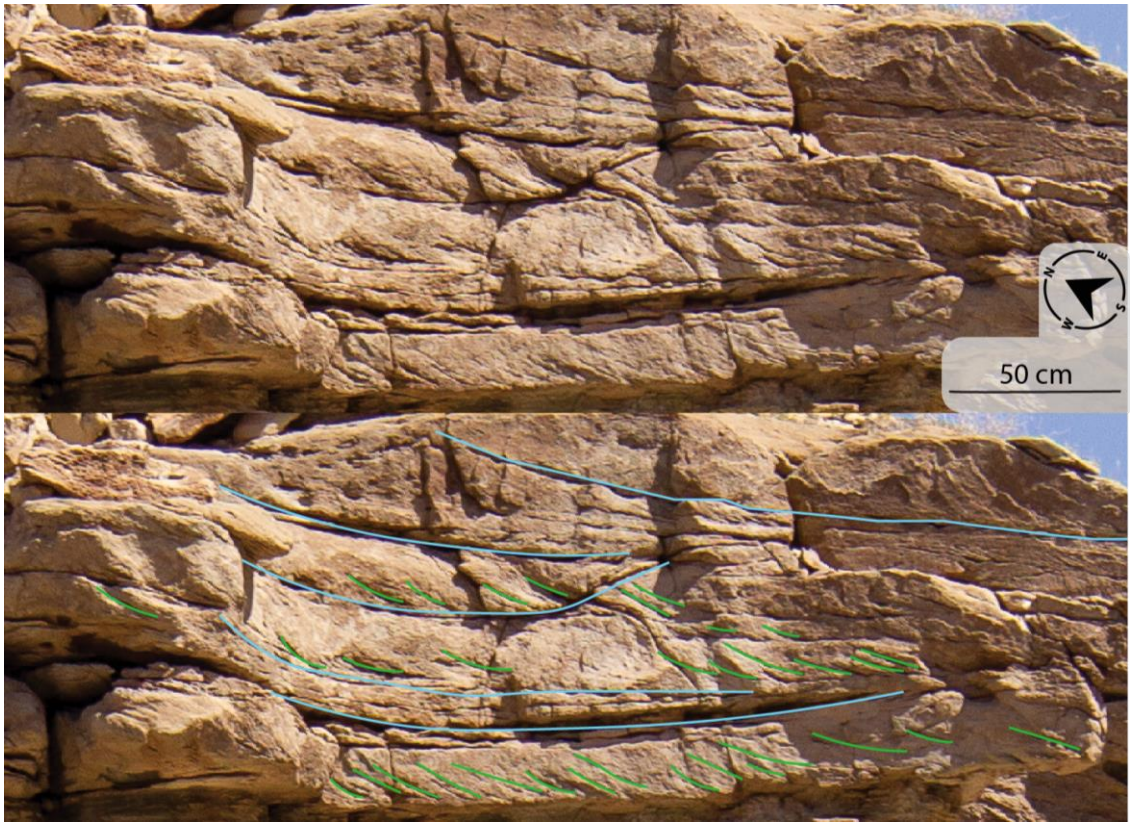

Fig. 5.6: Large-scale cross-beddings with smaller cross-beddings on the foresets.

Fig. 5.7 depicts a close-up of the sedimentary architecture within FA3 in 1SSW, where an abundance of cross-stratifications is visible. Plane parallel-stratification is also visible in the layer just above the sill.

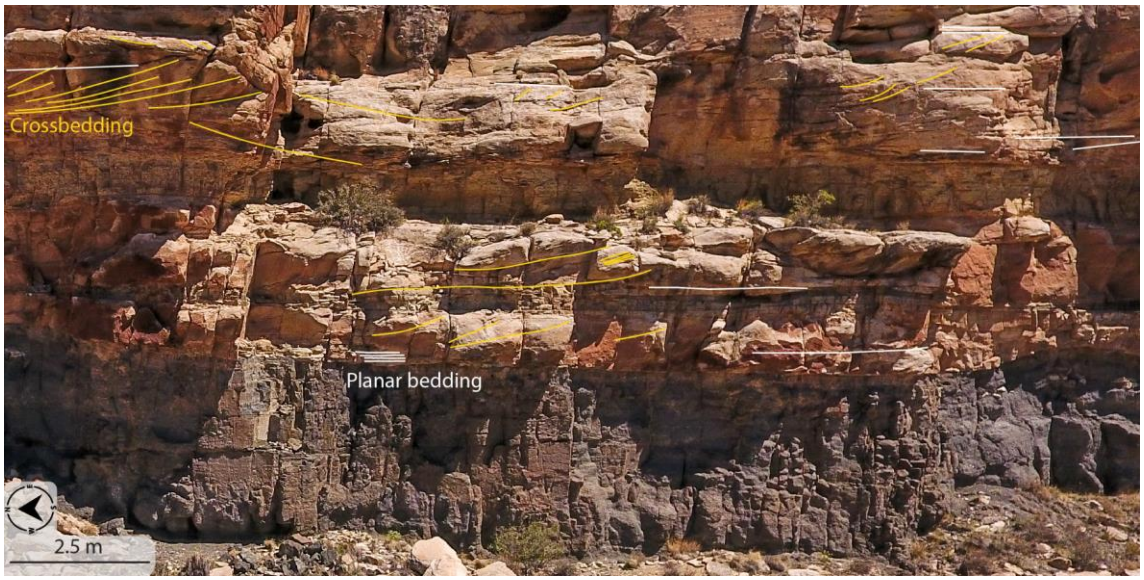

Fig. 5.7: Detailed look at the lithology and sill/sandstone contact in 1 South Swing. Yellow lines are cross-stratification and white lines are plane parallel-stratification.

Fig. 5.8: Erosive base underneath FA3. Tidal channels from FA3 are cutting into tidal flat deposits from FA1, leaving an erosive base.

5.2.3.2 Interpretation

The sedimentary structures visible in FA3 indicate an environment with higher energy than the two previous facies associations. Large-scale cross-stratification and plane parallel-stratification need high-energy streams to deposit coarser grained sediments. The mudstone draped foresets are good indicators for tidal influence. A study conducted by Visser (1980) investigated tidal deposits in Oosterschelde in the Netherlands. During their investigation, Visser (1980) examined crossbeds featuring mudstone-draped foresets. These specific mud-drapes on crossbeds were conclusively deposited during tidal slackwater phases. In this thesis, only single mudstone-draped foresets occurred, which is indicative for the intertidal zone (Visser, 1980). The hollow crossbeds depicted in Fig. 5.5E may represent mudstone-draped foresets where the mud was subsequently eroded or washed away. Tidal channels are characterized by strong tidal currents and tend to carry lots of sediments in suspension. Typical for tidal channels are erosive beds and erosion surfaces, in Fig. 5.8, FA3 erodes into the already existing FA1. 'Herringbone cross-stratification' is very common also in tidal channels, due to the reversing currents during ebb and flow. There has not been observed any bioturbation in this facies association either, indicating unfavorable environment for such burrowing organisms. This can be associated with perhaps rapid deposition of sand, or because of brackish water conditions (Smyrak-Sikora et al., 2019).

5.2.4 FA4: Tide influenced fluvial channel facies association

5.2.4.1 Observations

Facies FA4 is the rarest facies association in the study area, as it has only been recorded once during sedimentological logging (Fig. 5.10). It consists entirely of only F11 (conglomeratic sandstone) (Table 5.2). This facies consists of tangential cross-stratified poorly sorted conglomeratic medium sandstone with a sub-horizontal erosive base (Fig. 5.9). There is a 'fining-upwards' sequence, from coarse- to medium-grained sandstone (Fig. 5.4). The base is eroding into silty facies from FA1 or FA2 (Fig. 5.9). The unit thickness is 1.25 m with internal cross-stratification of 10-25 cm. It has sub- to rounded clasts with a diameter of maximum 2 cm, and it appears as if there is no preferred clast-orientation. The clasts within the layer exhibit an uneven distribution, appearing to cluster predominantly in the middle where the absence of visible trough-cross stratification is notable. The trough cross-stratification recorded displays a unidirectional pattern, with fewer clasts observed in its vicinity. The bedding has a reddish and greyish color. Bioturbation is 0, as there have been no burrows or fossils observed.

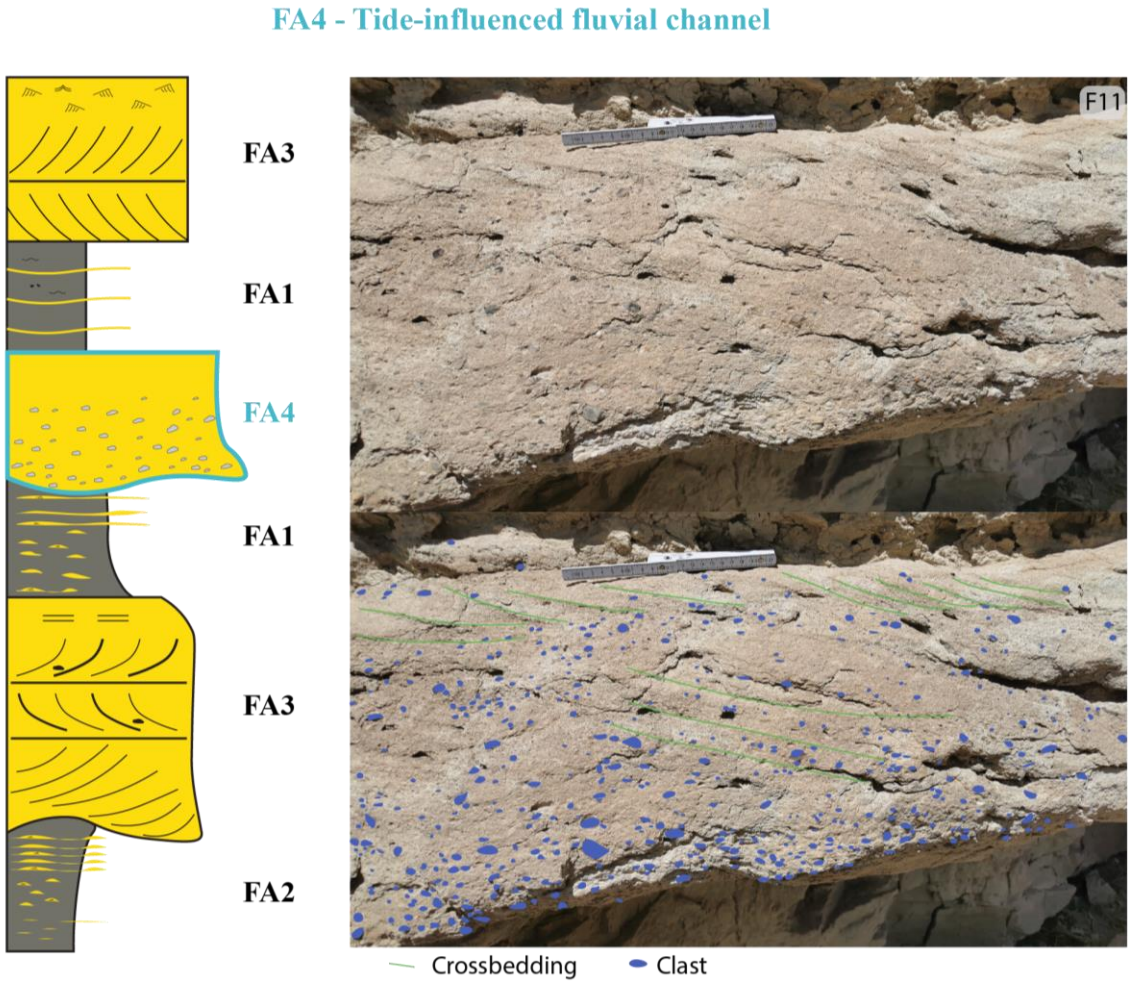

Fig. 5.9: Facies and a schematic log to display FA4 (tide-influenced fluvial channel facies association). The schematic log to the left displays a log from FA4. The green curved lines display crossbedding and the blue circles are clasts.

5.2.4.2 Interpretation

Based on the coarse grain size and the erosion of the underlying facies, deposition during high energy conditions is indicated. To transport bigger clasts, the stream needs both high capacity and competence. Capacity deals with the amount of detritus or particles a flow of water can carry, whereas competence involves the largest particle-size a water flow can transport. Typical for a fluvial channel with high energy and particle content is an erosive bed. F11 (conglomeratic sandstone) does exhibit this characteristic (Fig. 5.9). The gathering of clasts in the middle of the layer can indicate a period with high energy and chaotic deposition. FA4 is not recorded more than once in the logged study area; however, it displays a 'fining-upwards' sequence which is typical for fluvial channels (Fig. 5.4). Based on the observations made of this facies association, it is not entirely clear that the tidal channel is a tide-influenced fluvial channel. There have been observations of only unidirectional cross-stratification. This facies association

was only observed in one outcrop, 4 North Swing, and there might not have been enough observations to decide if it is a fluvial channel or a tide-influenced fluvial channel. However, based on the other facies associations determined in this thesis, as well as findings of tide-influenced conglomeratic dunes in the Curtis Formation in earlier studies (Gilluly & Reeside, 1928; Caputo & Pryor, 1991; Zuchuat et al., 2018), the FA4 is interpreted as a tide-influenced fluvial channel.

5.3 Sedimentary architecture of the Mussentuchit Wash and sill geometry

To achieve a comprehensive understanding of the effect of sedimentary architecture on sill architecture, it is necessary to showcase the sedimentary architecture of the entire Mussentuchit Wash and the sill geometry, connecting all the relevant components and elements. To achieve this, results such as the sedimentary logs obtained for this study are presented in Subchapter 5.3.1, as well as figures of the virtual outcrop models from each swing, and of the entire Mussentuchit Wash. The virtual outcrop models that have been generated and interpreted are displayed in Subchapter 5.3.1 where they display sedimentary architecture and sill geometry. The individual outcrops are first displayed without interpretation, then they are followed by figures where the sedimentary architecture and environment is displayed. Subchapter 5.3.2 will provide results from the sill geometry at the margins, such as sill/host rock-contact.

5.3.1 Sedimentary architecture and the large-scale sill geometry of the Mussentuchit Wash

The sedimentological logs are depicted in Fig. 5.10. Overall lithology and sedimentary architecture from the south overview and the north overview are displayed in Fig. 5.11 & 5.12, respectively. In both figures, individual virtual outcrop models from each swing are attached to present a more detailed sedimentary understanding. The sedimentological logs display the sedimentary architecture in two of the outcrops. The facies associations have been described in Subchapter 5.2. FA3 (tidal channel facies association) and FA1 (tidal flat facies association) are the dominant facies associations. It is FA2 (prodelta/delta front facies association) and FA4 (tide-influenced fluvial channel) are only observed once in the designated logging outcrops. The sedimentary architecture of the entire Mussentuchit Wash is characterized by several

incidents of tidal flat deposits being cut by tidal channel deposits. The sedimentological logs reveal predominantly thin tidal deposits that exhibit limited accumulation. The study area comprises mostly of fine-grained sediment in heterolithic strata with abundant sedimentary structures. There are observed no bioturbation or rootlets in the entire Mussentuchit Wash.

The overview models indicate varying continuity across most layers. The Entrada Sandstone, beneath the J-3 unconformity (explained in Subchapter 2.3.1) is partially visible (Fig. 5.11&5.12). The red line represents the upper Entrada position. Fig. 5.11 depicts the overall lithology of the Mussentuchit Wash in the south. Virtual outcrop models were created for three sections, revealing stepwise sill emplacement, considering the sill elevates and the sedimentary layer above the sill disappears. The gray areas, scree slopes, complicate layer visibility. Sandstone continuity is evident in sections C, B, and A, but data scarcity above the sill obscures it. However, thick sandstone under the north suggests stepped sill emplacement. Mud-rich layers appear below the sill in all sections, continuous in A and B. Plane bedding-dominated sandstone prevails, especially in the north. Mud-rich and plane bedding layers are continuous in B and C.

The overall lithology in the north of the Mussentuchit Wash is depicted in Fig. 5.12. Here, the dune-dominated sand layers as well as the mud-rich layers are continuous. The is only a single occurrence of plane bedding-dominated sandstone, restricted to 6 North Swing (Fig. 5.12C). The heterolithic layer in Fig. 5.12B and Fig. 5.12C is also continuous. Lack of visible layers below the sill (Fig. 5.12A) hinders confirming northside heterolithic continuity. The single mud-rich layer in Fig. 5.12C is also not possible to determine if it is continuous or not due to the lack of sedimentary layers underneath the sill.

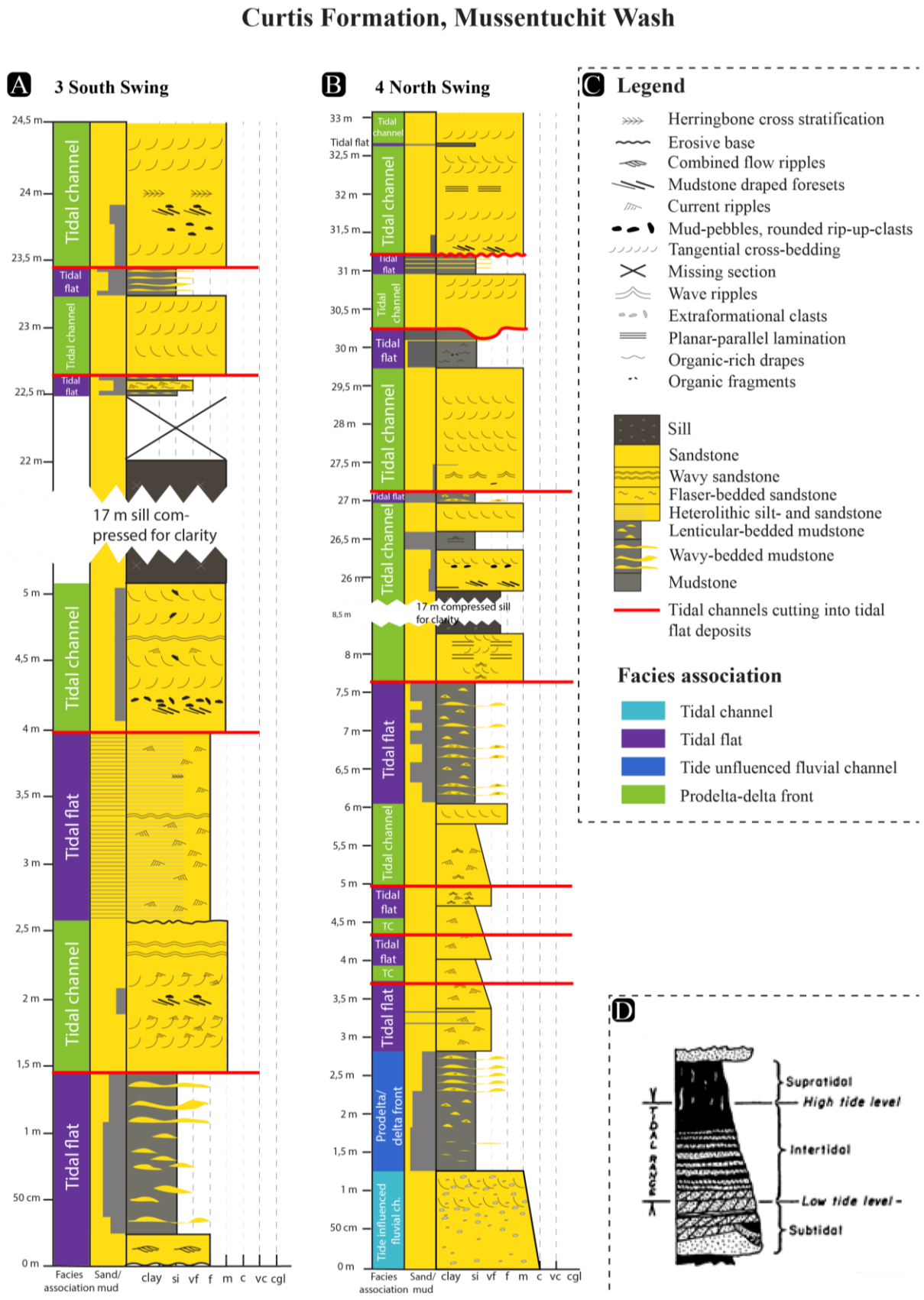

Fig. 5.10: (**A**) Sedimentological log from 3 South Swing (see Fig. 4.1 for location of log). Thickness of units, facies associations and sand/mud ratio are displayed for both logs. (**B**) Sedimentological log from 4 North Swing. (**C**) Legend for the sedimentological logs. (**D**) Ideal schematic log for a tidal flat (from Dalrymple (1992)). Red lines between FAs indicate tidal channels cutting into tidal flat deposits.

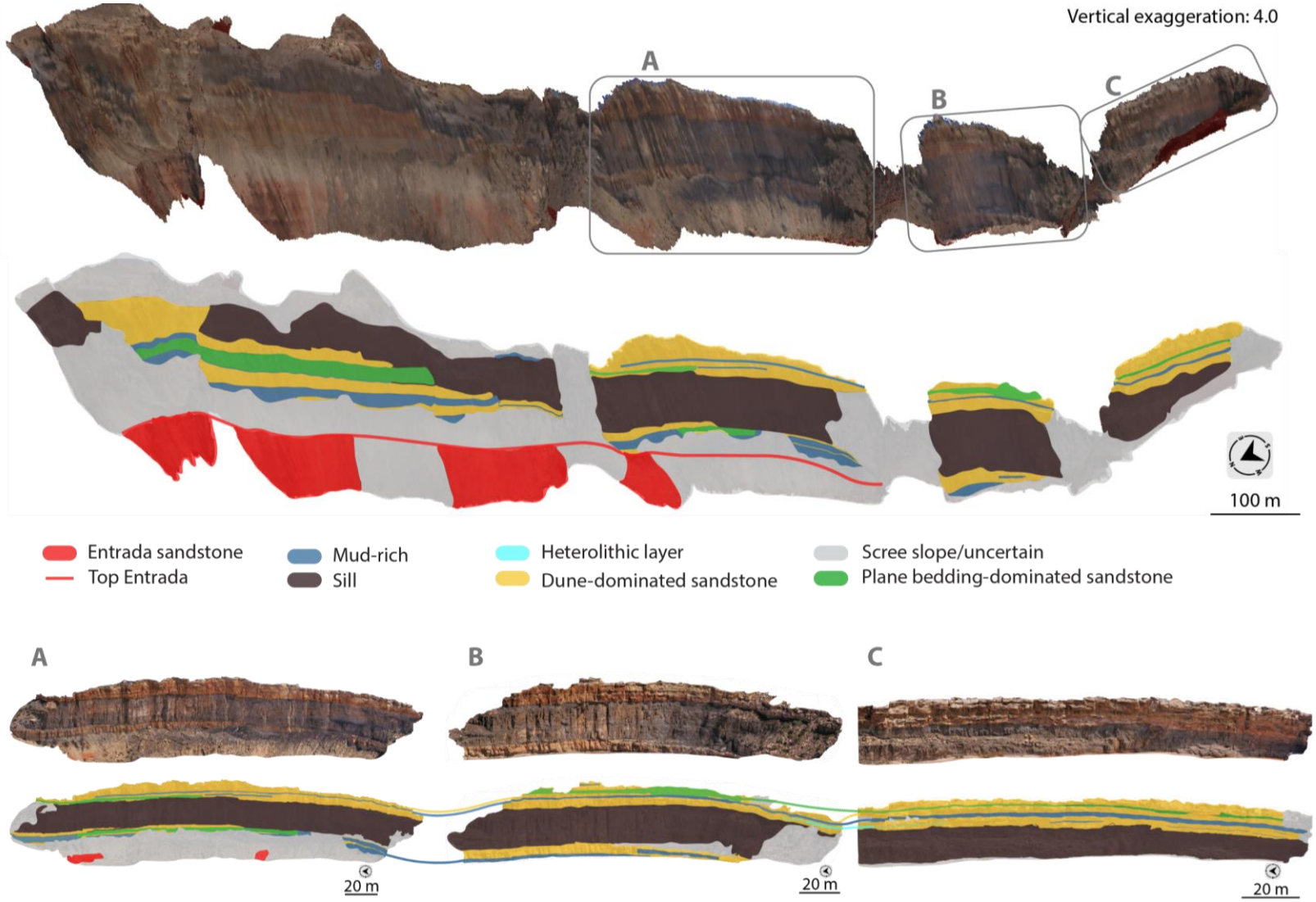

Fig. 5.11: Big model lithology south view with a vertical exaggeration of 4.0. The smaller virtual outcrop models are shown below. **A**: 5 South Swing, **B**: 3 South Swing and **C**: 1 South Swing.

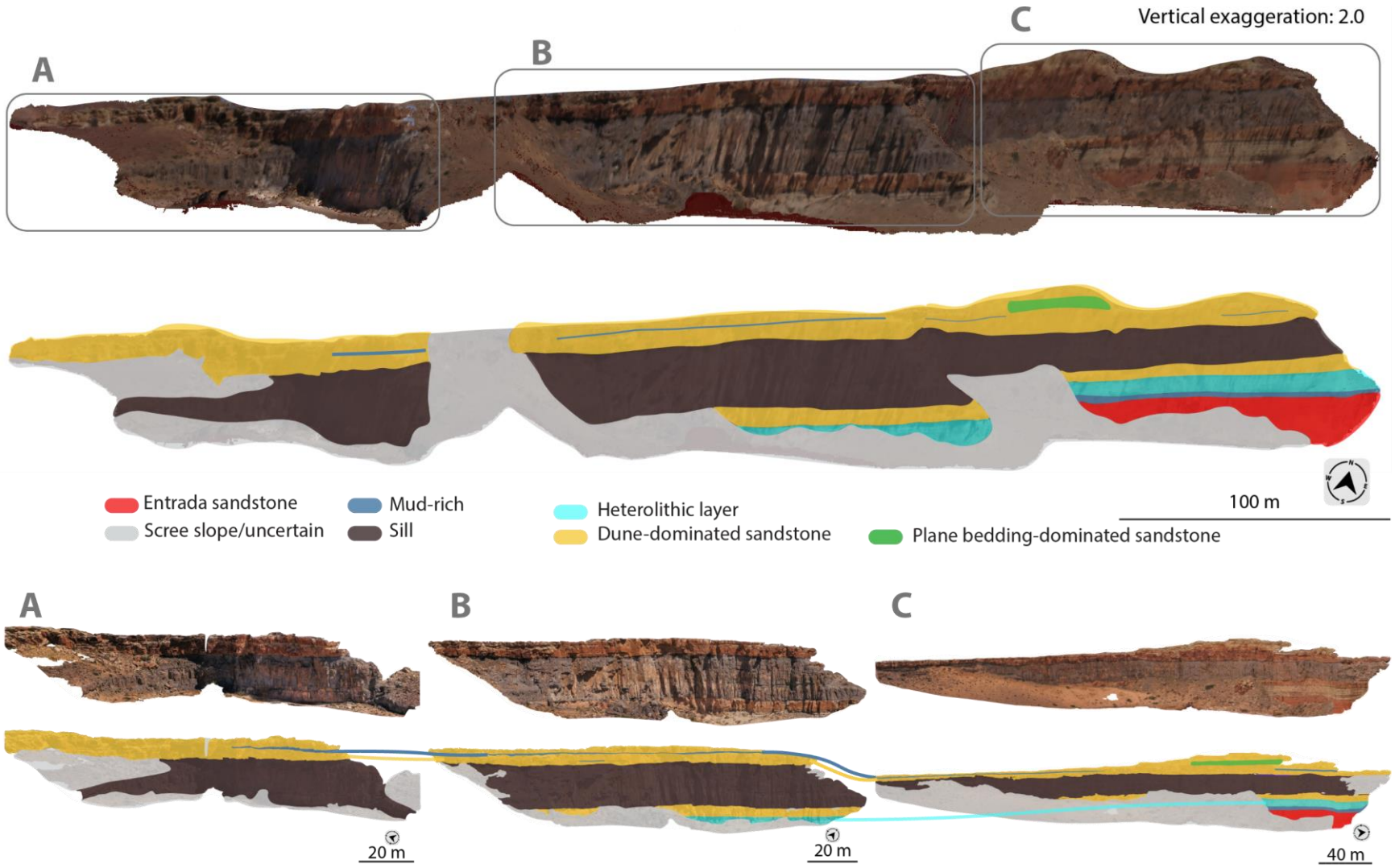

Fig. 5.12: Big model lithology north view with a vertical exaggeration of 2.0. The smaller virtual outcrop models are shown below. **A**: 2 North Swing, **B**: 4 North Swing and **C**: 6 North Swing.

A detailed look at 1 South Swing and 5 South Swing is displayed in Fig. 5.13, where in both the figures, crossbedding, mudstone-draped foresets, steps, splays and broken bridges are present. In Fig. 5.13A, the sill has emplaced itself in the dune-dominated sandstone layer and follows local sedimentary structures such as crossbedding. In Fig. 5.13B, it follows predominately the dune-dominated sandstone, but it also exploited the plane parallel-stratified sandstone layers. Fig. 5.14 displays a closer look at 6 North Swing (Fig. 5.12C) where steps are clearly visible in green resembling a staircase-morphology.

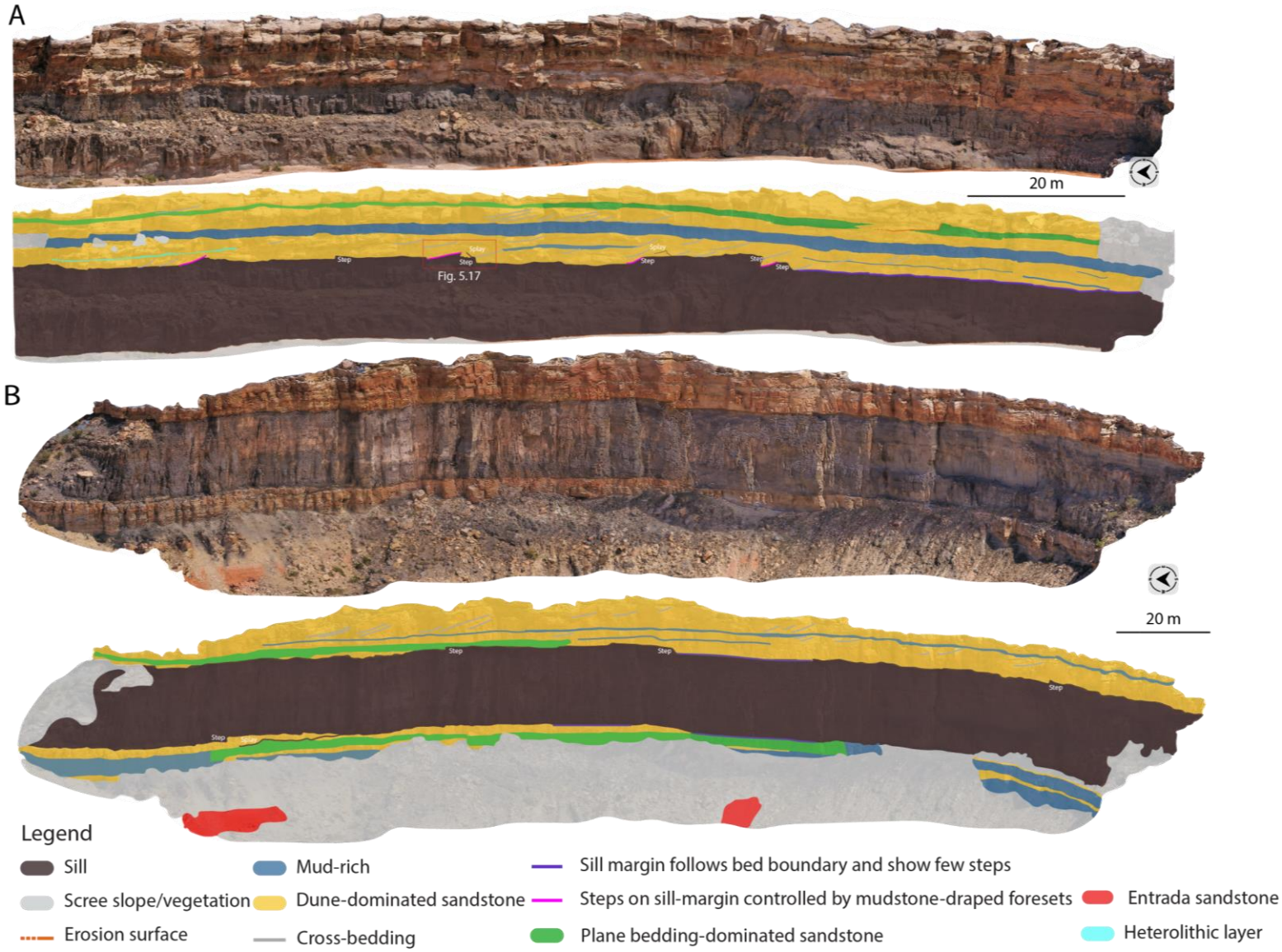

Fig. 5.13: Sill geometry and sedimentary architecture. (**A**) 1SSW without and with interpretation. Visible cross-bedding steps, mudstone-draped foresets and splays. (**B**) 5SSW without and with interpretation. Visible crossbedding, steps.

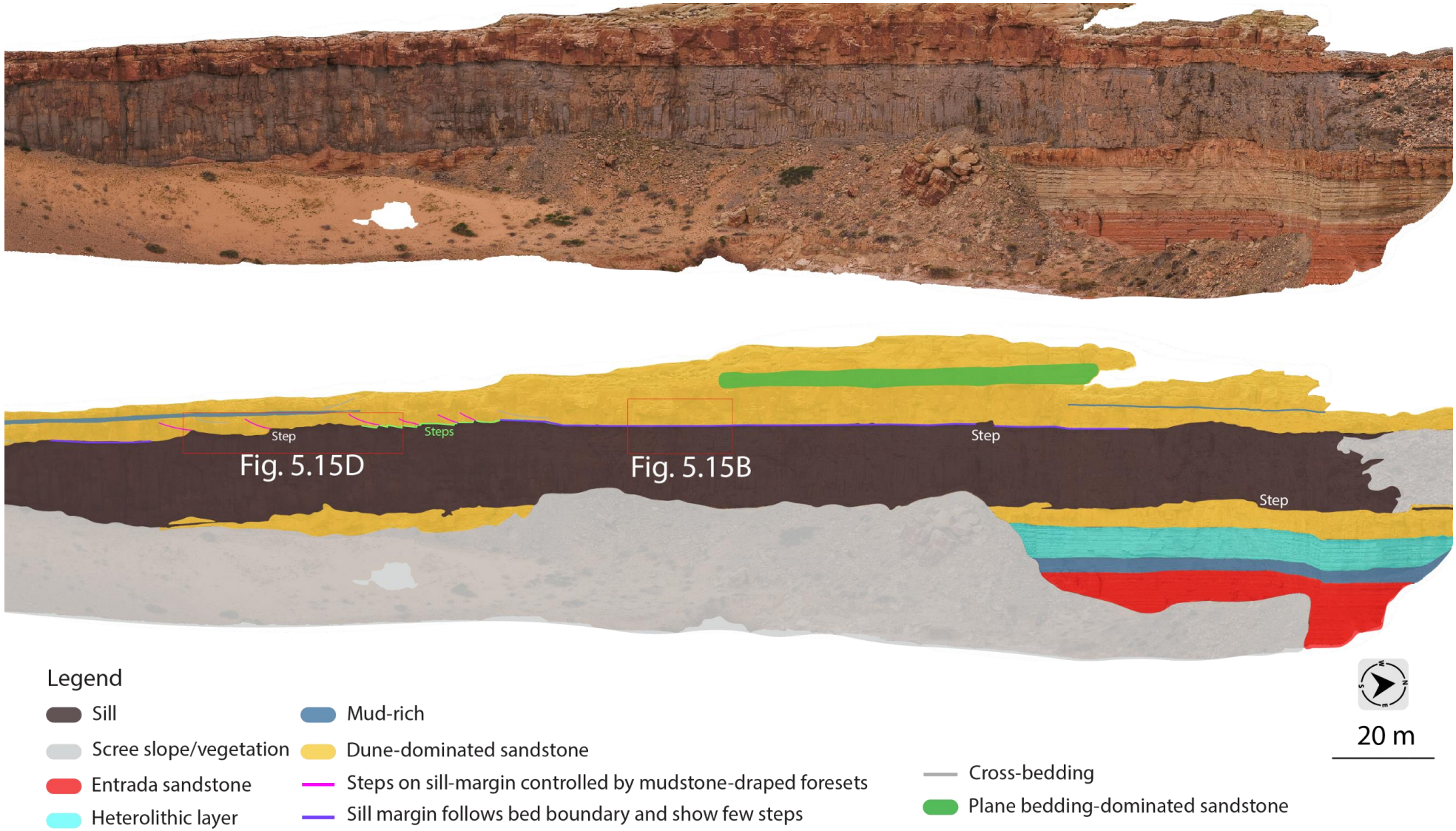

Fig. 5.14: Overview of the 6 North Swing from Fig. 5.12. The model shows several instances of planar contacts, as well as splays, mudstone-draped foresets and steps. The green line displays a stair-like geometry of several steps after each other.

As presented in this subchapter, the architecture of the sill is closely linked to the sedimentary architecture. There are numerous instances of the sill following local sedimentary such as crossbedding, and it displays several steps. The dune-dominated sandstone is the most intruded layer, which indicates that the sandstone is the preferred sedimentary layer to be emplaced in. There are many mud-rich layers present, but the sill does not seem to exploit them on a large scale. On a large-scale basis, the sill emplacement is mostly planar, apart from local sedimentary structures. The thickness of the sill is continuous, c. 15 m in all virtual outcrop models.

5.3.2 Sill geometry at the margins

There are many great field examples for examining the geometry of sill complexes, and the Mussentuchit Wash Sill is one of them. In the paragraphs below, the results and observations regarding the sill geometry at the margins are presented, focusing on the sill/host rock-contact. Different brittle emplacement structures that the Mussentuchit Wash Sill displays will also be presented. The contact displays predominantly two geometries: planar to bedding geometry (Fig. 5.15B and F) and irregular (5.15D). This study shows that the sill prefers to follow bed boundary, as well as the local sedimentary discontinuities present, such as crossbedding. Most crossbedding that the sill follows is mudstone-draped (Fig. 5.17). Instances where the sill follows crossbedding results in undulating geometries (Fig. 5.15A), and in Fig. 5.15C it follows wave ripples. An example of when the Mussentuchit Wash Sill displays a planar contact with the Curtis Formation is depicted below (Fig. 5.15B and F). There are no steps or bridges where the contact is planar, the sill follows the lithology and bedding of the sandstone.

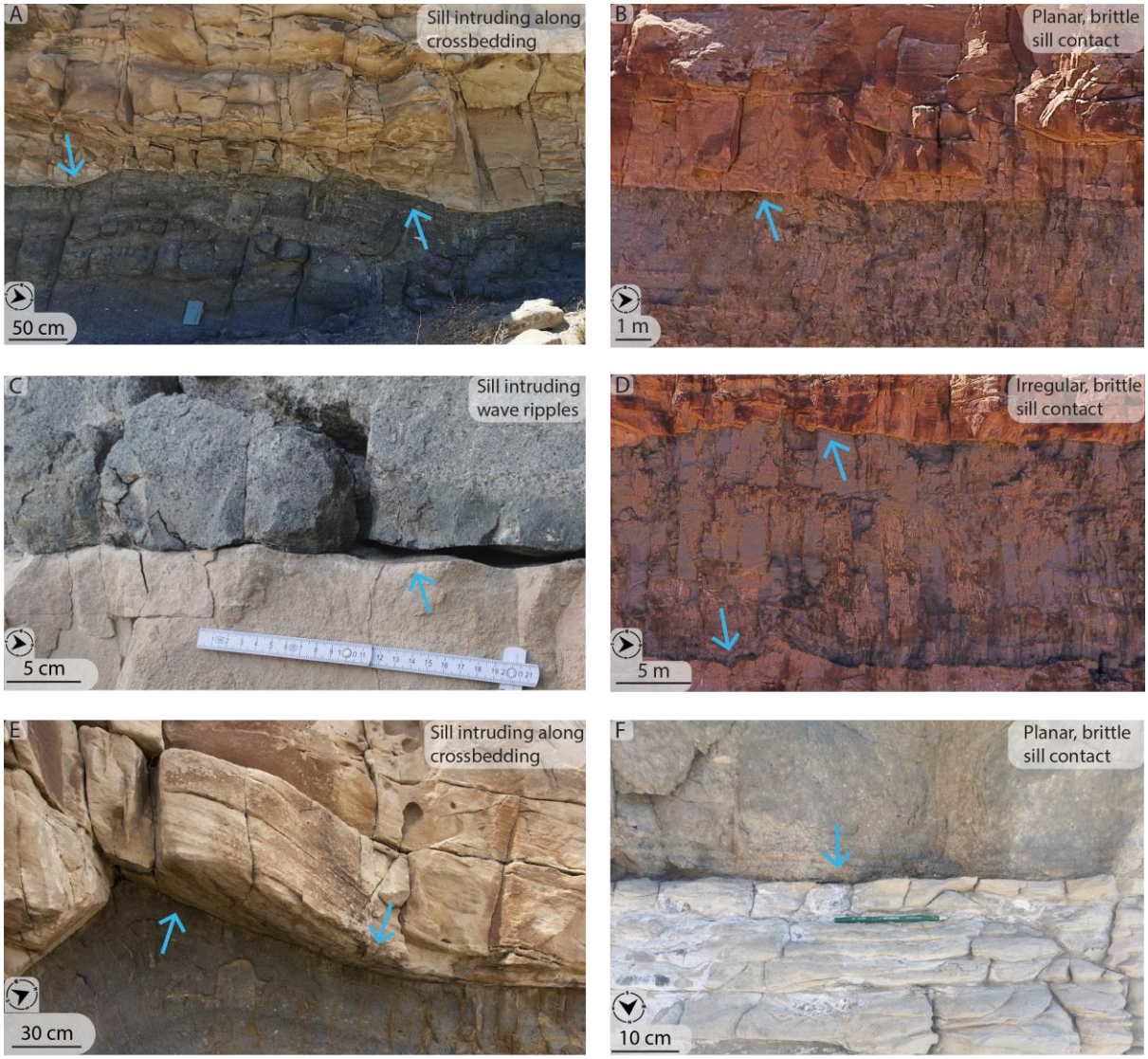

Fig. 5.15: Sill/host rock contacts and interplay. (**A**) Sill intruding along crossbedding. (**B**) Planar, brittle sill contact large-scale. (**C**) Sill intruding wave ripples. (**D**) Irregular, brittle sill contact large-scale. (**E**) Sill intruding along crossbedding. (**F**) Planar, brittle sill contact detail-scale.

The Mussentuchit Wash Sill also displays an irregular sill/host rock-contact (Fig. 5.15D). Both the lower and upper contact display irregular contacts. The irregular contact continues towards the north, whereas the contact gets more planar towards the south.

At the contact surface between the sill and the host rock of the Curtis Formation, the Mussentuchit Wash Sill exhibits various brittle emplacement structures, such as steps (Fig. 5.14) and bridges (Fig. 5.16). The sill shows a step-like geometry where it almost resembles a staircase. In other cases, the sill geometry can be irregular, appearing to completely disregard host rock lithology. Even though there are local changes in geometry, the sill appears to have a rather constant thickness of c. 15 m. Several broken magmatic bridges are evident in the study

area (Fig. 5.16). The lack of evidence for unbroken bridges indicates that they are rare or non-existent in the study area for this thesis.

Fig. 5.16: Example of a 'broken bridge' structure of the intruded Curtis Formation in 3 South Swing.

A great example of a case where the sill is following a mudstone draped foreset is depicted in the figure below (Fig. 5.17). The sill decides to follow the foreset before it abruptly changes into irregular contact. There is also a clear splay from the sill that has intruded almost vertically into the Curtis Formation. In cases where the studied sill follows crossbedding, the results are an undulating geometry (Fig. 5.15A).

Fig. 5.17: Example of where the Mussentuchit Wash Sill follows a mudstone draped foreset. Yellow curved lines display individual crossbeds whereas the purple curved line displays a mudstone draped foreset.

6.0 Discussion

This study of the emplacement of the Mussentuchit Wash Sill in the Curtis Formation provides a set of results presented in the previous chapter, which will be evaluated and discussed herein. Firstly, the sedimentary environment from this study interval will be discussed and compared to previous studies on tidal depositional environments, as well as specific studies on the Curtis Formation. Thereafter, the sill geometry will be evaluated in light of the facies associations established in this study, and the influence of sedimentary heterogeneity on sill geometry will be discussed. Finally, a discussion on sill intrusions and the relevance of lithological restraints on host rocks will be covered, in addition to previous studies on sill intrusions in mudstone and sandstone.

6.1 Sedimentary environment compared to previous studies

This subchapter will discuss the sedimentary environment in the study area for this thesis and compare it to 1) previous studies on tidal depositional environments and 2) previous studies on the Curtis Formation.

6.1.1 Previous studies on tidal depositional environments

Tidal flat depositional systems typically encompass tidal channels, sand flats, mixed flats, mud flats and a salt marsh on top with supratidal sediments (as explained in Subchapter 3.3) (S. Gao, 2019). An upwards fining sequence is expected in a perfect example of a tidal flat depositional system. Going from ‘herringbone cross-stratification’ (often present due to the reversing currents), bidirectional current ripples, and wave ripples in the tidal channels, to flaser-, wavy-, and lenticular bedding throughout sand flats, mixed flats, and mud flats. At the top, salt marshes can develop if there is enough vegetation (Dalrymple, 1992). Different types of cross-stratifications develop in tide-influenced environments, and they leave tidal signatures. These cross-stratifications are herringbone cross-stratification, reactivation surfaces and tidal bundles (Davis Jr., 2012).

Findings of this thesis indicate that the study area of the Curtis Formation does not display a perfect representation of a tidal flat. There has been no evidence of a salt marsh or supratidal deposits in the study area for this thesis. The absence of bioturbation, plants, raindrop marks,

and desiccation cracks further supports this conclusion. This lack of subaerial exposure can be an indicator for deposition in the subtidal to lower intertidal zone (Eide, Howell, et al., 2016). As depicted in Fig. 5.10, after each mudflat or sandflat episode, there is a new set of tidal channel facies association on top (red line). This may suggest that the study area in Mussentuchit Wash has been fed with lots of sediments from tidal channels, and that there has been enough energy in the channels to erode into pre-existing tidal flat deposits from the intertidal zone. This results in an erosion surface (Fig. 5.8). The tidal deposits in the study area are also relatively thin, which may suggest rapid deposition of sediments, in terms of it not being enough time to develop into a supratidal flat. A complete, expected tidal flat sequence with upwards fining deposits from tidal channel to supratidal is never observed in the study area. However, the study area in this thesis has shown recordings of sediments typical for tidal flats, such as herringbone cross-stratification (Fig. 5.5C), bidirectional current ripples (Fig. 5.5A), wave ripples (Fig. 5.2D). Reactivation surfaces are also prevalent in the study area (Fig. 6.1), suggesting significant impact from river floods and waves. The Mussentuchit Wash area resembles evidence of being a tidal depositional system in a low accommodation zone, meaning that the basin the sediments were deposited in does not subside significantly compared to sediment supply (Fig. 2.2) (Nuccio & Condon, 1996).

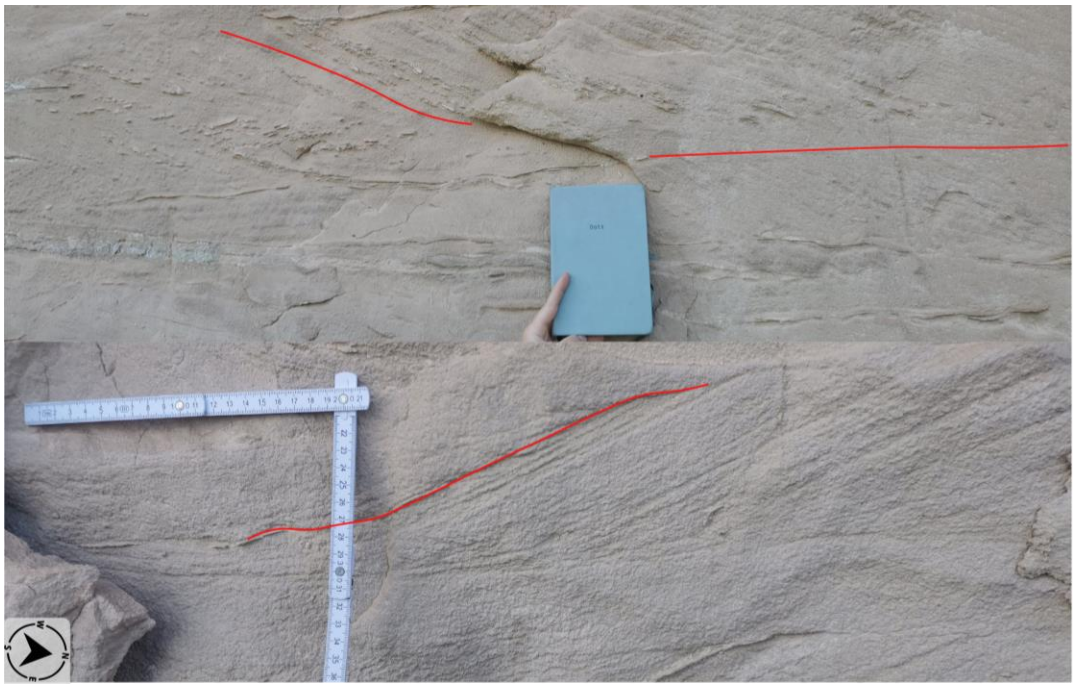

Fig. 6.1: Visible crossbedding with reactivation surfaces marked in red. These reactivation surfaces are erosion surfaces within sets of crossbedding.

6.1.2 Previous studies on the depositional setting of the Curtis Formation

Previous studies have shown that the Curtis Formation displays a greenish characteristic because of the mineral glauconite (Gilluly & Reeside, 1928; Zuchuat et al., 2018), which has also been used as evidence to support the identification of the formation. The greenish color has not been prevalent in the study area for this thesis, instead, the color has been ranging from whitish to yellow/orange. Nevertheless, since there were no microscopic examinations conducted in this thesis, it is not possible to be completely certain of the absence of glauconite. Observations from this study demonstrate many similarities with previous studies, however, there have been new observations that have shed light on new evidence for the Curtis Formation. This will be discussed in the subchapters below.

Common deposits on tidal flats are tidal bundles. Findings from this thesis show no observations of tidal bundles, as opposed to findings from Kreisa and Moiola (1986) and Zuchuat et al. (2018, 2019). This can indicate that the tidal bundles within the Curtis Formation are locally restricted. Earlier studies show evidence of the Curtis Formation being a great example of a typical tidal flat sequence with upwards fining deposits with supratidal deposits on top. However, the Mussentuchit Wash is not. The tidal deposits demonstrate several observations of tidal flat deposits being cut by tidal channel deposits. There have not been any studies on the Curtis Formation specifically in the Mussentuchit Wash, the study area for this thesis. This gives room for the fact that there can be differences in the observations for this study compared to previous studies.

General for all the facies associations established in this study, is the absence of trace fossils. There have not been observed any burrows or bioturbation in the logged outcrops. This is indicative of a stressed environment, possibly with brackish water-conditions (Smyrak-Sikora et al., 2019). This differs from previous studies, where marine trace fossils as well as burrows and rootlets have been observed (Gilluly & Reeside, 1928; Kreisa & Moiola, 1986; Caputo & Pryor, 1991; Zuchuat et al., 2018). Nevertheless, Zuchuat et al. (2018) observed limited bioturbation and diversity, also indicating stressed environmental conditions. Zuchuat et al. (2018) also proposed that the sediments were deposited in a confined, marginal-marine tidal flat setting characterized by hypoxic conditions and elevated salinity levels compared to normal marine standards. Based on the divisions made by Zuchuat et al. (2018), only lower and upper Curtis displayed bioturbation to a limited extent.

This study has shown findings of sediments deposited on a prodelta/delta front, which is not a uniform claim regarding the Curtis Formation. As a matter of fact, no other study has shown similar facies. Findings from this study support the claim that there might be prodelta/delta front deposits with the fact that there has been evidence of upward coarsening sequences in the heterolithic bedding (Fig. 5.2E). This was also evident in Caputo and Pryor's study (1991). As stated in Chapter 5, sediments from tidal flats and those of prodelta/delta front might appear almost identical. This claim stems from the several studies that have (Jorissen et al., 2018; Eide, Howell, et al., 2016; Smyrak-Sikora et al., 2019). However, it can be difficult to distinguish between tidal flat deposits and prodelta/delta front deposits that have later been reworked by tides. Other studies often observe an abundance of bioturbation in prodelta- and delta front deposits, nevertheless, it is not always the case. Findings from Eide and Howell et al. (2016), where a tide-influenced delta called Gule Horn Formation was investigated in Jameson Land, Greenland, show sparse bioturbation. This is explained by a stressed, brackish environment with low sandstone content, possibly due to rivers flowing into a restricted marine embayment (Eide, Howell, et al., 2016). Deposits from delta fronts are similar to those of prodeltas, however, it comprises of more sandstone deposits and mudstone draped foresets on crossbeds.

Despite the deviations in observed deposits compared to previous studies, data obtained from this study also display many similarities with earlier studies (e.g., (Gilluly & Reeside, 1928; Kreisa & Moiola, 1986; Caputo & Pryor, 1991; Zuchuat et al., 2018, 2019). Deposits from the Mussentuchit Wash comprise of sediments associated with tidal flats, such as heterolithic lenticular-, wavy-, and flaser bedding, cross-stratification with and without mudstone-draped foresets, bidirectional current ripples, cross-stratification ('herringbone cross-stratification') and rip up mud clasts. Plane parallel-stratification has also been recorded in this study, which coincides with earlier studies (Kreisa & Moiola, 1986; Caputo & Pryor, 1991; Zuchuat et al., 2018, 2019). The deposits in the Mussentuchit Wash are predominately fine-grained, such as silts, muds and up to fine-grained sandstone. As stated in Subchapter 2.3.2, Zuchuat et al. (2018) divided the Curtis Formation into lower-, middle-, and upper Curtis. In their study, the study area for this thesis, the Mussentuchit Wash, is situated where lower, middle, and upper Curtis have been observed. Sand-dominated heterolithic deposits from a subtidal flat of the lower Curtis have been observed in the study area for this thesis. Deposits from middle Curtis, sub- to intertidal channel-dune complex have also been documented in the study area for this thesis. Nevertheless, there is slightly more uncertainty surrounding the observation of deposits from the upper Curtis.

In one of the two sedimentological logs recorded for this thesis, the presence of gravel-rich dunes in medium-grained sandstone was documented within FA4, which represents a tide-influenced fluvial channel. This basal conglomerate is similar facies as found in earlier studies (Caputo & Pryor, 1991; Zuchuat et al., 2018). In the Mussentuchit Wash, FA4 is characterized by medium coarse-grained cross-stratified sandstones, containing an abundance of gravel. The lack of burrows and trace fossils is indicative of a stressed environment, which may be a result of rapid deposition of sand in a high-energy environment. The characteristics are all evidence for a tidal-fluvial depositional channel setting. Findings from this thesis have shown that there are several instances of erosive bases (Fig. 5.8), where the individual beds exhibit a sharp base.

The Curtis Formation has excellent exposures in the Mussentuchit Wash. This has been evident through the individual facies associations determined for the study area in this thesis. The Mussentuchit Wash displays tidal deposits from subtidal and intertidal zone; nonetheless, it lacks deposits from supratidal zone. FA4 (tide-influenced fluvial channel facies association), FA3 (tidal channel facies association), and FA1 (tidal flat facies association) as presented in Chapter 5, comprise deposits from the subtidal- and intertidal zone. These facies associations display deposits from sand flats, mixed flats, and mud flats. FA2 (prodelta-delta front facies association) has deposits belonging to the subtidal- and lower intertidal zone.

Despite not observing a perfect textbook representation of a tidal flat, there is enough evidence that the Mussentuchit Wash can be regarded as a tidal depositional system. This evidence stems from the deposits found in the study area that support the claim for tidal influence, such as heterolithic bedding, 'herringbone cross-stratification', reversing currents, sparse wave ripples (indicates limited reworking of sediments), and fine-grained sediments. Reactivation surfaces (Fig. 6.1) are also good indicators for tidal influence (Dalrymple, 1992).

6.2 Comparison of sill geometry and facies association

In the upcoming subchapters, the focus will be on exploring the geometry of the Mussentuchit Wash Sill and its impact on the facies associations established for the Curtis Formation in this thesis. This discussion aims to investigate how the sill has intruded into the different facies and how emplacement has potentially been influenced by the sedimentological characteristics of the Curtis Formation. Firstly, Subchapter 6.2.1 will discuss the geometry of the upper and lower boundaries of the Curtis Formation and investigate if and how the host rock has been deformed

to accommodate emplacement of the sill. Lastly, Subchapter 6.2.2 will discuss the morphology of the sill in the different sedimentary facies.

6.2.1 Geometry with and without the sill

The figures below show sedimentary architecture before and after digitally removing the sill to assess how the emplacement has been accommodated. In all the figures depicted below (Figs. 6.2-6.5), a precise match between the upper and lower boundaries of the sill could not be made, indicating slight displacement of the host rock above the sill out of the outcrop plane, and incorporation of host rock fragments into the sill. There is however no evidence of sill-related deformation of the host-rock away from the sill margin in the form of fractures, thrust faults or normal faults. In all the sections presented below, the sill has intruded into the dune-dominated sandstone.

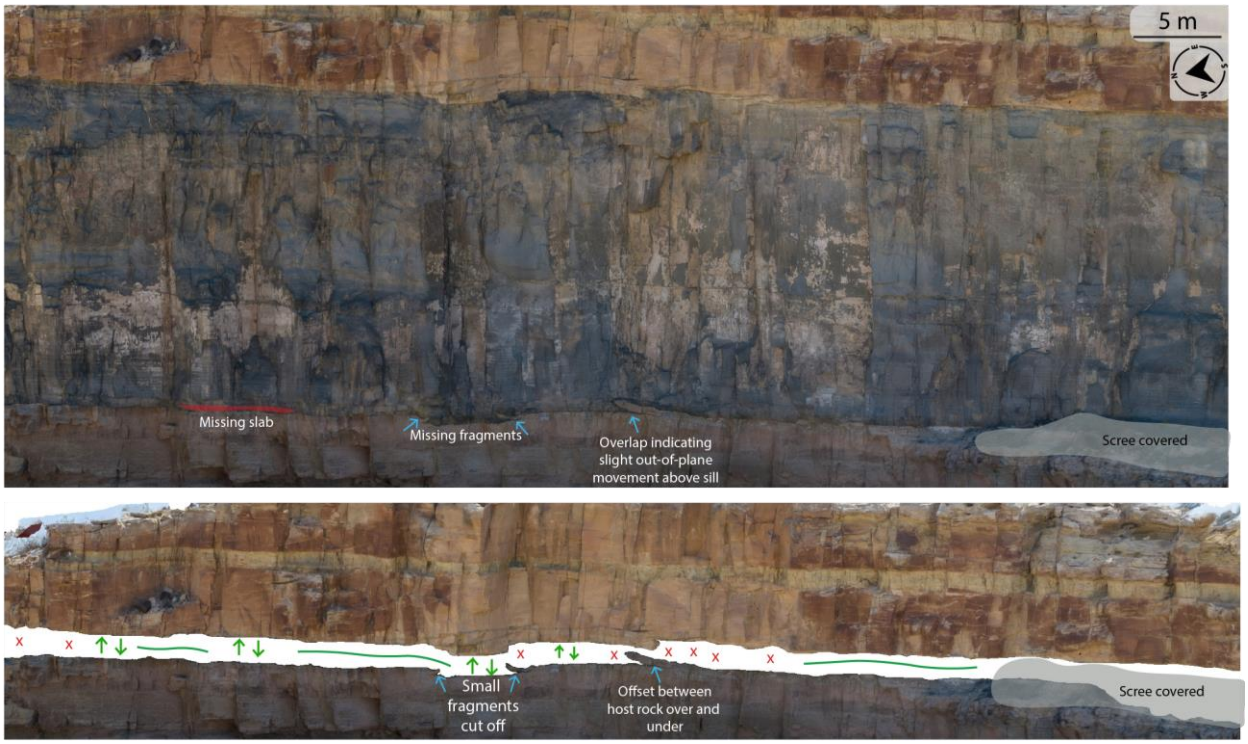

Fig. 6.2: Jack-up of host rock above the intrusion in 3SSW. The original image is at the top, and reconstructed pre-intrusion geometry obtained by removing the sill digitally in the image at the bottom. The top and bottom of the host rock does not display a perfect match, indicating that the sill has altered the host rock to an extent. Red cross means that the upper and lower strata does not match perfectly, whereas the green arrows/lines indicate a good match.

Fig. 6.2 displays a section of 3SSW, with the original photo at the top, and the altered photo at the bottom. The sedimentary strata above and below the sill do not seem to fit perfectly overall (red crosses in Fig. 6.2). Sill emplacement structures developed due to brittle deformation

processes such as broken bridges and steps are visible. For the rightmost broken bridge, the upper and lower segments show overlap of about 2 m. These two sections do not match, and the only way to explain this overlap is that the host rock above the sill has been displaced with respect to the host rock below. However, because of the overall very good match between the upper and lower boundary, this displacement cannot have been very large, only a few meters maximum. To the left in Fig. 6.2, there are two smaller, facing broken bridges. On the large scale, the upper and lower segments fit well, but there are small (< 1x1 m) fragments of host rock missing, indicating that during creation of broken bridges, host rock fragments were sometimes split off. Because these fragments are not visible within the sill, this indicates that they have been transported away by the flowing magma. As the host rock shows no evidence of melting anywhere else, since the magma shows no evidence of crustal assimilation (Germa et al., 2020), and since the sill shows several un-melted host-rock xenoliths, it is unlikely that these split-off fragments melted.

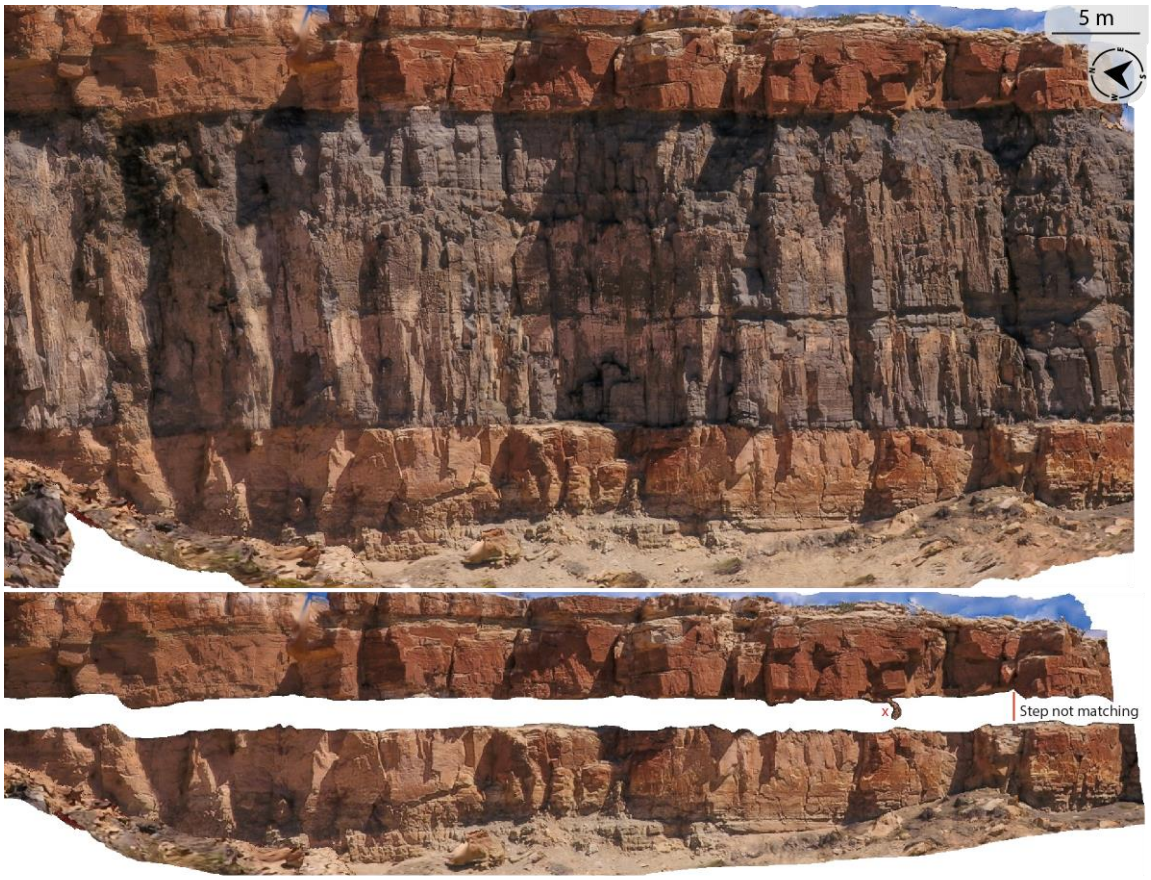

Fig. 6.3: Jack-up of host rock above the intrusion in 4NSW. The original image is at the top, and reconstructed pre-intrusion geometry obtained by removing the sill digitally in the image at the bottom. The top and bottom of the host rock does not display a perfect match, indicating that the sill has altered the host rock to an extent. Red cross means that the upper and lower strata does not match perfectly.

A section of 4NSW is shown in Fig. 6.3, where the original image is displayed on top, and the altered image is displayed at the bottom. This is a case where most of the top and bottom contact seem to fit, apart from the mismatch of the step (Fig. 6.3). Additionally, there is a section of the uppermost layer of the Curtis Formation that appears somewhat displaced, resembling a fragmented bridge of sorts. However, the underlying strata do not exhibit these characteristics.

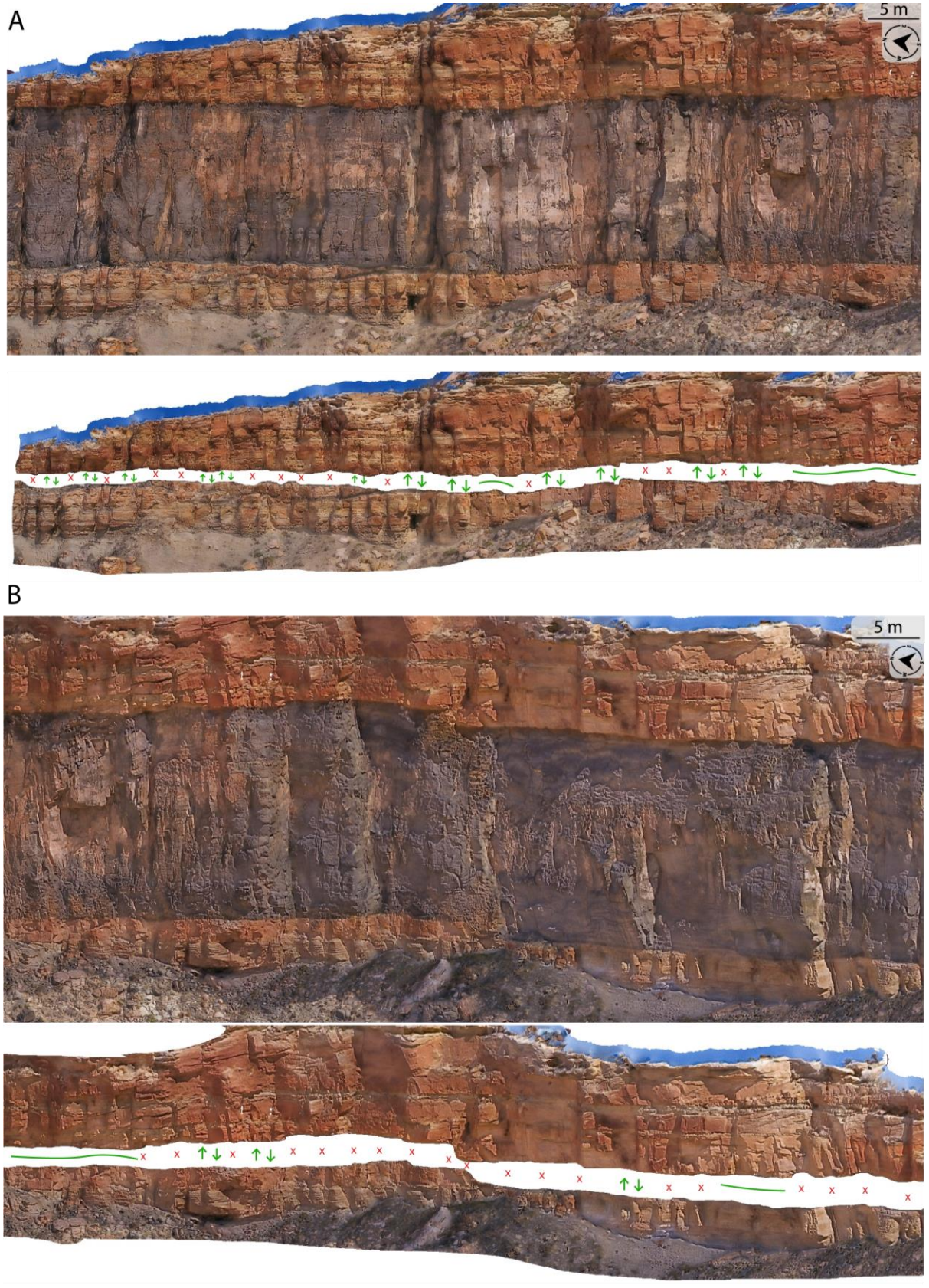

Fig. 6.4: Jack-up of host rock above the intrusion in 5SSW. (**A**) One section from 5SSW where the original image is at the top, and the reconstructed pre-intrusion geometry obtained by removing the sill digitally in the image at the bottom. (**B**) A different section displayed from 5SSW. In both cases, the top and bottom of the host rock does

not display a perfect match, indicating that the sill has altered the host rock to an extent. Red cross means that the upper and lower strata does not match perfectly, whereas the green arrows/lines indicate a good match.

Fig. 6.4 displays two different sections of 5SSW, with original images at the top, and altered images at the bottom. In Fig. 6.4A, there are visible steps and sill splays in the host rock strata. There is also an observation of a possible broken bridge in the top layer. This is another example of the sedimentary strata not matching perfectly overall. Nonetheless, there are many sections seeming to fit perfectly (green arrows). An interesting observation in the section in Fig. 6.4A is that in one of the steps visible, it seems like the strata would fit perfectly, however, it appears like the top layers have been moved to the left relative to the bottom layer. This is also the case in Fig. 6.4B, where a step is visible in the middle of the lower layer. The shape of the strata in the step, both above and underneath, display an almost perfect match. However, like in Fig. 6.4A, the top layer appears to have undergone a leftward displacement.

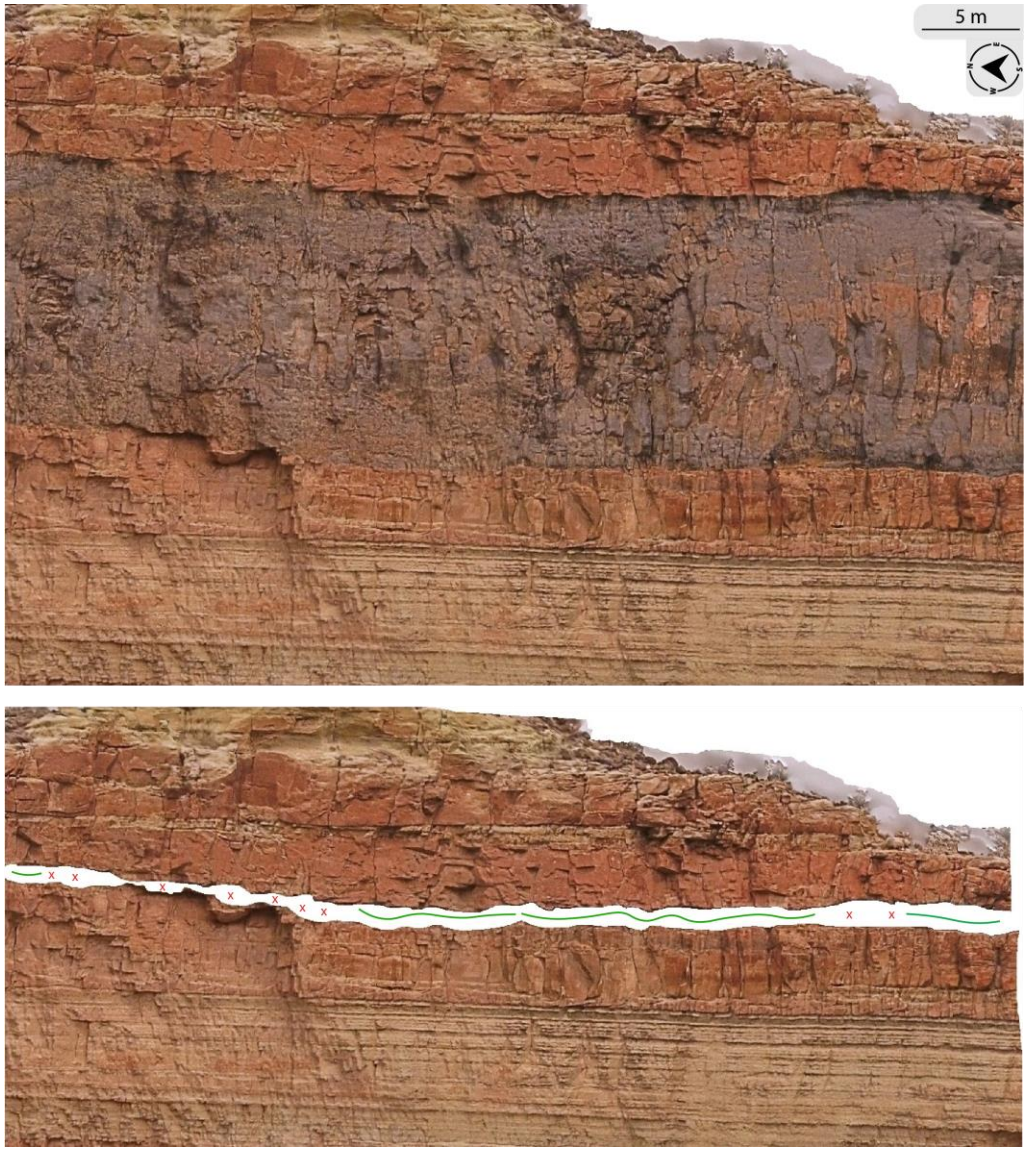

Fig. 6.5: Jack-up of host rock above the intrusion in 6NSW. Original image is at the top, and reconstructed pre-intrusion geometry obtained by removing the sill digitally in the image at the bottom. The top and bottom of the host rock does not display a perfect match, indicating that the sill has altered the host rock to an extent. Red cross means that the upper and lower strata does not match perfectly, whereas the green arrows/lines indicate a good match.

A section in 6NSW is depicted in Fig. 6.5, also displaying an original photo as well as an altered image underneath. In this case, the sedimentary strata above and underneath the sill appear to display several dissimilarities. While a few regions appear to align seamlessly, the majority of areas do not exhibit a perfect match. However, they seem to match to a certain extent. There are several steps visible, where none of them fit the sedimentary strata. In one instance, it appears as if there is a subsidence in the bottom layer, which is not traceable to the top layer.

The figures presented in this subchapter display different sill emplacement structures in the Mussentuchit Wash Sill, developed by brittle deformation processes, such as broken bridges

and steps. In each of the showcased models there was a mismatch between the upper and lower layer. This indicated deformation on the host rock. However, the strata above and underneath do not display thrust faults or appear extensively deformed. Some areas can have poorly imaged data, which can affect the results. The deformation on a small (maximum a few m) scale, and only along the sill boundary. This indicates that at the time of the intrusion, the small fragments of host rock were released along discontinuities and incorporated into the magma. This can also be the case for the broken bridges in Fig. 6.2. The broken bridges in the top and bottom layer do not match, and that might be due to the host rock being incorporated and transported with the magma. This can happen for example if smaller splays intrude between layers of the host rock and break it apart. From afar, the Mussentuchit Wash Sill does not look deformed by the sill. It looks like the intrusion has simply emplaced itself and lifted the Curtis Formation without deforming it. Nonetheless, this is not the case in the Mussentuchit Wash, as discussed in the figures above. Also, there are indications of the sedimentary strata not aligning fully in multiple occurrences. Moreover, there are signs of the sill intruding the Curtis Formation, lifting the strata of the host rock, and then pushing it towards the north.

6.2.2 Morphology of the sill in different facies

This subchapter aims to discuss the morphology of the sill in the sedimentary facies of the Curtis Formation. Due to the varied resolutions of the different 3D virtual outcrop models, the ability to identify individual facies and differentiate facies association in a comprehensive manner is limited. Nevertheless, the distinction of the sedimentary strata within the Curtis Formation has been achieved through the differentiation of dune-dominated sandstone, plane bedding-dominated sandstone, mud-rich layers, and heterolithic layers.

As presented in Chapter 5, the contacts between sill/host rock in Mussentuchit Wash are predominately strata-concordant and follow layer boundaries. This is a strong indication of the Curtis Formation being fully cemented at the time of the intrusion, as well as displaying high shear cohesion. The Curtis Formation was buried at depths between 2.45 and 2.86 km (Nuccio & Condon, 1996), which supports the claim that the sandstone was cemented at the time of intrusion. Due to this, the Mussentuchit Wash Sill deformed the host rock in a brittle manner. Mechanical strength of the host rock influences the sill emplacement structures, and this has been investigated in earlier studies (Kavanagh et al., 2017). The layering of the host rock, as well as local sedimentary structure may be utilized by the intrusion. This is depicted as local

sedimentary bedding (Fig. 5.15B & F), and crossbedding and ripple structures (Fig. 5.15C & E). In both cases, these beddings are used as pathways for the intrusion.

There have been observed irregular contacts as well in the study area (Fig. 5.15D & Fig. 6.6). This bedding propagation is not related to fracture-driven processes, but rather complex igneous textures. Kjenes et al. (2022) proposed that these were the result of fluidization and boiling of pore fluids at the time of intrusion. In the instances of irregular bedding contact, it appears as though the sill disregards bed boundaries (Fig. 6.6). In these cases, it does not appear that the sill is following the lithology on a large scale, but rather exploits local sedimentary heterogeneities. In areas where the sill is propagating along local crossbedding with mudstone-draped foresets, it is reasonable to assume that these foresets exhibit poor cementation and also low cohesive strength (Kjenes et al., 2022), making them susceptible to be exploited by the intrusion. Although there are several observations of the Mussentuchit Wash following mudstone draped foresets (Fig. 5.17), there is no evidence that this is the preferred pathway for the sill. This is evident in the numerous planar bedding contacts recorded in the study area (Fig. 5.15B).

Fig. 6.6: Irregular contact between the sill and the host rock.

As discussed in this subchapter, facies of the host rock control the morphology of the sill. Primarily, the sill appears to follow the bedding of strata, and is largely strata-concordant with the host rock. It follows mudstone-draped foresets as well as wave ripples, exploiting weaker sedimentary layers. Cemented sediments tend to advance brittle processes, such as bridges and steps (Pollard, 1973; Kavanagh et al., 2006), whereas insufficiently cemented sediments promote non-brittle emplacement mechanisms (Schofield et al., 2010, 2012; Spacapan et al., 2017). The Mussentuchit Wash Sill displays both mechanisms, but the non-brittle processes are

very rare and occur only locally, while brittle processes appear to have dominated during sill emplacement. Sedimentary structures and heterogeneities have a strong control on the local scale. However, on the large scale, the sill seems to propagate within the dune-dominated sandstone rather than the tidal flat and prodelta units, indicating that the sill does not always prefer mudstones as claimed by Eide, Schofield, et al. (2016). This sparks the discussion of why the sill avoided emplacement within the more mud-rich units of the Curtis Formation. Perhaps there is something about the sandstone or the mudstone that is either attracting or repelling the sill.

6.3 Processes controlling sill geometry

There have been many studies on sill geometry and what processes that control them (Francis, 1982; Thomson & Schofield, 2008; Schofield et al., 2012; Jackson et al., 2013; Eide, Schofield, et al., 2016). It is now widespread consensus that emplacement mechanisms and behavior of igneous sills are influenced by the lithology of the host rock (e.g. Schofield et al., 2012). These have mainly focused on sill emplacement mechanisms in mudstone and other clay-rich rocks. The upcoming subchapters will focus on discussing the factors influencing the intrusion of sills based on the lithology of the host rock. Furthermore, this discussion will encompass studies that specifically investigate sill intrusions in mudstone and explore the reasons behind its preference as a host rock. Additionally, relevant studies focused on sill intrusions in sandstone will be examined as well, facilitating a comparative analysis with the Mussentuchit Wash Sill.

The significance of examining the sill geometry in this study lies in recognizing the sill/host rock-contact, determining the extent to which the Mussentuchit Wash Sill conforms to the lithology of the Curtis Formation. It is also important to identify instances where it deviates from the expected lithology.

6.3.1 Previous studies on sill intrusions in mudstone

As aforementioned, the majority of previous studies on sill intrusions have focused on cases where the host rock consists of mudstone or clay-rich rocks (Eide, Schofield, et al., 2016; Spacapan et al., 2017; Mark et al., 2018). Eide et al (2016) conducted a study on the architecture of deeply emplaced sill complexes in Jameson Land, East Greenland. The investigated host rocks were sedimentary rocks from the Neill Klinter Group, specifically Early Jurassic

sandstones (poorly cemented, homogeneous sandstone), sandy heteroliths, and marine mudstone (Eide, Schofield, et al., 2016). The study revealed that the mudstones of the Albuen and Nathorst Fjeld members within the Neill Klinter Group were the intervals most frequently intruded.

The study's findings highlight the significant role of host rock lithology in determining sill morphology and emplacement locations. It is evident that the sills in the study area exhibit a preference for exploiting and occupying mudstones or discontinuities found between rocks of varying strength. Their findings also revealed that sills emplaced at greater depths (>1.5 km) typically exhibit planar geometries, in contrast to sills that are emplaced at more shallow levels. It is noteworthy that the Mussentuchit Wash Sill, which is emplaced at relatively shallow depths (around 0.8-1 km) (Delaney & Gartner, 1997), does not align with this observation. As presented in Chapter 5, the Mussentuchit Wash Sill displays predominately planar sill geometry. A possible reason for this can be that the Curtis Formation has been subjected to substantial amount of burial *prior to sill emplacement*, which led to quartz cementation and thus the diagenetic transition from sand to sandstone prior to the intrusion. After uplift and erosion, the rocks were still brittle, which might have led to planar intrusions and other brittle emplacement structures, rather than saucer-shaped intrusion and magma fingers. This might imply that the emplacement depth is less significant than what conditions the rocks are, i.e., brittle or ductile, cemented sandstone vs. unconsolidated sandstone. Due to the shallow emplacement of the Mussentuchit Wash Sill, one would expect predominant formation of emplacement structures would be a result of non-brittle processes, such as magma fingers (Schofield et al., 2012). This does not hold true to the Mussentuchit Wash Sill, where brittle deformation is prominent.

Mudstone is not a mechanically strong rock, and this might be the reason for the sill exploiting these layers. This can be due to the anisotropy of the mudstone, making it weak and due to the strong tensile strength. When magma is intruded into a host rock, the conduit will inflate due to the magma, and this will rupture and propagate the intrusion (Gudmundsson, 1990). According to Eide et al. (2021), clay-rich mudstones break easily along bedding planes, making it an easy target for intrusion. Tensile strength of the host rock (how much force the rock can withstand before breaking) has long been neglected, but it is proposed that this can have a great impact on emplacement of igneous intrusion (Eide et al., 2021). The measured tensile strength (in MPa) of mudstones is measured to be c. 300 times lower when measured parallel to the bedding plane compared to measurements taken perpendicular to the bedding plane (Q. Gao et

al., 2015). If mudstone demonstrates high tensile stress anisotropy, this phenomenon could elucidate its susceptibility to intrusion. The significant stress differential within mudstones can provide insight into their frequent susceptibility to intrusion. Furthermore, the strong anisotropy in tensile strength of mudstone could facilitate the creation of fractures within it, irrespective of the prevailing tectonic stress conditions.

6.3.2 To what extent does the sill follow host rock lithology?

This study has shown that most of the contacts between the Mussentuchit Wash Sill and the Curtis Formation follow layer boundaries and sedimentological discontinuities and are strata concordant. As mentioned in Subchapter 6.2.2, this is a good indicator of the sandstone being fully cemented at the time of the emplacement and made it possible for the sandstone to be deformed in a brittle manner. Intrusions at shallow depths often deform in a non-brittle manner, due to the host rock not being cemented enough (Jackson et al., 2013). If the host rock has been buried to great depths, such as the Curtis Formation, brittle deformation is indeed possible.

Crossbedding and local sedimentary discontinuities are utilized as passages for intrusion. The mudstone draped forests exhibit low cohesive strength, and this is due to the low cementation rate (Kjenes et al., 2022). Figures 6.6A & B illustrate cases in which the sill conforms to heterolithic bedding, aligning with the expectations based on prior studies of sill formations.

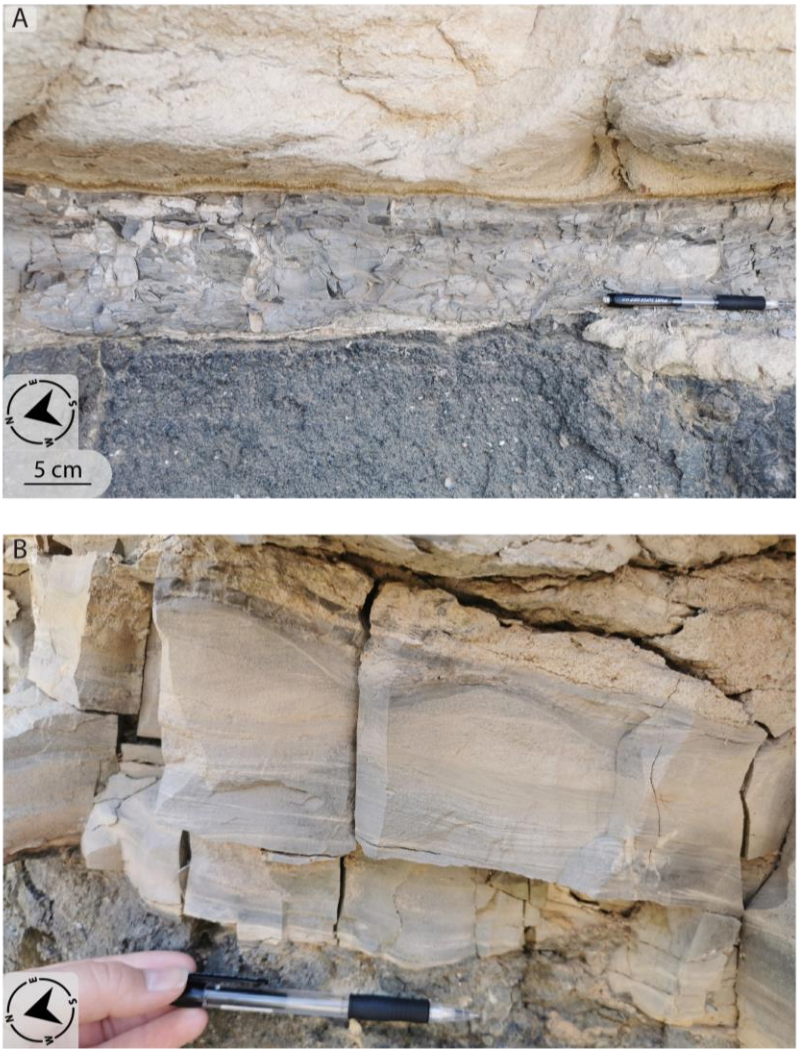

Fig. 6.7: Instances where the sill is following lithology and layer boundaries that is expected in term of earlier studies (Eide, Schofield, et al., 2016; Mark et al., 2018). (A) The sill exhibits planar contact with the Curtis Formation, following a mud-rich layer. (B) Sill following a heterolithic layer presented in Subchapter 5.2.1.

Based on the observations presented in Chapter 5, as well as the paragraphs discussed in this subchapter, it is reasonable to conclude that the Mussentuchit Wash Sill conforms to the overall lithology of the Curtis Formation. As previously stated, it displays a planar geometry on a large scale and most deviations occur at smaller scales. This will be discussed in the subchapter below, Subchapter 6.3.4.

6.3.3 Deviations from host rock lithology

The Mussentuchit Wash Sill follows host rock lithology to a great extent, nevertheless, there are several instances where the emplacement structures of the sill deviate from the expected. Such an example has been observed in a figure presented in Subchapter 5.3.2, where the sill follows the mudstone-draped foreset, before it abruptly changes layer (Fig. 5.17). There are

also several instances where the sill decides to leave the heterolithic bedding it is already following and go to the sandstone layer underneath (Fig. 6.5C). This is not expected, due to the findings of this thesis and several other studies (e.g. (Eide, Schofield, et al., 2016; Mark et al., 2018)) observing that sills often prefer to be emplaced in mudstone (Eide, Schofield, et al., 2016; Mark et al., 2018). This can indicate that the sill has different preferences on a large scale vs. on a small scale. In large scale, the Mussentuchit Wash Sill exhibits a planar characteristic, emplaced in sandstone layers and following the sedimentary boundaries. This is evident throughout the entire Mussentuchit Wash (Fig. 5.11 & 5.12). On a smaller scale, however, the sill tends to prefer weak layers such as mudstone-draped foresets. It follows these weak layers for a short distance until it abandons it in favor of a weak layer that conforms better to the overall shape the sill prefers, which is the crossbedding in the sandstone layer.

An interesting observation is presented in Fig. 6.5A, where the sill shows a step where it has thin deposits of heterolithic and or mud-rich sedimentary rock nearby, it does not exploit them. In Fig. 6.5B, a splay is depicted. Here, the sill appears to be following the bed boundary and the mudstone-draped crossbeds before it abruptly transgresses and intrudes into the sandstone layer. This layer is mud-rich, as several mud chips are present, making it seem like it intruded into FA3 (tidal channel facies association). Fig. 6.7C depicts an instance where the sill seems to be following a heterolithic layer, however, it also wants to follow the sandstone layer. There are also instances on a detail-scale where there are small splays moving regardless of the lithology of the host rock (Fig. 6.5D). This figure portrays a minor splay ascending through both the sandstone and heterolithic layers. What might have been expected was that the sill would intrude in the heterolithic layer, and then transgress downwards to the sides and conform to that layer.

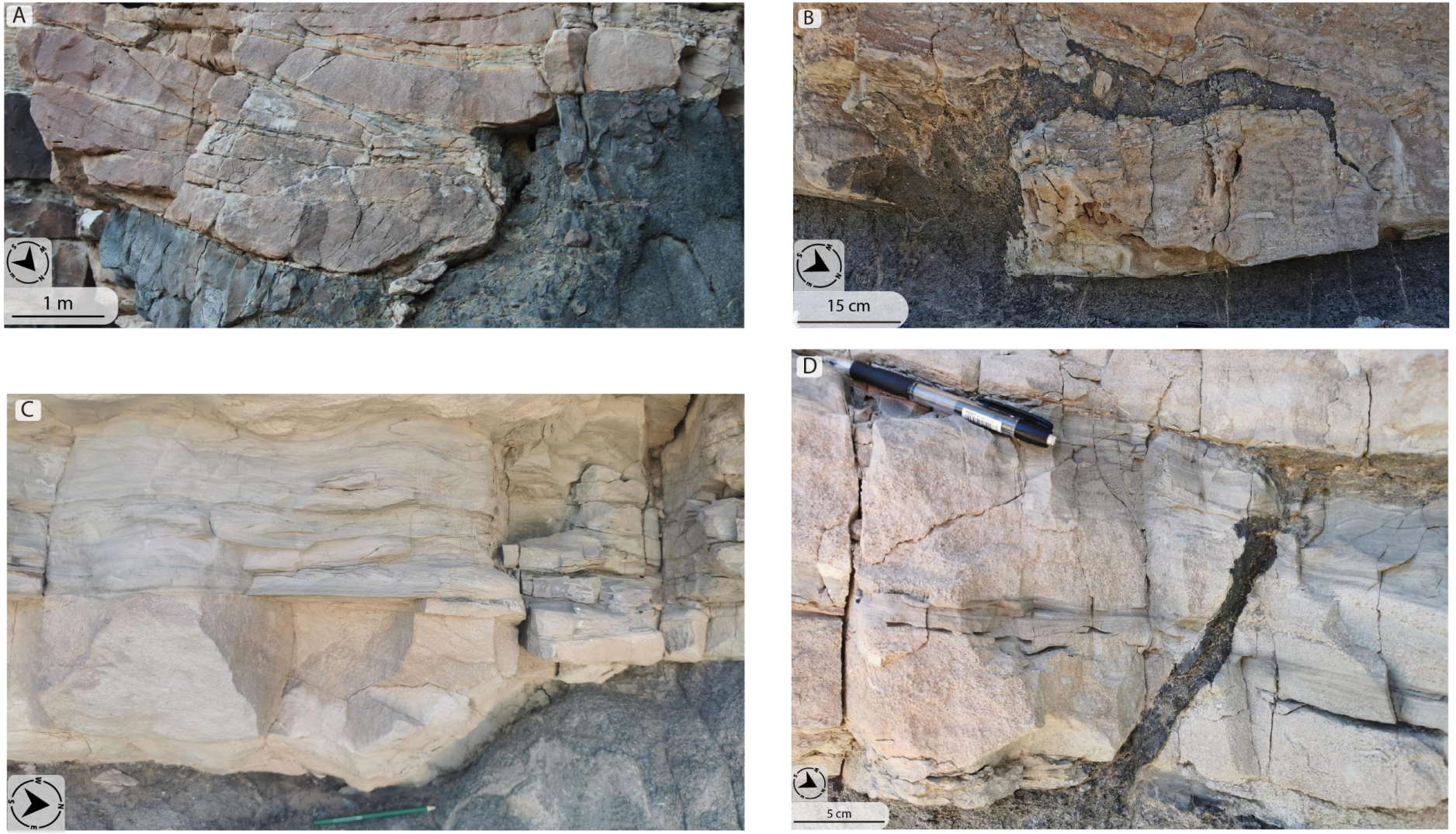

Fig. 6.8: Deviations from expected lithology. (**A**) Sill displaying a step and not choosing to move in the heterolithic facies. (**B**) The sill is exhibiting a chaotic splay, where the rest seems to follow local crossbedding. (**C**) The sill is following the heterolithic layer, but then it suddenly decides to leave the heterolithic layer and continue in the sandstone layer. (**D**) Small splay intruding through sandstone and heterolithic layer.

7.0 Summary and conclusions

This study has presented the observations of the Mussentuchit Wash Sill in SE Utah, emplaced in the Curtis Formation of the San Rafael Group. The interaction between the host rock and the sill has been investigated in a world-class exposure imaged in a virtual outcrop, displaying a c. 15 m thick sill. The Curtis Formation has been studied by investigating virtual outcrops combined with sedimentological field work. The detailed resolution of the models has allowed for the geometry and emplacement relationships of sill intrusions to be investigated. The results presented in this study and subsequent discussion emit the following conclusions about interaction between igneous intrusions and their host rocks:

- The Mussentuchit Wash Sill is predominately strata-concordant with the host rock, the Curtis Formation, and it exhibits numerous brittle deformation structures such as broken bridges and steps.
- Investigations of the sill/host rock interplay show that the architecture and geometry of the Mussentuchit Wash Sill is strongly controlled by host rock lithology on a larger scale, where they tend to follow sedimentary layers. On a smaller scale, the sill architecture is predominately controlled by weak mudstone beds, such as mudstone-draped foresets.
- Contrary to previous studies, igneous sills do not exclusively prefer to be emplaced in mudstone layers or clay-rich layers. The Mussentuchit Wash Sill is shown to prefer dune-dominated sandstone even though there are mudstone layers present.
- This study has shown that the properties of the host rock, such as mechanical strength or cementation state, can potentially outweigh the significance of emplacement depths. The Mussentuchit Wash Sill is a shallow emplaced intrusion that predominately displays brittle deformation processes and exhibits a planar geometry.

8.0 Further work

This thesis has provided a new and comprehensive study on the interaction between igneous sills and their host rocks. Nevertheless, there remain subjects requiring further research on the interaction between the host rock and sill in general that could enhance the comprehensiveness of this topic.

For further work, something that can enhance the comprehension of the interaction between host rocks and igneous intrusions would be to conduct microscopic analyses and investigate the petrophysical characteristics of the host rock. This can be used to see if the igneous intrusion has altered the host rock on a mineralogical scale, to figure out why the Mussentuchit Wash Sill prefers to stay emplaced in the sandstone units, and not in the tidal flat and prodelta units, and to investigate if there is something in particular about the mudstones in the Curtis Formations that makes them unviable to large-scale sill propagation.

Investigating the cementation of the sandstone will also be interesting, to see if the cementation of the host rock affects the intrusion. Examining to what extent quartz cementation compared to carbonate cementation matters for the emplacement of intrusion would be one important topic. In addition to investigating the cementation, getting more accurate data on burial depth in the Mussentuchit Wash would be interesting.

Numerous extensive investigations have been conducted concerning the sedimentology of the Curtis Formation; however, there are no other studies focusing specifically on the interplay between the Curtis Formation and the Mussentuchit Wash Sill. Therefore, acquiring additional sedimentological logs could enhance the comprehension of the dynamic between the sill and its host rock.

Getting a comprehensive understanding of the sills and dykes complex in the San Rafael Swell would hold significant interest. To perform this, seismic data in the area could aid the comprehension of the sills and determining the shape of them (saucer-shaped, planar etc.). Getting seismic of the area could potentially give insight into the source of the magmatism in the area as well.

Bibliography

Agisoft, M. (2023). *Agisoft User Manual: Professional Edition* (2.0) [Computer software].

Ágústsdóttir, T., Woods, J., Greenfield, T., Green, R. G., White, R. S., Winder, T., Brandsdóttir, B., Steinthórsson, S., & Soosalu, H. (2016). Strike-slip faulting during the 2014 Bárðarbunga-Holuhraun dike intrusion, central Iceland. *Geophysical Research Letters*, *43*(4), 1495–1503. https://doi.org/10.1002/2015GL067423

Amos, C. L. (1995). Chapter 10 Siliciclastic Tidal Flats. In G. M. E. Perillo (Ed.), *Developments in Sedimentology* (Vol. 53, pp. 273–306). Elsevier. https://doi.org/10.1016/S0070-4571(05)80030-5

Bjerrum, C. J., & Dorsey, R. J. (1995). Tectonic controls on deposition of Middle Jurassic strata in a retroarc foreland basin, Utah-Idaho trough, western interior, United States. *Tectonics*, *14*(4), 962–978.

Blakey, R. C. (2019). Chapter 7—Pennsylvanian-Jurassic Sedimentary Basins of the Colorado Plateau and Southern Rocky Mountains. In A. D. Miall (Ed.), *The Sedimentary Basins of the United States and Canada (Second Edition)* (pp. 315–367). Elsevier. https://doi.org/10.1016/B978-0-444-63895-3.00007-3

Blakey, R. C., & Ranney, W. D. (2018a). Flat-Slab Subduction, the Laramide Orogeny, Uplift of the Colorado Plateau and Rocky Mountains: Paleocene and Eocene: Ca. 65–35 Ma. In R. C. Blakey & W. D. Ranney (Eds.), *Ancient Landscapes of Western North America: A Geologic History with Paleogeographic Maps* (pp. 131–148). Springer International Publishing. https://doi.org/10.1007/978-3-319-59636-5_9

Blakey, R. C., & Ranney, W. D. (2018b). The Arrival of Wrangellia and the Nevadan Orogeny: Late Triassic to Late Jurassic: Ca. 240–145 Ma. In R. C. Blakey & W. D. Ranney (Eds.), *Ancient Landscapes of Western North America: A Geologic History with Paleogeographic Maps* (pp. 89–101). Springer International Publishing. https://doi.org/10.1007/978-3-319-59636-5_7

Buckley, S. J., Ringdal, K., Naumann, N., Dolva, B., Kurz, T. H., Howell, J. A., & Dewez, T. J. B. (2019). LIME: Software for 3-D visualization, interpretation, and communication of virtual geoscience models. *Geosphere*, *15*(1), 222–235. https://doi.org/10.1130/GES02002.1

Bump, A., & Davis, G. (2003). Late Cretaceous–early Tertiary Laramide deformation of the northern Colorado Plateau, Utah and Colorado. *Journal of Structural Geology*, *25*, 421–440. https://doi.org/10.1016/S0191-8141(02)00033-0

Caputo, M., & Pryor, W. (1991). Middle Jurassic Tide- and Wave-influenced Coastal Facies and Paleogeography, Upper San Rafael Group, East-central Utah. *Utah Geological Association 1991 Field Symposium*, *Publication 19*, 9–28.

Dalrymple, R. W. (1992). Tidal Depositional Systems. *Facies Models Response to Sea-Level Change.*, 195–218.

Davis Jr., R. A. (2012). Tidal Signatures and Their Preservation Potential in Stratigraphic Sequences. In *Principles of Tidal Sedimentology* (pp. 35–55). https://doi.org/10.1007/978-94-007-0123-6_3

Delaney, P. T., & Gartner, A. E. (1997). Physical processes of shallow mafic dike emplacement near the San Rafael Swell, Utah. *GSA Bulletin*, *109*(9), 1177–1192. https://doi.org/10.1130/0016-7606(1997)109<1177:PPOSMD>2.3.CO;2

Demko, T. M., Currie, B. S., & Nicoll, K. A. (2004). Regional paleoclimatic and stratigraphic implications of paleosols and fluvial/overbank architecture in the Morrison Formation (Upper Jurassic), Western Interior, USA. *Sedimentary Geology*, *167*(3), 115–135. https://doi.org/10.1016/j.sedgeo.2004.01.003

Díez, M., Connor, C. B., Kruse, S. E., Connor, L., & Savov, I. P. (2009). Evidence of small-volume igneous diapirism in the shallow crust of the Colorado Plateau, San Rafael Desert, Utah. *Lithosphere*, *1*(6), 328–336. https://doi.org/10.1130/L61.1

Duffield, W. A., Bacon, C. R., & Delaney, P. T. (1986). Deformation of poorly consolidated sediment during shallow emplacement of a basalt sill, Coso Range, California. *Bulletin of Volcanology*, *48*, 97–107. https://doi.org/10.1007/BF01046545

Eide, C. H., Howell, J. A., Buckley, S. J., Martinius, A. W., Oftedal, B. T., & Henstra, G. A. (2016). Facies model for a coarse-grained, tide-influenced delta: Gule Horn Formation (Early Jurassic), Jameson Land, Greenland. *Sedimentology*, *63*(6), 1474–1506. https://doi.org/10.1111/sed.12270

Eide, C. H., Schofield, N., Howell, J. A., & Jerram, D. A. (2021). Transport of mafic magma through the crust and sedimentary basins: Jameson Land, East Greenland. *Journal of the Geological Society*, *179*(3), jgs2021-043. https://doi.org/10.1144/jgs2021-043

Eide, C. H., Schofield, N., Jerram, D. A., & Howell, J. A. (2016). Basin-scale architecture of deeply emplaced sill complexes: Jameson Land, East Greenland. *Journal of the Geological Society*, *174*(1), 23–40. https://doi.org/10.1144/jgs2016-018

Eide, C. H., Schofield, N., Lecomte, I., Buckley, S. J., & Howell, J. A. (2018). Seismic interpretation of sill complexes in sedimentary basins: Implications for the sub-sill imaging problem. *Journal of the Geological Society*, *175*(2), 193–209. https://doi.org/10.1144/jgs2017-096

Fan, D., Yuan, W., & Min, L. (2013). Classifications, sedimentary features and facies associations of tidal flats. *Journal of Palaeogeography*, *2*(1), 66–80. https://doi.org/10.3724/SP.J.1261.2013.00018

Farmin, R. (1941). Host-rock inflation by veins and dikes at Grass Valley. California. *Econ. Geol.*, *36*, 143–174.

Francis, E. H. (1982). Magma and sediment-I Emplacement mechanism of late Carboniferous tholeiite sills in northern Britain. *Journal of the Geological Society*, *139*(1), 1–20. https://doi.org/10.1144/gsjgs.139.1.0001

Galland, O., Bertelsen, H. S., Eide, C. H., Guldstrand, F., Haug, Ø. T., Leanza, H. A., Mair, K., Palma, O., Planke, S., Rabbel, O., Rogers, B., Schmiedel, T., Souche, A., & Spacapan, J. B. (2018). Chapter 5—Storage and Transport of Magma in the Layered Crust—Formation of Sills and Related Flat-Lying Intrusions. In S. Burchardt (Ed.), *Volcanic and Igneous Plumbing Systems* (pp. 113–138). Elsevier. https://doi.org/10.1016/B978-0-12-809749-6.00005-4

Galloway, W. (1975). Process framework for describing the morphologic and stratigraphic evolution of deltaic depositional system. *Society of Economic Paleontologists and Mineralogist (SEPM), Special Publication No. 31*, 127–156.

Gao, Q., Tao, J., Hu, J., & Yu, X. (Bill). (2015). Laboratory study on the mechanical behaviors of an anisotropic shale rock. *Journal of Rock Mechanics and Geotechnical Engineering*, *7*(2), 213–219. https://doi.org/10.1016/j.jrmge.2015.03.003

Gao, S. (2019). Chapter 10—Geomorphology and Sedimentology of Tidal Flats. In G. M. E. Perillo, E. Wolanski, D. R. Cahoon, & C. S. Hopkinson (Eds.), *Coastal Wetlands (Second Edition)* (pp. 359–381). Elsevier. https://doi.org/10.1016/B978-0-444-63893-9.00010-1

Gardiner, D., Schofield, N., Finlay, A., Mark, N., Holt, L., Grove, C., Forster, C., & Moore, J. (2019). Modeling petroleum expulsion in sedimentary basins: The importance of igneous intrusion timing and basement composition. *Geology*, *47*(10), 904–908. https://doi.org/10.1130/G46578.1

Germa, A., Koebli, D., Wetmore, P., Atlas, Z., Arias, A., Savov, I. P., Diez, M., Greaves, V., & Gallant, E. (2020). Crystallization and Segregation of Syenite in Shallow Mafic Sills: Insights from the San Rafael Subvolcanic Field, Utah. *Journal of Petrology*, *61*(9), egaa092. https://doi.org/10.1093/petrology/egaa092

Gilluly, J., & Reeside, J. B. (1928). Sedimentary rocks of the San Rafael Swell and some adjacent areas in eastern Utah. *Professional Paper*, Article 150-D. https://doi.org/10.3133/pp150D

Gonzales, D. A., & Lake, E. T. (2017). Geochemical constraints on mantle-melt sources for Oligocene to Pleistocene mafic rocks in the Four Corners region, USA. *Geosphere*, *13*(1), 201–226. https://doi.org/10.1130/GES01314.1

Gudmundsson, A. (1990). Emplacement of dikes, sills and crustal magma chambers at divergent plate boundaries. *Tectonophysics*, *176*(3), 257–275. https://doi.org/10.1016/0040-1951(90)90073-H

Haug, Ø. T., Galland, O., Souloumiac, P., Souche, A., Guldstrand, F., Schmiedel, T., & Maillot, B. (2018). Shear Versus Tensile Failure Mechanisms Induced by Sill Intrusions: Implications for Emplacement of Conical and Saucer-Shaped Intrusions. *Journal of Geophysical Research: Solid Earth*, *123*(5), 3430–3449. https://doi.org/10.1002/2017JB015196

Hughes, Z. J. (2012). Tidal Channels on Tidal Flats and Marshes. In R. A. Davis Jr. & R. W. Dalrymple (Eds.), *Principles of Tidal Sedimentology* (pp. 269–300). Springer Netherlands. https://doi.org/10.1007/978-94-007-0123-6_11

Humphreys, E. D. (1995). Post-Laramide removal of the Farallon slab, western United States. *Geology*, *23*(11), 987–990. https://doi.org/10.1130/0091-7613(1995)023<0987:PLROTF>2.3.CO;2

Hutton, D. (2009). Insights into magmatism in volcanic margins: Bridge structures and a new mechanism of basic sill emplacement - Theron Mountains, Antarctica. *Petroleum Geoscience - PETROL GEOSCI*, *15*, 269–278. https://doi.org/10.1144/1354-079309-841

Ichaso, A. A., & Dalrymple, R. W. (2014). Eustatic, tectonic and climatic controls on an early syn-rift mixed-energy delta, Tilje Formation (Early Jurassic, Smørbukk field, offshore mid-Norway). In *From Depositional Systems to Sedimentary Successions on the Norwegian Continental Margin* (pp. 339–388). John Wiley & Sons, Ltd. https://doi.org/10.1002/9781118920435.ch13

Jackson, C., Schofield, N., & Golenkov, B. (2013). Geometry and controls on the development of igneous sill-related forced folds: A 2-D seismic reflection case study from offshore southern Australia. *Geological Society of America Bulletin*, *125*, 1874–1890. https://doi.org/10.1130/B30833.1

Jerram, D., & Bryan, S. (2015). Plumbing Systems of Shallow Level Intrusive Complexes. In *Advances in Volcanology*. https://doi.org/10.1007/11157_2015_8

Jorissen, E. L., de Leeuw, A., van Baak, C. G. C., Mandic, O., Stoica, M., Abels, H. A., & Krijgsman, W. (2018). Sedimentary architecture and depositional controls of a Pliocene river-dominated delta in the semi-isolated Dacian Basin, Black Sea. *Sedimentary Geology*, *368*, 1–23. https://doi.org/10.1016/j.sedgeo.2018.03.001

Kavanagh, J. L., Menand, T., & Sparks, R. S. J. (2006). An experimental investigation of sill formation and propagation in layered elastic media. *Earth and Planetary Science Letters*, *245*(3), 799–813. https://doi.org/10.1016/j.epsl.2006.03.025

Kavanagh, J. L., Rogers, B. D., Boutelier, D., & Cruden, A. R. (2017). Controls on sill and dyke-sill hybrid geometry and propagation in the crust: The role of fracture toughness. *Tectonophysics*, *698*, 109–120. https://doi.org/10.1016/j.tecto.2016.12.027

Kjenes, M., Eide, C. H., Schofield, N., & Chedburn, L. (2022). Alkaline sill intrusions in sedimentary basins: Emplacement of the Mussentuchit Wash Sill in San Rafael Swell, Utah. *Journal of the Geological Society*, *180*(1), jgs2021-139. https://doi.org/10.1144/jgs2021-139

Klein, G. deVries. (1985). Intertidal Flats and Intertidal Sand Bodies. In R. A. Davis (Ed.), *Coastal Sedimentary Environments* (pp. 187–224). Springer. https://doi.org/10.1007/978-1-4612-5078-4_3

Kreisa, R. D., & Moiola, R. J. (1986). Sigmoidal tidal bundles and other tide-generated sedimentary structures of the Curtis Formation, Utah. *GSA Bulletin*, *97*(4), 381–387. https://doi.org/10.1130/0016-7606(1986)97<381:STBAOT>2.0.CO;2

Magee, C., D., M., Karvelas, A., Holford, S., Jackson, C., Bastow, I., Schofield, N., Stevenson, C., Mclean, C., Mccarthy, W., & Shtukert, O. (2016). Lateral Magma Flow in Mafic Sill-complexes. *Acta Geologica Sinica - English Edition*, *90*, 4–5. https://doi.org/10.1111/1755-6724.12848

Mark, N. J., Schofield, N., Pugliese, S., Watson, D., Holford, S., Muirhead, D., Brown, R., & Healy, D. (2018). Igneous intrusions in the Faroe Shetland basin and their implications for hydrocarbon exploration; new insights from well and seismic data. *Marine and Petroleum Geology*, *92*, 733–753. https://doi.org/10.1016/j.marpetgeo.2017.12.005

Nicholson, R., & Pollard, D. D. (1985). Dilation and linkage of echelon cracks. *Journal of Structural Geology*, *7*(5), 583–590. https://doi.org/10.1016/0191-8141(85)90030-6

Nuccio, V. F., & Condon, S. M. (1996). *Burial and Thermal History of the Paradox Basin, Utah and Colorado, and Petroleum Potential of the Middle Pennsylvanian Paradox Formation* (United States - Colorado; Report USGS Bulletin 2000-O). Geological Survey (U.S.). https://digital.library.unt.edu/ark:/67531/metadc304484/

Nyberg, B., & Howell, J. A. (2016). Global distribution of modern shallow marine shorelines. Implications for exploration and reservoir analogue studies. *Marine and Petroleum Geology*, *71*, 83–104. https://doi.org/10.1016/j.marpetgeo.2015.11.025

Pipiringos, G. N., & O'Sullivan, R. B. (1978). Principal unconformities in Triassic and Jurassic rocks, western interior United States—A preliminary survey. In *Principal unconformities in Triassic and Jurassic rocks, western interior United States—A preliminary survey* (USGS Numbered Series 1035-A; Professional Paper, Vols. 1035-A, p. 35). United States Government Printing Office. https://doi.org/10.3133/pp1035A

Planke, S., Rasmussen, T., Rey, S. S., & Myklebust, R. (2005). Seismic characteristics and distribution of volcanic intrusions and hydrothermal vent complexes in the Vøring and Møre basins. *Geological Society, London, Petroleum Geology Conference Series*, *6*(1), 833–844. https://doi.org/10.1144/0060833

Pollard, D. D. (1973). Derivation and evaluation of a mechanical model for sheet intrusions. *Tectonophysics*, *19*(3), 233–269. https://doi.org/10.1016/0040-1951(73)90021-8

Pollard, D. D., Muller, O. H., & Dockstader, D. R. (1975). The Form and Growth of Fingered Sheet Intrusions. *GSA Bulletin*, *86*(3), 351–363. https://doi.org/10.1130/0016-7606(1975)86<351:TFAGOF>2.0.CO;2

Reineck, H.-E. (1967). *Layered sediments of tidal flats, beaches, and shelf bottoms of the North Sea*.

Reineck, H.-E., & Singh, I. B. (1980). *Depositional Sedimentary Environments*. Springer. https://doi.org/10.1007/978-3-642-81498-3

Reineck, H.-E., & Wunderlich, F. (1968). Classification and Origin of Flaser and Lenticular Bedding. *Sedimentology*, *11*(1–2), 99–104. https://doi.org/10.1111/j.1365-3091.1968.tb00843.x

Richardson, J. A., Connor, C. B., Wetmore, P. H., Connor, L. J., & Gallant, E. A. (2015). Role of sills in the development of volcanic fields: Insights from lidar mapping surveys of the San Rafael Swell, Utah. *Geology*, *43*(11), 1023–1026. https://doi.org/10.1130/G37094.1

Rickwood, P. C. (1990). *The anatomy of a dyke and the determination of propagation and, magma flow directions* (Mafic Dykes and Emplacement Mechanisms). Parker, A.J., Rickwood, P.C. & Tucker, D.H. (eds).

Schmiedel, T., Galland, O., & Breitkreuz, C. (2017). Dynamics of Sill and Laccolith Emplacement in the Brittle Crust: Role of Host Rock Strength and Deformation Mode. *Journal of Geophysical Research: Solid Earth*, *122*(11), 8860–8871. https://doi.org/10.1002/2017JB014468

Schofield, N., Brown, D., Magee, C., & Stevenson, C. (2012). Sill morphology and comparison of brittle and non-brittle emplacement mechanisms. *Journal of the Geological Society*, *169*, 127–141. https://doi.org/10.1144/0016-76492011-078

Schofield, N., Stevenson, C., & Reston, T. (2010). Magma fingers and host rock fluidization in the emplacement of sills. *Geology*, *38*(1), 63–66. https://doi.org/10.1130/G30142.1

Smyrak-Sikora, A., Osmundsen, P. T., Braathen, A., Ogata, K., Anell, I. M., Mulrooney, M. J., & Zuchuat, V. (2019). Architecture of growth basins in a tidally influenced, prodelta to delta-front setting: The Triassic succession of Kvalpynten, East Svalbard. *30*. https://doi.org/10.1111/bre.12410

Spacapan, J., Galland, O., Leanza, H., & Planke, S. (2017). Igneous sill and finger emplacement mechanism in shale-dominated formations: A field study at Cuesta del

Chihuido, Neuquén Basin, Argentina. *Journal of the Geological Society*, *174*, jgs2016-056. https://doi.org/10.1144/jgs2016-056

Terwindt, J. H. J., & Breusers, H. N. C. (1972). Experiments on the Origin of Flaser, Lenticular and Sand-Clay Alternating Bedding. *Sedimentology*, *19*(1–2), 85–98. https://doi.org/10.1111/j.1365-3091.1972.tb00237.x

Thompson, G. A., & Zoback, M. L. (1979). Regional geophysics of the Colorado Plateau. *Tectonophysics*, *61*(1), 149–181. https://doi.org/10.1016/0040-1951(79)90296-8

Thomson, K., & Schofield, N. (2008). Lithological and structural controls on the emplacement and morphology of sills in sedimentary basins. *Geological Society, London, Special Publications*, *302*(1), 31–44. https://doi.org/10.1144/SP302.3

Tibaldi, A. (2015). Structure of volcano plumbing systems: A review of multi-parametric effects. *Journal of Volcanology and Geothermal Research*, *298*. https://doi.org/10.1016/j.jvolgeores.2015.03.023

Tibaldi, A., & Pasquarè, F. A. (2008). A new mode of inner volcano growth: The "flower intrusive structure." *Earth and Planetary Science Letters*, *271*(1), 202–208. https://doi.org/10.1016/j.epsl.2008.04.009

Tingey, D. G., Christiansen, E. H., Best, M. G., Ruiz, J., & Lux, D. R. (1991). Tertiary minette and melanephelinite dikes, Wasatch Plateau, Utah: Records of mantle heterogeneities and changing tectonics. *Journal of Geophysical Research: Solid Earth*, *96*(B8), 13529–13544. https://doi.org/10.1029/91JB00327

Turcotte, D. L., & Oxburgh, E. R. (1978). Intra-plate volcanism. *Philosophical Transactions of the Royal Society of London. Series A, Mathematical and Physical Sciences*, *288*(1355), 561–579. https://doi.org/10.1098/rsta.1978.0034

van Straaten, L. M. J. U. (1954). Composition and structure of recent marine sediments in the Netherlands. *Leidse Geologische Mededelingen*, *19*(1), 1–108.

Vigneresse, J. L., & Clemens, J. D. (2000). Granitic magma ascent and emplacement: Neither diapirism nor neutral buoyancy. *Geological Society, London, Special Publications*, *174*(1), 1–19. https://doi.org/10.1144/GSL.SP.1999.174.01.01

Visser, M. J. (1980). Neap-spring cycles reflected in Holocene subtidal large-scale bedform deposits: A preliminary note. *Geology*, *8*(11), 543–546. https://doi.org/10.1130/0091-7613(1980)8<543:NCRIHS>2.0.CO;2

Wentworth, C. K. (1922). A Scale of Grade and Class Terms for Clastic Sediments. *The Journal of Geology*, *30*(5), 377–392.

Williams, S. N. (1983). Plinian airfall deposits of basaltic composition. *Geology*, *11*(4), 211–214. https://doi.org/10.1130/0091-7613(1983)11<211:PADOBC>2.0.CO;2

Yoshida, S., Steel, R., & Dalrymple, R. (2007). Changes in Depositional Processes—An Ingredient in a New Generation of Sequence-Stratigraphic Models. *Journal of Sedimentary Research - J SEDIMENT RES*, *77*, 447–460. https://doi.org/10.2110/jsr.2007.048

Zuchuat, V., Sleveland, A. R. N., Pettigrew, R. P., Dodd, T. J. H., Clarke, S. M., Rabbel, O., Braathen, A., & Midtkandal, I. (2019). Overprinted allocyclic processes by tidal resonance in an epicontinental basin: The Upper Jurassic Curtis Formation, east-central Utah, USA. *The Depositional Record*, *5*(2), 272–305. https://doi.org/10.1002/dep2.69

Zuchuat, V., Sleveland, A. R. N., Sprinkel, D., Rimkus, A., Braathen, A., & Midtkandal, I. (2018). New Insights on the Impact of Tidal Currents on a Low-gradient, Semi-enclosed, Epicontinental Basin—The Curtis Formation, East-central Utah, USA. *Geology of the Intermountain West*, *5*, 131–165. https://doi.org/10.31711/giw.v5.pp131-165

Zuchuat, V., Steel, E., Mulligan, R. P., Collins, D. S., & Green, J. A. M. (2022). Tidal dynamics in palaeo-seas in response to changes in physiography, tidal forcing and bed shear stress. *Sedimentology*, *69*(4), 1861–1890. https://doi.org/10.1111/sed.12975

APPENDIX

APPENDIX I:

Generated reports from the 3D virtual outcrop models in Agisoft Metashape

Appendix I: Generated reports from six 3D virtual outcrop models: 1 South Swing, 2 North Swing, 3 South Swing, 4 North Swing, 5 South Swing, and 6 North Swing. All the technical parameters and details are included.